

**Fakultät für Medizin
Medizinische Klinik und Poliklinik
für Innere Medizin II der
Technischen Universität München
Klinikum rechts der Isar**



**Characterization of tumor initiation and development
in a mouse model of primary liver cancer**

Christian Lechler

Vollständiger Abdruck der von der Fakultät für Medizin der
Technischen Universität München zur Erlangung des akademischen
Grades eines

Doktors der Naturwissenschaften

genehmigten Dissertation.

Vorsitzender: Prof. Dr. Percy A. Knolle

Prüfer der Dissertation:

1. Priv.-Doz. Dr. Fabian Geisler
2. Prof. Dr. Gabriele Multhoff

Die Dissertation wurde am 16.08.2019 bei der Technischen
Universität München eingereicht und durch die Fakultät für Medizin
am 31.12.2019 angenommen.

Contents

	List of Tables	V
	List of Figures	VI
	List of Abbreviations	VII
1	Abstract	1
2	Zusammenfassung	2
3	Introduction	3
3.1	Primary liver cancer	3
3.2	Cancer initiation and cell of origin	4
3.3	Molecular pathways in liver cancer	4
3.4	Kras-driven mouse model for primary liver cancer	6
3.5	KRAS effector pathways	7
3.5.1	MEK/ERK signaling	7
3.5.2	PI3K/AKT signaling	8
3.6	Liver specific targeting	10
3.7	Lentiviral systems for <i>in vivo</i> transfection of hepatocytes	13
3.8	Deleted in malignant brain tumors 1	13
3.9	Aims	14
4	Materials	16
4.1	Technical equipment	16
4.2	Disposables	19
4.3	Reagents and enzymes	20
4.4	Antibodies	23
4.5	Molecular biology	24
4.5.1	Primers	31

4.6	Cell culture	32
4.7	Histology	33
4.8	Software	34
5	Methods	35
5.1	Mouse experiments	35
5.1.1	Mouse strains	35
5.1.2	Genotyping	36
5.1.3	Tamoxifen treatment of mice	36
5.1.4	Hydrodynamic tail vein injection	36
5.1.5	Doxycycline treatment of mice	37
5.1.6	Mouse dissection and fixation of organs	37
5.2	Histological analysis	37
5.2.1	Paraffin sections	37
5.2.2	Hematoxylin and eosin staining of tissue sections	37
5.2.3	Immunohistochemistry	38
5.2.4	Immunofluorescence	39
5.2.5	Analysis of stainings	40
5.3	Cell Culture	40
5.3.1	Cryopreservation of cell lines	40
5.3.2	Transfection of RPK cells lines with shRNA constructs	40
5.3.3	MTT assay	41
5.3.4	Clonogenic assay	42
5.4	Molecular biology	42
5.4.1	Isolation of genomic DNA	42
5.4.2	Polymerase chain reaction	43

5.4.3	Separation of DNA by agarose gel electrophoresis	44
5.4.4	RNA isolation and cDNA synthesis	44
5.4.5	Quantitative real time PCR	44
5.5	Protein biochemistry	45
5.5.1	Protein extraction	45
5.5.2	Protein concentration estimation	45
5.5.3	SDS polyacrylamide gel electrophoresis	45
5.5.4	Immunoblot	46
5.6	Statistical analysis	47
6	Results	48
6.1	Novel mouse model for the development of primary liver cancer	48
6.2	Liver tumors in RPK mice show characteristics of hepatocyte and biliary differentiation	50
6.3	Tumors in RPK mice develop from hepatocytes	51
6.4	Microarray and KEGG pathway analysis	53
6.5	Activation of ERK and PI3K-dependent AKT activation in RPK liver tumors <i>in vivo</i>	55
6.6	Inhibition of MEK activity in RPK liver tumor and control cell lines <i>in vitro</i>	56
6.7	Inhibition of PI3K activity in RPK liver tumor and control cell lines <i>in vitro</i>	58
6.8	Genetic inactivation of Pdk1 increases the survival of RPK mice	60
6.9	Genetic inactivation of Pdk1 decreases proliferation in RPK livers	61
6.10	Screening of cancer associated genes	62
6.11	shDMBT1 expression decreases cell viability <i>in vitro</i>	64
6.12	Injection of shDMBT1 increases survival compared to control RPK mice	66
7	Discussion and outlook	68
	Conclusion	75

Publications resulting from my PhD work	76
Acknowledgements	77
References	78

List of Tables

Table 1	Technical equipment	16
Table 2	Disposables	19
Table 3	Reagents and enzymes	20
Table 4	Antibodies	23
Table 5	Buffers and solutions for molecular biology	24
Table 6	Kits for molecular biology	25
Table 7	Bacterial strains	25
Table 8	Plasmids	25
Table 9	shRNA sequences	25
Table 10	PCR genotyping primers	31
Table 11	Primers for quantitative real time PCR	32
Table 12	Cell culture media and their components	32
Table 13	Reagents and kits for cell culture	33
Table 14	Reagents and kits for histological analysis	34
Table 15	Secondary antibodies for histological analysis	34
Table 16	Software	34
Table 17	Mouse strains	35
Table 18	TAM concentration per strain	36
Table 19	Transfection mix	41
Table 20	Composition of PCR	43
Table 21	Conditions for standard PCR	43
Table 22	Annealing temperatures and PCR products	43
Table 23	Composition of running and stacking gel	46

List of Figures

Figure 1	Mutation distribution on a cohort of 24 HCC samples (exome sequencing), the mutations or deletions of the color labeled genes were validated in a set of 125 HCC samples	5
Figure 2	Effector kinase cascade of MEK/ERK signaling	8
Figure 3	Effector kinase cascade of PI3K/AKT signaling	9
Figure 4	Mechanism of hydrodynamic tail vein injection	11
Figure 5	Transposon construct extended by an entry vector with a specific shRNA and a GFP reporter gene under the control of a DOXY-inducible TRE promoter	13
Figure 6	Liver tumor development in RPK mice	49
Figure 7	Liver tumors in RPK mice show characteristics of mixed hepatocyte and biliary differentiation	50
Figure 8	Tumors in RPK mice develop from hepatocytes	52
Figure 9	Microarray and KEGG pathway analysis	54
Figure 10	Activation of ERK and PI3K-dependent AKT in RPK liver tumors <i>in vivo</i>	55
Figure 11	Inhibition of MEK activity in RPK liver tumor and mouse and human cancer cell lines <i>in vitro</i>	57
Figure 12	Inhibition of PI3K activity in RPK liver tumor cells and mouse and human cancer cell lines <i>in vitro</i>	59
Figure 13	Genetic inactivation of Pdk1 increases median survival of RPK mice	60
Figure 14	Genetic inactivation of PDK1 decreases proliferation in RPK livers	61
Figure 15	Screening of cancer associated genes	63
Figure 16	Inducible shDMBT1 expression decreases cell viability <i>in vitro</i>	65
Figure 17	Injection of shDMBT1 increases survival compared to non-treated RPK mice <i>in vivo</i>	67

List of Abbreviations

°C	degree Celsius
AAV	adeno-associated virus
AFP	alpha-fetoprotein
<i>Alb</i>	albumin gene
ANOVA	analysis of variance, a statistical model
AKT	protein kinase B
pAKT ^{Ser473}	phosphorylated protein kinase B at serin 473
pAKT ^{Thr308}	phosphorylated protein kinase B at threonine 308
attB1/attB2	attB recombination sites
ApoE	apolipoprotein E
APS	ammonium persulphate
BDH	bile duct hyperplasia
BILIN-3	Biliary intraepithelial neoplasia, grade 3
bp	base pair
BSA	bovine serum albumin
Cas9	CRISPR-associated 9 endonuclease
CD24a	cluster of differentiation 24a
CD44	cluster of differentiation 44
cDNA	complementary deoxyribonucleic acid
CK19	Cytokeratin 19
c-Met	tyrosine-protein kinase Met
CreER	inducible cre recombinase
CRISPR	clustered regularly interspaced short palindromic repeats
Da	Dalton
DMBT1	deleted in malignant brain tumors 1
DMEM	Dulbecco's modified Eagle medium
DMSO	dimethylsulfoxide

DNA	deoxyribonucleic acid
dNTP	deoxynucleoside triphosphate
DOXY	Doxycyclin
DTT	dithiothreitol
EDTA	ethylenediaminetetraacetic acid
EGFR	epidermal growth factor receptor
ER	endoplasmic reticulum
ERK	extracellular signal-related kinase
EtOH	ethanol
FCS	fetal calf serum
FOXG1	forkhead box protein G1
GAPDH	glyceraldehyde 3-phosphate dehydrogenase
GFP	<i>Green fluorescent protein</i>
GKN2	gastrokine 2
h	hour
H&E	hematoxylin and eosin
hAAT	human alpha1-Antitrypsin
HBS 2x	HEPES buffered saline 2x
HCC	Hepatocellular carcinoma
HCR	hepatic locus control region of the ApoE gene
HEK	human embryonic kidney
HEPES	2-[4-(2-hydroxyethyl)piperazin-1-yl]ethanesulfonic acid
HMGA2	high-mobility group AT-hook 2
Hnf1 β	hepatocyte nuclear factor 1 homeobox B
HTVI	hydrodynamic tail vein injection
i.p.	intraperitoneal
ICC	intrahepatic cholangiocarcinoma/bile duct cancer
IGF	Insulin-like growth factor

IHC	immunohistochemistry
kb	kilo base
Kras	v-Ki-ras2 Kirsten rat sarcoma viral oncogene homolog
L	liter
LB	Luria Broth Bertani
LSL	loxP-stop-loxP
M	molar
MAPK	mitogen-activated protein kinase
MEK	mitogen-activated protein kinase kinase
mg	milligram
min	minute
mL	milliliter
mm	millimeter
mM	millimolar
mRNA	messenger ribonucleic acid
mTOR	mammalian target of rapamycin
MTT	3-(4,5-dimethyl-2-thiazolyl)-2,5-diphenyl-tetrazolium bromide
MW	molecular weight
ng	nanogram
nm	nanometer
nM	nanomolar
OD	optical density
PAGE	polyacrylamide gel electrophoresis
PBS	phosphate buffered saline
PCR	polymerase chain reaction
PDGFR	platelet-derived growth factor receptor
PDK1	3-phosphoinositide-dependent protein kinase 1
PDK2	3-phosphoinositide-dependent protein kinase 2

PH	pleckstrin homology
PI3K	phosphoinositide 3-kinase
PVDF	polyvinylidene fluoride
qPCR	quantitative real time PCR
Raf	rapidly accelerated fibrosarcoma
Ras	Rat sarcoma
RB	retinoblastoma
RNA	ribonucleic acid
<i>Rosa26</i>	ubiquitously expressed gene locus
<i>RPK</i>	<i>Rb^{lox/lox}; p53^{lox/lox}; Kras/Isl-Kras^{G12D}</i>
rpm	revolutions per minute
RPMI	Roswell Park Memorial Institute medium
RT	room temperature
rtTA	reverse tetracycline-controlled transactivator
SB	<i>Sleeping Beauty</i>
SD	standard deviation
SDS	sodium dodecyl sulphate
SEM	standard error of mean
shRNA	short hairpin RNA
SOX4	sex-determining region Y - related high mobility group-box4
SOX9	sex-determining region Y - related high mobility group-box9
S.O.C.	Super Optimal Broth with catabolite repression
TAE	tris-acetate-EDTA
TAM	tamoxifen
TBS	tris-buffered saline
TBST	tris-buffered saline tween-20
TCGA	The Cancer Genome Atlas; Project for the genetic characterization of tumors

TE	tris-EDTA buffer
TEMED	N,N,N',N'-tetramethylethylenediamine, 1,2-bis(dimethylamino)-ethane
TKO	triple-Knock out
TP53 / Trp53	transformation related protein 53
TRE	tetracyclin-responsive element
TSPAN8	tetraspanin 8
β -Tub	β -Tubulin
U	unit of enzyme activity
V	volt
VEGF	vascular endothelial growth factor
WT	wild type
w/v	weight per volume
YFP	<i>yellow fluorescent protein</i>
μ g	microgram
μ L	microliter
μ m	micrometer
μ M	micromolar

1 Abstract

Primary liver cancer is mostly diagnosed in intermediate or advanced stages of the disease, where therapeutic options are limited. The heterogeneity of primary liver cancer renders it difficult to find the key signaling pathways and key drivers, which also complicates the establishment of suitable mouse models. Here, we present a mouse model that by genetically inactivating p53 and RB, along with a persistent activation of oncogenic Kras, targets 3 commonly altered signaling pathways in human liver cancer. After a few months, these *RPK* animals develop hepatic tumors expressing biliary and hepatocyte differentiation markers. The cell of origin from which the primary tumors arise in the *RPK* mouse model are hepatocytes.

Hepatic tumors from our mouse model show a positive staining for pERK or pAKT^{Thr308}, respectively, confirming the activation of Ras-dependent signaling pathways *in vivo*. *RPK* cell lines derived from *RPK* tumors show a high sensitivity against PI3K/AKT or MEK/ERK inhibitors, respectively. Combinations of MEK and AKT inhibitors synergistically provided greater inhibition of *in vitro* cell growth and survival than the individual drugs alone. In *RPK* mice *in vivo*, genetic inactivation of *Pdk1*, as part of the Ras-dependent PI3K/AKT effector cascade, is associated with decreased hepatocyte proliferation in comparison to control *RPK* mice at early time points after gene mutation. Furthermore, our data indicate that RAS driven AKT activation is required for early tumor development in our model.

Microarray analysis of *RPK* tumors revealed a variety of upregulated genes. In an *in vitro* shRNA-screen in *RPK* tumor cell lines, the most promising candidate *Dmbt1* was tested *in vivo* in *RPK* mice. Strikingly, *RPK* mice with concomitant knock-down of *Dmbt1* show a prolonged lifespan.

In summary, the *RPK* mouse model presents a novel platform to study key molecular mechanisms in liver carcinogenesis. The identification of relevant Ras-dependent signaling pathways may offer improved therapeutic benefits through simultaneous targeting of MEK/ERK and PI3K/AKT signaling. Additionally, DMBT1 has been identified as a novel target that contributes to tumor development in our model. The mechanism of how DMBT1 exerts its oncogenic activity is under further investigation.

2 Zusammenfassung

Primärer Leberkrebs wird meist im intermediären oder fortgeschrittenen Krankheitsstadium diagnostiziert, in denen die therapeutischen Möglichkeiten begrenzt sind. Die Heterogenität der hepatischen Malignome macht es schwierig, relevante Schlüssel-Signalwege zu identifizieren, was auch die Etablierung geeigneter Mausmodelle erschwert. Hier stellen wir ein Mausmodell vor, das durch genetische Inaktivierung von p53 und RB zusammen mit einer dauerhaften Aktivierung von onkogenem Kras, 3 häufig veränderte Signalwege in humanen Lebermalignomen nachstellt. Nach kurzer Zeit entwickeln diese *RPK*-Tiere Lebertumore mit biliärer und hepatozytärer Differenzierung. Die Ursprungszelle, aus der die primären Tumoren im *RPK*-Mausmodell entstehen, sind Hepatozyten.

Die hepatischen Tumore aus unserem Mausmodell zeigen in der Immunhistochemie eine positive Färbung für pERK bzw. pAKT^{Thr308}, was die Aktivierung von Ras-abhängigen Signalwegen *in vivo* bestätigt. *RPK*-Zelllinien aus *RPK*-Tumoren zeigen eine hohe Sensitivität gegenüber PI3K/AKT- oder MEK/ERK-Inhibitoren. Kombinationen von MEK/ERK- und PI3K/AKT-Inhibitoren zeigen synergistisch eine stärkere Hemmung des Zellwachstums und -überlebens *in vitro* als die jeweils einzelnen Inhibitoren. *In vivo* führt die zusätzliche genetische Inaktivierung von *Pdk1* als Teil der Ras-abhängigen PI3K/AKT-Effektorkaskade zu einer verminderten Proliferation der Hepatozyten im Vergleich zu *RPK*-Tieren zu frühen Zeitpunkten nach Cre-Aktivierung. Unsere Daten weisen darauf hin, dass die RAS-abhängige AKT-Aktivierung für die frühe Tumorentwicklung in unserem Modell erforderlich ist.

In Microarray-Analysen von *RPK*-Tumoren und Kontrolllebern konnte eine Vielzahl von im *RPK*-Modell überexprimierten Genen identifiziert werden. In einem shRNA-Screeningansatz in *RPK*-Zelllinien wurde *Dmbt1* als vielversprechendes Kandidatengen identifiziert. *In vivo* zeigen *RPK*-Mäuse mit *Dmbt1*-Kock-down eine verlängerte Lebensdauer. Das *RPK*-Mausmodell bietet somit eine Plattform, um wichtige molekulare Mechanismen und Veränderungen in der hepatischen Karzinogenese zu untersuchen. Die Identifizierung von relevanten RAS-abhängigen Signalwegen kann möglicherweise einen verbesserten therapeutischen Nutzen durch gleichzeitige Inhibition der MEK/ERK- und PI3K/AKT-Signalkaskaden bringen. *DMBT1* wurde als ein neues Zielprotein identifiziert, das direkt oder indirekt Tumorentwicklung in unserem Modell beiträgt. Der Mechanismus, wie *DMBT1* die hepatischen Karzinogenese beeinflusst wird in weiteren Studien untersucht.

3 Introduction

3.1 Primary liver cancer

Primary liver cancer is one of the leading causes of cancer related mortality worldwide with a rising incidence in Europe and the United States of America [4]. With almost 800,000 cancer related deaths annually, liver cancer ranks third in cancer mortality in men and sixth in women [5]. Accounting for up to 85% of all primary tumors, hepatocellular carcinoma (HCC) is the most common type of primary liver cancer, followed by intrahepatic cholangiocarcinoma (ICC). Both are characterized by a rising incidence over the recent years [6-8]. In a number of cases, tumors exhibit histological characteristics of both HCC and ICC, but whether these tumors arise from two different entities or if they share the same cell of origin is still debated [9]. Viral hepatitis as well as repeated exposure to hepatotoxins such as alcohol or aflatoxin present major risk factors in liver disease and are associated with chronic hepatic inflammation, liver cirrhosis, and HCC [10, 11]. In contrast to HCC, most cases of ICC or combined tumors cannot be associated to the presence of specific risk factors. However, the increased risk for ICC in infection with liver flukes, biliary-duct cysts, hepatolithiasis, and primary sclerosing cholangitis links the etiology of this disease to chronic inflammation, similar to HCC [12]. In 70-80% of cases, liver cancer is diagnosed in intermediate or advanced stages of the disease where therapeutic options remain limited, rendering few patients subject to curative therapy such as tumor resection or liver transplantation [13, 14]. The multityrosine kinase inhibitor sorafenib has been the only effective therapy option for years, but even with this treatment, mean overall survival remains less than a year [15, 16]. Novel systematic tumor therapies show promising results with an average overall survival of around 13 months [17-19]. With sequential treatment regimens, average survival can extend beyond 2 years in selected patients [20]. Even with the rise of these new systemic treatment options, 5-year survival will probably not significantly improve. The limited treatment options in advanced tumor stages outlined above together with an up to 70% recurrence rate after curative therapy [21] contribute to the high mortality of HCC and a 5-year survival rate of less than 20% in the Western world [7]. Therefore, there is an urgent need for effective systemic therapies that can control tumor growth, especially in advanced stages. Further insights in the key drivers is mandatory for the improvement of existing cancer therapies and for the identification of future therapeutic targets in liver cancer.

3.2 Cancer initiation and cell of origin

The common molecular traits in ICC, tumors of mixed differentiation, and poorly differentiated HCC suggest for a potential continuum between these tumors and indicate that they might originate from the same cell of origin [22]. Over the recent years, hepatocytes as well as liver progenitor cells have been discussed as the potential tumor initiating cells in these cancers. Previous reports indicated that liver progenitor cells do not only play a role in physiological tissue turnover but might also contribute to liver carcinogenesis [23-26]. Gene expression profiling of HCC, ICC, and combined hepatocellular-cholangiocarcinomas identified subtypes with “stem-like” characteristics [27], leading to the assumption that the cell of origin in these cancers might be a stem or progenitor cell. Additionally, several mouse models highly suggested for an origin of hepatic cancers from liver progenitor cells [28, 29]. However, this view has been challenged by recent research indicating that HCCs and even ICCs, can arise from transformed mature hepatocytes [30, 31]. Characterization of the highly debated cell of origin in primary liver cancer will help us to understand the molecular mechanisms in cancer initiation and could identify early diagnostic markers as well as therapeutic targets in preventive cancer therapy.

3.3 Molecular pathways in liver cancer

In the last two decades, the molecular characterization of tumor diseases has triggered the development of new therapies that specifically inhibit tumor-relevant signaling pathways. For the identification of targetable signaling pathways, a knowledge of the molecular changes that occur in tumor development is essential. In the analysis of human hepatocellular carcinoma – including data of the Cancer Genome Atlas (TCGA) – numerous mutations in known oncogenes or tumor suppressor genes were detected [1, 32-34]. The HCCs analyzed in these studies showed a high intertumoral heterogeneity and a diverse mutational profile, which makes it difficult to identify the genetic alterations that are essential during carcinogenesis. In addition to the gene mutations, deletions, or gene amplifications that were identified in sequence analyzes, signaling pathways may be altered by epigenetic or other regulatory changes [35, 36]. However, despite this heterogeneity, accumulation of mutations in different tumor-associated pathways has been shown by gene expression profiling and cancer genome

β-catenin	p53/cell cycle	chromatin remodelling	PI3K/ Ras signaling	oxidative and ER stress
<div style="border: 1px solid black; padding: 2px; display: inline-block;">FZR1</div> <div style="border: 1px solid black; padding: 2px; display: inline-block;">CSNK1E</div> <div style="border: 1px solid red; padding: 2px; display: inline-block; color: red;">CTNNB1 32,8%</div> <div style="border: 1px solid black; padding: 2px; display: inline-block;">AXIN1 15,2%</div> <div style="border: 1px solid black; padding: 2px; display: inline-block; margin-left: 10px;">APC 1,6%</div> <div style="border: 1px solid black; padding: 2px; display: inline-block;">MCC</div>	<div style="border: 1px solid blue; padding: 2px; display: inline-block;">IRF2 4,8%</div> <div style="border: 1px solid black; padding: 2px; display: inline-block;">MDM2</div> <div style="border: 1px solid blue; padding: 2px; display: inline-block;">TP53 20,8%</div> <div style="border: 1px solid black; padding: 2px; display: inline-block; margin-left: 10px;">RB1</div> <div style="border: 1px solid blue; padding: 2px; display: inline-block;">CDKN2A 7,2%</div> <div style="border: 1px solid black; padding: 2px; display: inline-block;">CDKN1B</div> <div style="border: 1px solid black; padding: 2px; display: inline-block; margin-left: 10px;">PAK2</div> <div style="border: 1px solid black; padding: 2px; display: inline-block;">CDK11A</div> <div style="border: 1px solid black; padding: 2px; display: inline-block; margin-left: 10px;">CDKN2C</div> <div style="border: 1px solid black; padding: 2px; display: inline-block;">CDK11B</div>	<div style="border: 1px solid black; padding: 2px; display: inline-block;">SMARCA2</div> <div style="border: 1px solid black; padding: 2px; display: inline-block;">SMARCA4</div> <div style="border: 1px solid black; padding: 2px; display: inline-block;">SMARCB1</div> <div style="border: 1px solid blue; padding: 2px; display: inline-block; margin-left: 20px;">ARID1A 16,8%</div> <div style="border: 1px solid blue; padding: 2px; display: inline-block; margin-left: 20px;">ARID2 5,6%</div> <div style="border: 1px solid black; padding: 2px; display: inline-block; margin-left: 40px;">PBRM1</div> <div style="border: 1px solid black; padding: 2px; display: inline-block;">SMARCA1</div> <div style="border: 1px solid black; padding: 2px; display: inline-block; margin-left: 10px;">SMARCA1</div> <div style="border: 1px solid black; padding: 2px; display: inline-block; margin-left: 10px;">SMARCA1</div> <div style="border: 1px solid black; padding: 2px; display: inline-block;">JMJD8</div> <div style="border: 1px solid black; padding: 2px; display: inline-block; margin-left: 10px;">JMJD1C</div> <div style="border: 1px solid black; padding: 2px; display: inline-block; margin-left: 10px;">EP300</div> <div style="border: 1px solid black; padding: 2px; display: inline-block;">CHD3</div> <div style="border: 1px solid black; padding: 2px; display: inline-block; margin-left: 10px;">CHD4</div> <div style="border: 1px solid black; padding: 2px; display: inline-block; margin-left: 10px;">HAT1</div> <div style="border: 1px solid black; padding: 2px; display: inline-block;">HDAC9</div> <div style="border: 1px solid black; padding: 2px; display: inline-block; margin-left: 10px;">Hist1H2BF</div> <div style="border: 1px solid black; padding: 2px; display: inline-block; margin-left: 10px;">MCM6</div>	<div style="border: 1px solid red; padding: 2px; display: inline-block; color: red;">Kras 1,6%</div> <div style="border: 1px solid black; padding: 2px; display: inline-block; margin-left: 20px;">PIK3CA 1,6%</div> <div style="border: 1px solid black; padding: 2px; display: inline-block;">MAPK8</div> <div style="border: 1px solid black; padding: 2px; display: inline-block; margin-left: 10px;">PIK3CG</div> <div style="border: 1px solid black; padding: 2px; display: inline-block;">MAP3K12</div> <div style="border: 1px solid black; padding: 2px; display: inline-block; margin-left: 10px;">PTEN</div> <div style="border: 1px solid blue; padding: 2px; display: inline-block; margin-left: 20px;">RPS6KA3 9,6%</div> <div style="border: 1px solid black; padding: 2px; display: inline-block; margin-left: 20px;">PRKCB</div> <div style="border: 1px solid black; padding: 2px; display: inline-block;">STK11</div> <div style="border: 1px solid black; padding: 2px; display: inline-block; margin-left: 10px;">DLC1</div> <div style="border: 1px solid black; padding: 2px; display: inline-block; margin-left: 10px;">STRADA</div>	<div style="border: 1px solid black; padding: 2px; display: inline-block;">ERN1</div> <div style="border: 1px solid red; padding: 2px; display: inline-block; color: red;">NFE2L2 6,4%</div> <div style="border: 1px solid black; padding: 2px; display: inline-block; margin-left: 10px;">EDEM1</div> <div style="border: 1px solid black; padding: 2px; display: inline-block; margin-left: 10px;">PDIA2</div> <div style="border: 1px solid black; padding: 2px; display: inline-block;">KEAP1</div> <div style="border: 1px solid black; padding: 2px; display: inline-block; margin-left: 10px;">PARK7</div> <div style="border: 1px solid black; padding: 2px; display: inline-block; margin-left: 10px;">DNAJB3</div> <div style="border: 1px solid black; padding: 2px; display: inline-block;">NOX5</div> <div style="border: 1px solid black; padding: 2px; display: inline-block; margin-left: 10px;">NOS3</div> <div style="border: 1px solid black; padding: 2px; display: inline-block; margin-left: 10px;">DNAJC22</div> <div style="border: 1px solid black; padding: 2px; display: inline-block;">SOD1</div> <div style="border: 1px solid black; padding: 2px; display: inline-block; margin-left: 10px;">CYP2E1</div> <div style="border: 1px solid black; padding: 2px; display: inline-block; margin-left: 10px;">CCT8L2</div> <div style="border: 1px solid black; padding: 2px; display: inline-block;">CYP2F1</div> <div style="border: 1px solid black; padding: 2px; display: inline-block; margin-left: 10px;">BAG3/4</div>

Figure 1: Mutation distribution on a cohort of 24 HCC samples (exome sequencing), the mutations or deletions of the color-labeled genes (red: activated, blue: inactivated) were validated in a set of 125 HCC samples (modified according to [1])

sequencing and identified several commonly altered pathways involved in hepatic carcinogenesis, including genes in cell cycle control and chromatin remodeling, Wnt/β-catenin signaling, EGFR/Ras/ERK and PI3K/AKT/mTOR pathways, growth factor signaling (c-MET, IGF, VEGF and PDGFR), oxidative and ER stress pathways as well as inflammatory signaling pathways [15, 32, 37, 38] (Fig. 1). Similar to HCC, ICCs display a great heterogeneity in their molecular expression profile, with the most common mutations found in the *p53* and *KRAS* genes [39]. Gene expression analyses further indicate that several subtypes of ICC exist, which differ in prognosis and therapeutic response [40-42]. The mutation spectrum in combined hepatocellular-cholangiocarcinomas shares similarities with both ICC and HCC. The molecular expression profiles of these tumors exhibit features of liver progenitor cells with down-regulation of hepatocyte differentiation programs [27]. One of the pathways that is activated in the majority of human HCC as well as ICC is Ras signaling [43] and the expression of RAS activated proteins such as RAF-1 and pMEK is associated with poorer overall survival in patients [44]. On the molecular level, the Ras signaling cascade transduces extracellular signals from growth factor receptors such as EGFR, IGFR, or c-MET and subsequently activates RAF, MEK, and ERK, resulting in activation of a plethora of proliferative and anti-apoptotic signaling pathways. To date, our understanding of critical RAS effectors in liver cancer remains limited: While several animal studies indicated that inhibition of MEK/ERK alone or in combination with other compounds could be a promising approach in the therapy of liver cancer [45-48]. Further research is needed to characterize the key mediators of Ras signaling in liver cancer as a basis for the development of novel therapeutic strategies in the treatment of HCC or ICC.

3.4 Kras-driven mouse model for primary liver cancer

The use of animal models in cancer research requires systems that closely match the human disease in pathophysiology, clinical and histological appearance as well as gene expression profiling. The great heterogeneity of primary liver cancer hampers the finding of suitable mouse models. The absence of reliable mouse models has been a major limitation in the study of advanced, metastatic liver cancer in the past. In our lab, we generated a novel genetically engineered mouse model of primary liver cancer. In this model, activation of oncogenic Kras together with functional inactivation of the tumor suppressor proteins RB and p53 in the liver of adult *RPK* mice mimic molecular events that occur in the majority of human liver cancers. The functional inactivation of the retinoblastoma signaling pathway is observed in the majority of human hepatocellular carcinomas [49]. The p53 pathway was identified as the second pathway the most frequently altered in HCC with around 20% of mutations that lead to inactivation of p53 [1]. Since activation of p53 may act as a tumor suppressive mechanism in RB-deficient cells [50, 51], combined functional inactivation of the two major tumor suppressors RB and p53 will likely promote tumor development. Interestingly, combined loss of RB and p53 does lead to spontaneous tumor formation only with long latency [138]. However, in the presence of continuously hepatocarcinogenic stress, such as viral infection, exposure to hepatotoxins, or metabolic stresses, an aberrant DNA damage signaling response occurs which can contribute to tumor formation. Inactivation *KRAS* mutations are mainly found in extra aggressive tumors, leading to a short survival of patients. A previous study analyzing biliary tract cancer found that *KRAS* was mutated in 18% and p53 in 26% of the cases, indicating for a role as top drivers of biliary tract cancer [52]. In HCC p53 also belongs to the top mutated genes with a frequency of approximately 20%. In contrast, the frequency of *KRAS* mutations is at rather low with a frequency of less than 5%. However, the presence of *KRAS* was associated with poor survival [1]. Independent of the presence of *KRAS* mutations, PI3K/Ras signaling is activated in the majority of HCC either by mutations in other genes of the signaling pathway or other mechanisms [1]. Simultaneously targeting three commonly altered signaling pathways in hepatocellular carcinoma and also cholangiocarcinoma was therefore used in our mice to mimic one of the most common molecular changes in human primary liver cancer. After hepatic gene recombination, these *RPK* mice rapidly develop hepatic tumors with hepatocytic and biliary differentiation. To date, many open questions remain in hepatic

carcinogenesis. Here, we used the *RPK* model to gain insight into the molecular mechanisms that drive tumor initiation and progression.

3.5 KRAS effector pathways

RAS activation is usually mediated by EGFR, which, after binding to EGF, alters its conformation leading to activation of tyrosine kinase activity on the cytoplasmic side of the receptor. KRAS is activated by binding to GTP, which triggers a downstream signal kinase cascade. Continuously activated oncogenic KRAS leads to increased activation of effector pathways important for cancer initiation and development such as MEK/ERK and PI3K/AKT signaling. The continuously activating *KRAS* mutations are a prognostic marker for bad prognosis for patients in different tumor entities, resulting in a decreased overall survival [53]. *KRAS* mutations are observed at low frequencies in HCC, but are quite common mutations in ICC [1, 54]. Several studies using mouse models containing *Kras*^{G12D} mutations report an increased number of ICC tumors, underlining the important role of KRAS as a driver of hepatic carcinogenesis [55, 56]. Since KRAS itself is considered non-targetable, various clinical studies have tried to inhibit KRAS effector downstream kinases.

3.5.1 MEK/ERK signaling

The importance of the MEK/ERK signaling pathway in hepatocarcinogenesis has been confirmed in several *in vivo* studies. In mice with continuously liver-specific expression of activated proteins of the MEK/ERK cascade, there is an increased proliferation in hepatocytes finally resulting in HCC development [57]. The backbone of the MEK/ERK signaling consists of RAS-activated isoforms of RAF (cRaf, B-Raf, and A-Raf) that phosphorylate and activate MEK, which in turn phosphorylates and therefore activates ERK (Fig. 2) [58]. Active pERK directly or indirectly mediates the activation of several genes that play an important role for cell growth, survival, apoptosis, proliferation, and differentiation. Significant upregulation of pERK in 60% of patients with advanced HCC and poor prognosis has been observed underlining the clinical relevance of this pathway in human advanced primary liver cancer [43, 59, 60]. Downstream effectors of MEK/ERK signaling include NF- κ B and c-MYC signaling. NF- κ B activation leads to the expression of anti-apoptotic genes and plays a major role in wound healing response in chronic liver diseases and proliferation that can ultimately contribute to HCC development

[61-63]. c-MYC targets and regulates cell cycle genes such as CDK4 and influences cell growth

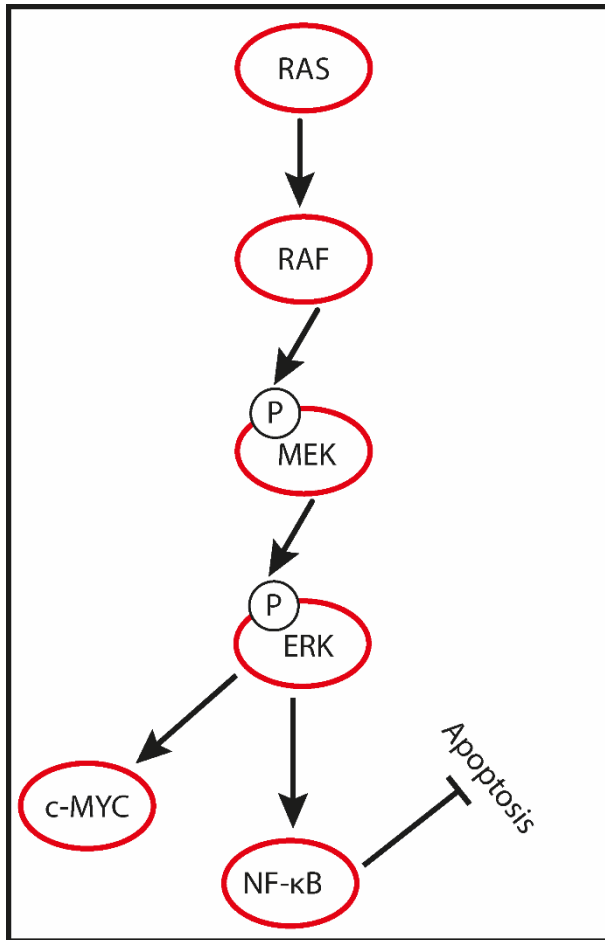


Figure 2: Effector kinase cascade of MEK/ERK signaling

and cell cycle arrest [64]. A disruption of the MEK/ERK signaling pathway can lead to uncontrolled cell proliferation and cancer development, with aberrant c-MYC and NF-κB signaling contributing to chronic liver disease and increasing the risk of primary liver cancer formation [62, 65]. Pharmacological inhibition of RAF or MEK tested in several clinical studies could therefore be a promising approach in the therapy of primary liver cancer with activated Ras signaling. Sorafenib, a Raf, VEGFR, and PDGFR-β inhibitor showed promising results and prolonged overall survival but has modest efficacy in advanced HCC patients [66, 67]. Patients with advanced HCC showed no sufficient anti-tumor responses by the MEK inhibitor

Selumetinib either [68]. The effect of single inhibitors is promising but the effect might be too small. Of note, combinational therapy of the MEK inhibitor Refametinib together with Sorafenib in HCC patients showed a better clinical response in patients with *KRAS* mutations than patients without mutated *RAS* [69]. Combination of Selumetinib and Sorafenib in patients with mostly HBV-related advanced HCC showed an encouraging anti-tumor activity [70]. In summary, these studies indicate that the MEK/ERK pathway is a key mediator of primary liver cancer for cell growth, survival, apoptosis, proliferation, and differentiation and a strong driver of carcinogenesis.

3.5.2 PI3K/AKT signaling

Ras-induced signaling also leads to the activation of the intracellular PI3K/AKT signaling pathway also known as the PI3K/AKT/mTOR pathway. Overexpression of PI3K/AKT pathway members is commonly observed in different cancers including acute myeloid leukemia, breast

cancer, and HCC [71-73]. The pathway consists of an activating signaling cascade of RAS, PI3K,

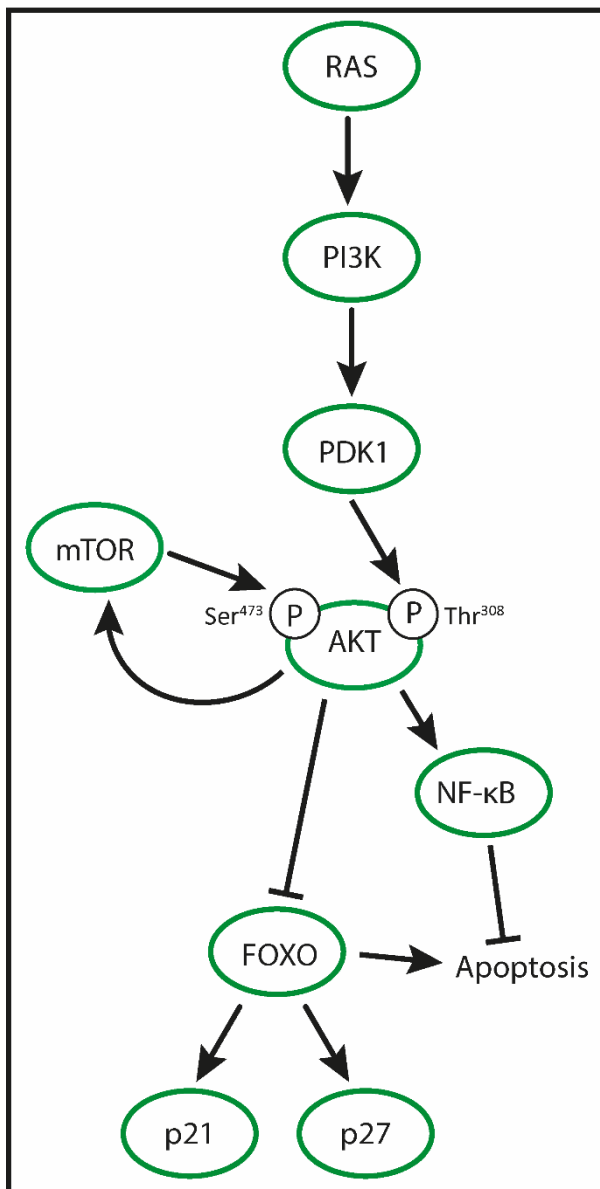


Figure 3: Effector kinase cascade of PI3K/AKT signaling

and PDK1. The kinase PDK1 finally activates AKT at threonine 308, initiating pAKT^{Thr308} downstream signaling. PDK1 is a serine/threonine kinase and seen as a candidate pro-oncogene and a potential prognostic biomarker for HCC, based on the observation of high PDK1 levels in HCC patients [74]. This finding is probably based on the downstream activation of AKT and the resulting activation of various potentially oncogenic target genes. There are many different mechanisms of how pAKT affects cellular processes whose disruption promotes cancer development, including survival, proliferation, apoptosis, and cell growth. Downstream effector signaling includes activation of mTOR and NF-κB [75], as well as the inhibition of FOXO. FOXO belongs to the forkhead box transcription factor family can only enter the nucleus when non-phosphorylated. pAKT phosphorylation

inhibits FOXOs regulation of the transcription of the tumor suppressors p21 and p27 and expression of proapoptotic Bcl-2 family members, making the cell more susceptible to cancer development [76, 77]. Another important aspect is that AKT can activate the mTOR complex which in turn phosphorylates AKT at the Serine residue 473, necessary for full activation of pAKT [78]. mTOR up-regulation is often seen in HCC and associated with bad prognosis outcome for patients [79-81]. However, clinical trials with inhibitors of mTOR signaling gave mixed results. The mTOR inhibitor temsirolimus achieved a disease stabilization among HCC patients with chronic liver disease [82]. On the other hand, second-line treatment with the mTOR inhibitor everolimus did not result in any survival benefit over best supportive care [83]

and a combinational therapy of sorafenib and everolimus did not show any improvement of efficacy compared to sorafenib therapy alone [84]. PI3K/AKT signaling is a strong oncogenic RAS sub-pathway with the ability to promote cancers in different tissues. The up-regulation of several downstream effector kinases of PI3K/AKT signaling are reported as bad prognosis markers in HCC patients. However, treatment of mTOR signaling alone does not seem to have a significant benefit in the liver.

3.6 Liver specific targeting

Various methods are available for the analysis of oncogenic and tumor suppressive signaling pathways in the liver. Targeted genetic changes in hepatocytes are used effectively to investigate the relevance of specific genes or associated signaling pathways [85, 86]. The generation of genetically modified mouse lines is mostly indispensable to investigate tumors-associated pathways, but also time-consuming, labor-intensive and expensive. Therefore, in recent years, alternative methods have been increasingly developed for genetic manipulation of the liver *in vivo*, including virus-mediated transduction of hepatocytes to express target genes or direct *in vivo* transfection by hydrodynamic tail vein injection (HTVI) [87-89]. In HTVI, dissolved plasmid vectors harboring the desired target DNA are injected intravenously into mice in a large-volume of saline within a short time via the tail vein (Fig. 4B). The applied volume exceeds the cardiac output of the animals resulting in a backflow of the volume into the sinusoids of the liver parenchyma and a pressure-mediated uptake of the dissolved DNA into hepatocytes. Due to the methodology, mainly hepatocytes close to central veins become transfected (Fig. 4A). Depending on the efficiency of the injection, the vector size and amount of injected DNA, up to 40% of the hepatocytes can be transfected by this method [3]. When using a DNA sequence flanked by transposon elements and simultaneous injection of a transposase expression vector, integration of the target DNA into the genomic DNA of hepatocytes is achieved [89]. In contrast to introduction of DNA by adenoviruses or adeno-associated viruses (AAV), the most commonly used viral vector systems for targeted gene manipulation of murine hepatocytes, transposon-mediated genomic integration can provide stable long-term expression even after multiple cell divisions, such as in liver regeneration or in tumors [87, 89]. Although it is also possible to achieve genomic integration in numerous *in vitro* and *in vivo* models via lentiviral vectors, the efficiency of this integration in the liver of

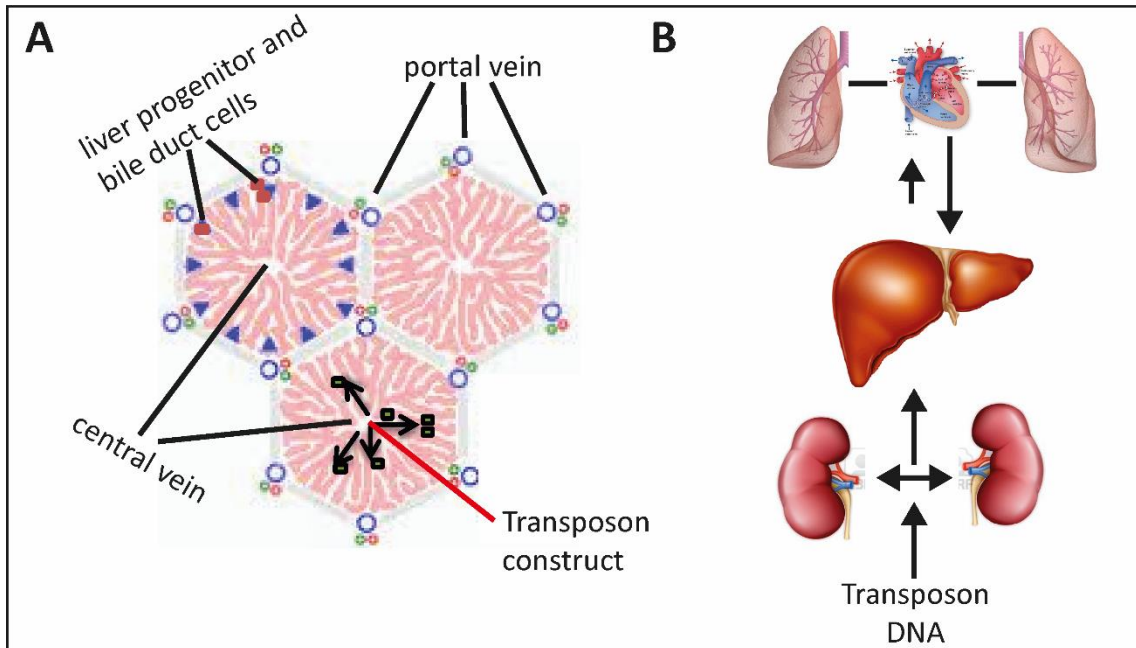


Figure 4: Mechanism of hydrodynamic tail vein injection

(A) The injected transposon construct integrates into the genomic DNA of hepatocytes near the central vein.

(B) The transposon DNA solution is injected into the tail vein, exceeding cardiac output. The volume is stowed back into the liver and the transposon DNA is pushed through the central vein directly into the hepatocytes (modified according to [2])

adult animals is very low as the majority of hepatocytes are in a quiescent state. Additionally, proteins of the lentiviral envelope are immunogenic, probably resulting in clearing of infected hepatocytes by the immune system [90]. Further advantages of stable transfection via HTVI are a low to absent immunogenicity, as well as a comparatively simple generation of the transposon vectors without the peculiarities of an increased biosafety level, as required for the preparation of almost all viral vectors [91, 92]. Because of these advantages, HTVI has become established in recent years as a method of choice for achieving stable long-term expression of genes in murine hepatocytes. It has been used successfully in preclinical models for the evaluation of gene therapy approaches [89] and has enabled the functional analysis of numerous oncogenes in hepatocellular carcinoma in tumor research [87]. In combination with targeted gene knockdown or gene knockout using small hairpin RNA (shRNA) or CRISPR/Cas9 constructs, the method was successfully used for the identification and targeted modification of relevant signaling pathways in liver regeneration and carcinogenesis [93-96]. Due to the relatively high capacity of the transposon vectors, expression of two or more transgenes can be done by a single vector, although increasing the size of the vectors may result in reduction of transfection efficiency [97, 98]. A combination of transgene expression and gene knockdown is also possible and has been successfully used in *in vivo* screens [93, 99]. We were able to establish a system that extends this approach to reversibly inducible expression of

transgenes or shRNA. In this system, a constitutive gene expression of inducible Cre-recombinase is combined with tetracycline-inducible gene expression or knockdown, which makes it possible to test the relevance of target genes at different times, particularly in models for hepatocarcinogenesis [98, 100]. In addition to the induction of tumors and the analysis of relevant oncogenes and tumor suppressor genes, HTVI also offers promising potential applications in other areas of liver research, such as mouse models for metabolic liver diseases or in regeneration models [94]. We used the *Sleeping Beauty* (SB) transposon system for a stable transfection of the desired vector into hepatocytes. In a previous study, a transposon system with a tamoxifen (TAM)-inducible Cre-recombinase (CreERT2) under the control of the liver specific ApoE.HCR.hAAT promotor was established [2]. The liver specificity of the ApoE.HCR.hAAT promotor and the successful transgene expression in mouse livers *in vivo* was shown previously [2, 101]. When adult *RPK* mice are injected with a construct containing a sequence for constitutive CreERT2 by HTVI, specific recombination in targeted hepatocytes can be induced by intraperitoneal injection of TAM. The genetic background of our mice contains a *Rosa26^{LSL-YFP}* reporter gene, which allows for visualization of recombined hepatocytes after activation of transfected Cre-recombinase. Transfection efficiency therefore can be proven and quantified. A small, but notable disadvantage of the system is the variable targeting efficiency, mainly based on the size of the transposon system, the DNA concentration, the injection volume and the injection time [3, 102, 103].

Another variant for hepatocyte specific targeting is the expansion of our *RPK* mouse model with a hepatocyte specific CreER expression driven by the Albumin promotor (*Alb^{CreER}*) [104]. Albumin is continuously expressed by hepatocytes, which leads to extensive liver specific Cre recombinase activity even after low-dose TAM treatment. Activation of the Cre recombinase in *Alb^{CreER}* mice was carried out by one time TAM injection of 100 ng/g body weight as described before [105]. *Alb^{CreER}* mouse strains are efficient to target the hepatocyte compartment, but at higher doses cells from the small biliary ductules are also targeted, giving the rational to use low doses of TAM to ensure almost complete hepatocyte specificity [105]. For specific targeting of the biliary compartment, we crossed our *RPK* mice with *Hnf1 β -CreER* and *Sox9-CreER* mice, respectively. Hnf1 β -positive cells are found in bile ducts and periportal ductules of the canals of Hering, staining of these cells revealed a positive staining of the biliary markers CK19 and SOX9 [105]. Since the Cre recombination activity in *RPK;Hnf1 β -CreER* and

RPK;Sox9-CreER mice is limited to the biliary compartment, we can clarify whether our tumors do strictly arise of hepatocytes or also from the biliary compartment.

3.7 Adaption of inducible lentiviral systems for *in vivo* transfection of hepatocytes

The *SB* transposon system described above was extended to specifically express shRNA under the control of a doxycycline (DOXY)-inducible tetracycline-responsive element (TRE) promoter (Fig. 5) [98, 100]. From the starting point of the TAM induced liver specific Cre recombination that leads to primary liver cancer in our model, DOXY chow was fed to the mice which induces the TRE promoter and therefore specific shRNA/GFP expression. This extended inducible system is a valuable tool to study the effect of the specifically expressed shRNA on hepatic cancer initiation, development and progression. This system was used for *in vivo* validation of candidate genes identified in the *in vitro* shRNA screening approach using specific shRNA against candidate genes.

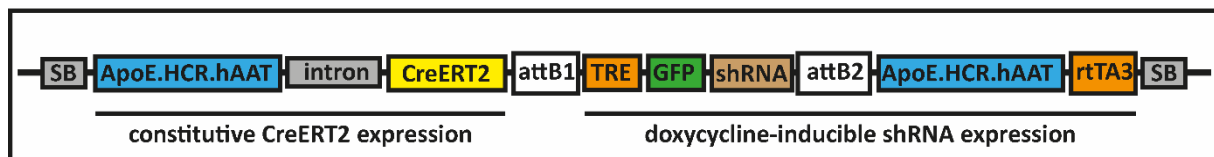


Figure 5: Transposon construct extended by an entry vector with a specific shRNA and a *GFP* reporter gene under the control of a DOXY-inducible TRE promoter [98, 100]

3.8 Deleted in malignant brain tumors 1

Candidate genes were defined by microarray analysis of gene expression data from *RPK* liver tumors. The variety of significant up-regulated genes highly expressed in *RPK* liver tumors but not in control livers are related to cancer and metastasis. Our gene list includes several putative oncogenes (*Sox4*, *Foxg1*, *Tspan8*, *Hmga2*), markers of cancer stem cells (*Cd24a* and *Cd44*) in liver cancer [106], as well as genes that have been reported as tumor suppressors in other tissues but might have a different function in hepatocarcinogenesis (*Dmbt1*, *Gkn2*). Comparison with publicly available data from human liver tumors [25, 107] revealed that the expression of these genes was elevated in hepatic malignancies in human patients. However, their functional role in liver carcinogenesis is mostly unknown to date. For our screen, we infected *RPK* cancer cell lines with lentiviral particles harboring gene-specific shRNA constructs and evaluated infected cell lines for knockdown efficiency of the desired gene on mRNA and

protein level and the impact of this knockdown on cell viability and clonogenic capabilities. One of the most promising screened candidate genes that was highly upregulated in *RPK* tumors is deleted in malignant brain tumors 1 (DMBT1). DMBT1 is a protein that belongs to the scavenger receptor cysteine-rich superfamily. DMBT1 deletion was observed in brain tumor cell lines and was therefore first described as a putative tumor suppressor [108]. Additionally studies support the tumor suppressor hypothesis, because of the loss or downregulation of DMBT1 in melanoma [109], pancreatic adenocarcinoma [110], lung cancer [111, 112], epithelial skin cancer [113], breast cancer [114], oral squamous cell carcinoma [115], prostate cancer [116], and oesophageal cancer [117]. Functionally, DMBT1 is described as a contributor to the innate immune defense system and functions as a pattern recognition molecule for pathogens [118]. In the liver, there are only a few studies available that describe a connection between DMBT1 and cancer, but neither of them present a reliable mechanism. A splice variant of DMBT1 called Ebnerin has been reported to have a role in liver regeneration from transit-amplifying ductular (oval) cells by deciding their fate and differentiation [119]. However, the role of oval cells in liver regeneration has been debated recently [88] and the role of DMBT1 in this setting remains unclear. DMBT1 is described as a potential biomarker for bile duct hyperplasia (BDH) [120] and DMBT1 expression induces a proliferation of cholangiocytes which results in BDH [121]. In another study, DMBT1 expression has been reported in transformed biliary epithelial cells with high expression of DMBT1 in biliary intraepithelial neoplasia, grade 3 (BillN 3) and lower expression in bile duct cancer compared to BillN 3. This study indicates that upregulation of DMBT1 occurs at early stages during ICC formation that might be followed by downregulation at later time points [122]. To date the functions DMBT1 in the liver are not clear and one can only speculate about the underlying mechanism by which DMBT1 mediates cancer initiation and development.

3.9 Aims

By establishing the *RPK* mouse model as a system that recapitulates many aspects of human primary liver cancer with poor prognosis, we aimed to study various aspects of initiation, development, and progression.

Aim 1: Recent studies indicate that HCC and ICC arise primarily from hepatocytes, whereas cells from the periportal cell compartment, so-called liver progenitor cells or oval cells, do not

play a significant role in the development of HCCs. However, it is not fully understood whether direct development of cholangiocarcinoma from adult hepatocytes is possible without activation of pathways that drive bile duct development such as Notch signaling. The characterization of tumor initiating cells might not only be important in the early diagnosis of cancer, but will also help to identify potential targets in tumor prevention. To date, the potential cell of origin in primary liver cancer remains highly debated. In this aim we characterized the cell of origin in our cancer model and combined detailed analyses of early stages in tumor development with *in vivo* lineage tracing systems that specifically target the potential tumor initiating cells in liver carcinogenesis.

Aim 2: Due to the wide variety of molecular changes in human primary liver cancer, the identification of the most relevant signaling pathways that drive tumor development presents a challenging task. Genetically engineered mice recapitulate molecular events that contribute in human carcinogenesis and provide the opportunity to characterize the role of oncogenic pathways in liver cancer. The expression of mutant, constitutively active Kras presents a strong oncogenic signal that induces cell proliferation through various downstream effector kinases. Ras signaling represents one of the most critical oncogenic signaling pathways in early and advanced hepatocarcinogenesis. To test the relevance of Ras signaling in our *RPK* mouse model, inhibition of PI3K and MEK as downstream effector kinases and their effect on proliferation in *RPK* hepatocytes *in vitro* was investigated.

Aim 3: We used a screening approach to test for the functional relevance of highly expressed candidate oncogenes identified in gene expression microarrays of advanced *RPK* liver tumors. To this aim, we employed *in vitro* and *in vivo* systems to analyze the effects of gene knock-down on tumor cell proliferation, survival, anchorage-independent growth, and cell viability. We anticipate that the aims of this project will be able to answer important question in tumor biology of hepatic malignancies and will help to identify novel therapeutic targets for the treatment of human liver cancer.

4 Materials

4.1 Technical equipment

Table 1: Technical equipment

Device	Source
Analytical balance ABS-N/ABJ-NM	KERN & SOHN GmbH, Balingen-Frommern
Autoclave 2540 EL	Tuttnauer Europe B.V., Breda, The Netherlands
AxioCam HRc	Carl Zeiss AG, Oberkochen
AxioCam MRc	Carl Zeiss AG, Oberkochen
Bag sealer Folio FS 3602	Severin Elektrogeräte GmbH, Sundern
Centrifuge 5424 R	Eppendorf AG, Hamburg
Centrifuge 5702 R	Eppendorf AG, Hamburg
Centrifuge 5810 R	Eppendorf AG, Hamburg
CO ₂ incubator HERAcell®	Heraeus Holding GmbH, Hanau
CO ₂ incubator MCO-5AC 17AI	Sanyo Sales & Marketing Europe GmbH, Munich
Compact shakers KS 15 A	Edmund Bühler GmbH, Bodelshausen
Cryo Storage Vessels BSS-6000	VWR International GmbH, Darmstadt
Dewar carrying flask, type B	KGW-Isotherm, Karlsruhe
EcoVac	schuett-biotec GmbH, Göttingen
EG1130 cooling plate	Leica Microsystems GmbH, Wetzlar
Forma™ 900 Series Upright Ultra-Low Temperature Freezers	Thermo Fisher Scientific, Inc., Waltham, MA, USA
Gel Doc™ XR+ system	Bio-Rad Laboratories GmbH, Munich
Glass ware, Schott Duran®	Schott AG, Mainz
Heated paraffin embedding module EG1150 H	Leica Microsystems GmbH, Wetzlar
Herasafe™ KS (NSF) Class II, Type A2 Biological Safety Cabinets	Thermo Fisher Scientific, Inc., Waltham, MA, USA

Heracell™ 240 incubator	Thermo Fisher Scientific, Inc., Waltham, MA, USA
Homogenizer SilentCrusher M with tool 6F	Heidolph Instruments GmbH & Co. KG, Schwabach
Horizontal shaker	Titertek Instruments, Inc., Huntsville, AL, USA
Incubator B6120	Heraeus Holding GmbH, Hanau
Incubator shaker Thermoshake	C. Gerhardt GmbH & Co. KG, Königswinter
Laboratory balance 2.5kg	KERN & SOHN GmbH, Balingen-Frommern
Magnetic stirrer, Ikamag® RCT	IKA® Werke GmbH & Co. KG, Staufen
Mastercycler™ Nexus Thermal Cycler	Eppendorf AG, Hamburg
Maxwell® 16 Instrument	Promega GmbH, Mannheim
Microplate reader Anthos 2001	Anthos Mikrosysteme GmbH, Krefeld
Microscope Axio Imager A1	Carl Zeiss AG, Oberkochen
Microscope Axiovert 25	Carl Zeiss AG, Oberkochen
Microscope DM LB	Leica Microsystems GmbH, Wetzlar
Microtome Microm HM355	Thermo Fisher Scientific, Inc., Waltham, MA, USA
Microtome Microm HM355S	Thermo Fisher Scientific, Inc., Waltham, MA, USA
Microwave R-631	SHARP business systems Deutschland GMBH, Köln
Mini Centrifuge Spectrafuge C1301-b 230V	Labnet International, Inc., Edison, NJ, USA
Mini Trans-Blot Cell	Bio-Rad Laboratories GmbH, Munich
Mini-PROTEAN® Tetra Cell	Bio-Rad Laboratories GmbH, Munich
MR 2002 Hotplate/Magnetic Stirrer	Heidolph Instruments GmbH & Co. KG, Schwabach
Multipipette® stream	Eppendorf AG, Hamburg

Neubauer hemocytometer, improved	LO-Laboroptik GmbH, Bad Homburg
Owl™ EasyCast™ B2 minigel-electrophoresis	Bio-Rad Laboratories GmbH, Munich
Paraffin tissue floating bath Microm SB80	Thermo Fisher Scientific, Inc., Waltham, MA, USA
pH meter 521	WTW Wissenschaftlich-Technische Werkstätten GmbH, Weilheim
Pipettes Reference®, Research®	Eppendorf AG, Hamburg
Pipetus®	Hirschmann Laborgeräte GmbH & Co. KG, Eberstadt
PowerPac™ Basic Power Supply	Bio-Rad Laboratories GmbH, Munich
Reax top	Heidolph Instruments GmbH & Co. KG, Schwabach
Shaker DRS-12	neoLab Migge GmbH, Heidelberg
Spectrophotometer NanoDrop 1000	Peqlab Biotechnologie GmbH, Erlangen
StepOnePlus™ real time PCR system	Applied Biosystems, Inc., Carlsbad, CA, USA
Stereomicroscope Stemi SV 11	Carl Zeiss AG, Oberkochen
Surgical instruments	Thermo Fisher Scientific, Inc., Waltham, MA, USA
T100™ Thermal Cycler	Bio-Rad Laboratories GmbH, Munich
Thermomixer compact	Eppendorf AG, Hamburg
Tissue processor ASP300	Leica Microsystems GmbH, Wetzlar
Tumbling Table WT 17	Biometra GmbH, Göttingen
Vortex-Genie 2	Scientific Industries Inc., Bohemia, NY, USA
Water bath 1003	GFL Gesellschaft für Labortechnik GmbH, Burgwedel

4.2 Disposables

Table 2: Disposables

Disposable	Source
Cell culture plastics	FALCON® Corning Incorporated, Corning, NY, USA; Sarstedt AG & Co., Nümbrecht; Greiner Bio-One GmbH, Frickenhausen
CHROMAFIL® Color-coded cellulose mixed ester syringe filters A-20/25	MACHEREY-NAGEL GmbH & Co. KG, Düren
Chromatography paper, 3 mm	GE Healthcare Europe GmbH, Munich
CL-Xposure™ Film	Thermo Fisher Scientific, Inc., Waltham, MA, USA
Combitips BioPur®	Eppendorf AG, Hamburg
Conical tubes, 15 mL	TPP Techno Plastic Products AG, Trasadingen, Switzerland
Conical tubes, 50 mL	Sarstedt AG & Co., Nümbrecht
Cover slips	Thermo Fisher Scientific, Inc., Waltham, MA, USA
CryoPure tubes	Sarstedt AG & Co., Nümbrecht
Cuvettes	Greiner Bio-One GmbH, Frickenhausen
Disposable scalpels	Feather Safety Razor Co., Ltd., Osaka, Japan
Pierce™ ECL Western Blotting Substrate	Thermo Fisher Scientific, Inc., Waltham, MA, USA
Amersham ECL™ Prime Western Blotting Detection Reagent	GE Healthcare Europe GmbH, Munich
Filtropur S 0.2	Sarstedt AG & Co., Nümbrecht
Filtropur S 0.45	Sarstedt AG & Co., Nümbrecht
Glass slides Superfrost® Plus	Thermo Fisher Scientific, Inc., Waltham, MA, USA
MicroAmp® optical 96-well reaction plate	Applied Biosystems, Inc., Carlsbad, CA, USA
Microtome blades S35 and C35	Feather Safety Razor Co., Ltd., Osaka, Japan
Pasteur pipettes	Hirschmann Laborgeräte GmbH & Co. KG, Eberstadt

PCR reaction tubes	Brand GmbH + Co. KG, Wertheim; Eppendorf AG, Hamburg
Petri dishes	Sarstedt AG & Co., Nümbrecht
Pipette tips	Sarstedt AG & Co., Nümbrecht
Reaction tubes, 0.5 mL, 1.5 mL and 2 mL	Eppendorf AG, Hamburg
Safe seal pipette tips, professional	Biozym Scientific GmbH, Hessisch Oldenburg
Serological pipettes	Sarstedt AG & Co., Nümbrecht
Single use needles Sterican® 27 gauge	B. Braun Melsungen AG, Melsungen
Single use syringes Omnifix®	B. Braun Melsungen AG, Melsungen
Tissue embedding cassette system	Medite GmbH, Burgdorf

4.3 Reagents and enzymes

Table 3: Reagents and enzymes

Reagent	Source
1,4-Dithiothreitol (DTT)	Carl Roth GmbH + Co. KG, Karlsruhe
2-Log DNA ladder (0.1–10.0 kb)	New England Biolabs GmbH, Frankfurt am Main
2-MercaptoEtOH, 98%	Sigma-Aldrich Chemie GmbH, Munich
2-Propanol (isopropanol)	Carl Roth GmbH + Co. KG, Karlsruhe
Acetic acid 100%	Carl Roth GmbH + Co. KG, Karlsruhe
Ammonium persulfate	Sigma-Aldrich Chemie GmbH, Munich
Ampicillin sodium salt	AppliChem GmbH, Darmstadt
Biozym LE Agarose	Biozym Scientific GmbH, Hessisch Oldenburg
Blotting grade blocker non-fat dry milk	Bio-Rad Laboratories GmbH, Munich
Bovine serum albumin	Carl Roth GmbH + Co. KG, Karlsruhe
Bromphenol blue	Sigma-Aldrich Chemie GmbH, Munich
Calcium chloride dihydrate	Carl Roth GmbH + Co. KG, Karlsruhe
Chloramphenicol	Sigma-Aldrich Chemie GmbH, Munich
Complete, EDTA-free, protease inhibitor cocktail tablets	Roche Deutschland Holding GmbH, Grenzach-Wyhlen

Corn oil, delivery vehicle for fat-soluble compounds	Sigma-Aldrich Chemie GmbH, Munich
disodium phosphate (KCl)	Carl Roth GmbH + Co. KG, Karlsruhe
dNTP mix, 10mM each	Bioline GmbH, Luckenwalde
Dodecylsulfate Na-salt in pellets (SDS)	Serva Electrophoresis GmbH, Heidelberg
Dulbecco's phosphate buffered saline, powder	Biochrom AG, Berlin
EtOH (80%) denatured with Butan-2-on	BrüggemannAlcohol GmbH, Heilbronn
EtOH absolut (100%)	Merck KGaA, Darmstadt
Ethidium bromide	Sigma-Aldrich Chemie GmbH, Munich
Ethylenediaminetetraacetic acid (EDTA)	Invitrogen GmbH, Karlsruhe
Formaldehyde solution 37%	Carl Roth GmbH + Co. KG, Karlsruhe
Gel loading dye, blue	New England Biolabs GmbH, Frankfurt am Main
GeneRuler 1 kb Plus DNA Ladder	Thermo Fisher Scientific, Inc., Waltham, MA, USA
Glycerol Rotipuran®	Carl Roth GmbH + Co. KG, Karlsruhe
Glycin Pufferan®	Carl Roth GmbH + Co. KG, Karlsruhe
GREENTaq® ReadyMix™ PCR reaction mix	Sigma-Aldrich Chemie GmbH, Munich
HEPES	Carl Roth GmbH + Co. KG, Karlsruhe
Hydrogen peroxide 30% Rotipuran®	Carl Roth GmbH + Co. KG, Karlsruhe
Isotonic sodium chloride solution 0,9 %	Fresenius Kabi Deutschland GmbH, Bad Homburg
LB agar (Luria/Miller)	Carl Roth GmbH + Co. KG, Karlsruhe
LB broth (Luria/Miller)	Carl Roth GmbH + Co. KG, Karlsruhe
Magnesium chloride	Carl Roth GmbH + Co. KG, Karlsruhe
MEtOH	Carl Roth GmbH + Co. KG, Karlsruhe
Nonidet® P40	AppliChem GmbH, Darmstadt
Orange G	Carl Roth GmbH + Co. KG, Karlsruhe
Phosphatase inhibitor mix I	Serva Electrophoresis GmbH, Heidelberg
Polyethylene glycol 4000	Merck KGaA, Darmstadt

Ponceau S	Carl Roth GmbH + Co. KG, Karlsruhe
Potassium chloride	Sigma-Aldrich Chemie GmbH, Munich
Precision Plus Protein™ all blue standard	Bio-Rad Laboratories GmbH, Munich
Proteinase K, recombinant, PCR grade	Roche Deutschland Holding GmbH, Grenzach- Wyhlen
QuantiFast® SYBR® green PCR master mix	Qiagen GmbH, Hilden
REDTaq® ReadyMix™ PCR reaction mix	Sigma-Aldrich Chemie GmbH, Munich
Restriction endonucleases	New England Biolabs GmbH, Frankfurt am Main
RNase-free DNase set	Qiagen GmbH, Hilden
RnaseA	Fermentas GmbH, St. Leon-Rot
Rotiphorese® gel 30	Carl Roth GmbH + Co. KG, Karlsruhe
S.O.C. medium	Thermo Fisher Scientific, Inc., Waltham, MA, USA
Sodium acetate buffer solution	Sigma-Aldrich Chemie GmbH, Munich
Sodium chloride (NaCl)	Carl Roth GmbH + Co. KG, Karlsruhe
Sodium hydroxide solution (NaOH)	Carl Roth GmbH + Co. KG, Karlsruhe
SuperScript II	Thermo Fisher Scientific, Inc., Waltham, MA, USA
Tamoxifen	Sigma-Aldrich Chemie GmbH, Munich
TaqMan® reverse transcription reagents	Applied Biosystems, Inc., Carlsbad, CA, USA
TE buffer, pH 8.0	AppliChem GmbH, Darmstadt
TEMED	Carl Roth GmbH + Co. KG, Karlsruhe
Tissue-Tek® O.C.T.™ compound	Sakura Finetek Europe B.V, Alphen aan den Rijn, Netherlands
Tris buffered saline 1X, pH 7.6, Tablets	Th. Geyer GmbH & Co. KG, Renningen
Tris hydrochloride Pufferan®	Carl Roth GmbH + Co. KG, Karlsruhe
Tris Pufferan®	Carl Roth GmbH + Co. KG, Karlsruhe
Triton® X-100	Merck KGaA, Darmstadt
Tween® 20	Sigma-Aldrich Chemie GmbH, Munich

4.4 Antibodies

Table 4: Antibodies

Antibody	Source
Akt (pan) (C67E7), #4691	Cell Signaling Technology, Inc., Danvers, MA, USA
Anti- α -Tubulin, T9026	Sigma-Aldrich Chemie GmbH, Munich
Anti- β -actin, A5316	Sigma-Aldrich Chemie GmbH, Munich
Anti-DMBT1 (C-terminal), SAB2700429	Sigma-Aldrich Chemie GmbH, Munich
Anti-DMBT1, ABN256	Merck KGaA, Darmstadt
Anti-GFP, rabbit IgG fraction	Invitrogen GmbH, Karlsruhe
Anti-GFP, chicken IgY fraction, unconj.	Thermo Fisher Scientific, Inc., Waltham, MA, USA
Anti-Ki-67	BD Biosciences, Franklin Lakes, NJ, USA
DMBT1 (H-130), sc-28239	Santa Cruz Biotechnology, Inc., Dallas, TX, USA
GAPDH (D16H11) XP [®] , #5174	Cell Signaling Technology, Inc., Danvers, MA, USA
GFP Tag Polyclonal Antibody	Thermo Fisher Scientific, Inc., Waltham, MA, USA
Hsp90 α / β (f-8), sc-13119	Santa Cruz Biotechnology, Inc., Dallas, TX, USA
p44/42 MAPK (Erk1/2), #9102	Cell Signaling Technology, Inc., Danvers, MA, USA
Phospho-Akt (Ser473), #9271	Cell Signaling Technology, Inc., Danvers, MA, USA
Phospho-Akt (Ser473) (D9E) XP [®] , #4060	Cell Signaling Technology, Inc., Danvers, MA, USA
Phospho-Akt (Thr308) (C31E5E), #2965	Cell Signaling Technology, Inc., Danvers, MA, USA
Phospho-p44/42 MAPK (Erk1/2) (Thr202/Tyr204) (D13.14.4E) XPC, #4370	Cell Signaling Technology, Inc., Danvers, MA, USA
Rab11 (D4F5) XP [®] , #5589	Cell Signaling Technology, Inc., Danvers, MA, USA

4.5 Molecular biology

All buffers were prepared with bi-distilled H₂O.

Table 5: Buffers and solutions for molecular biology

Buffer	Component
HBS 2x (HEPES buffered saline)	273 mM NaCl 10 mM KCL 1.4 mM Na ₂ HPO ₄
TENSV lysis buffer, pH 7.9	50 mM HEPES 150 mM NaCl 1 mM EDTA 0.5% Nonidet P40 10% Glycerol Protease inhibitor (added prior to use)
Running buffer	25 mM Tris 192 mM Glycine 0.1% SDS
Transfer buffer, pH 8.3	25 mM Tris 192 mM Glycine 20% MetOH
5x Protein loading buffer (Laemmli), pH 6.8	10% SDS 50% Glycerol 228 mM Tris hydrochloride 0.75 mM Bromphenol blue 5% 2-MercaptoEtOH
6x Loading buffer orange G	60% Glycerol 60 mM EDTA 0.24% Orange G
50x Tris acetate EDTA (TAE) buffer, pH 8.5	2 M Tris 50 mM EDTA 5.71% Acetic acid

Table 6: Kits for molecular biology

Kit	Source
Maxwell® 16 LEV simplyRNA Purification Kit	Promega GmbH, Mannheim
NucleoBond® Xtra Maxi	MACHEREY-NAGEL GmbH & Co. KG, Düren
Pierce™ BCA Protein Assay Kit	Thermo Fisher Scientific, Inc., Waltham, MA, USA
QIAquick Gel Extraction Kit	Qiagen GmbH, Hilden
Zyppy™ Plasmid Midiprep Kit	Zymo Research Europe GmbH, Freiburg
Zyppy™ Plasmid Miniprep Kit	Zymo Research Europe GmbH, Freiburg

Table 7: Bacterial strains

Bacterial strain	Source
One Shot® Stbl3™ chemically competent <i>E. coli</i>	Invitrogen GmbH, Karlsruhe

Table 8: Plasmids

Plasmid	Source
pLKO.1 puro (#8453)	Addgene, Cambridge, MA, USA
pLKO.1 puro shScrambled	gift from Roland Rad, Munich
pTC ApoE-Tet	[98]

Table 9: shRNA sequences

Target	Name	Sequence	Source
Dmbt1	Dmbt1_1	CCGGCCTGGGAATTATCCTAA TAATCTCGAGATTATTAGGAT AATTCCCAGGTTTTTG	Mission TRC 1.0/TRC 1.5 mouse shRNA library, gift from A. Sweet-Cordero, Stanford, CA, USA
Dmbt1	Dmbt1_2	CCGGCCCTTCAAACCTATCCAAA CAACTCGAGTTGTTTGGATAG TTTGAAGGGTTTTTG	Mission TRC 1.0/TRC 1.5 mouse shRNA library, gift from A. Sweet-Cordero, Stanford, CA, USA
Dmbt1	Dmbt1_3	CCGGCCCTTCAAACCTATCCTAA CAACTCGAGTTGTTAGGATAG TTTGAAGGGTTTTTG	Mission TRC 1.0/TRC 1.5 mouse shRNA library, gift from A. Sweet-Cordero, Stanford, CA, USA

Dmbt1	Dmbt1_4	CCGGCGTTCCTGATTATACACC AATCTCGAGATTGGTGTATAA TCAGGAACGTTTTTG	Mission TRC 1.0/TRC 1.5 mouse shRNA library, gift from A. Sweet- Cordero, Stanford, CA, USA
Tspan8	Tspan8_1	GTACCGGGGAACTGACTGTGC AACTTATCTCGAGATAAGTTG CACAGTCAGTTCCTTTTTTG	Mission TRC 1.0/TRC 1.5 mouse shRNA library, gift from A. Sweet- Cordero, Stanford, CA, USA
Tspan8	Tspan8_2	GTACCGGTGATCTTGGGACTG GCCATATCTCGAGATATGGCC AGTCCCAAGATCATTTTTTG	Mission TRC 1.0/TRC 1.5 mouse shRNA library, gift from A. Sweet- Cordero, Stanford, CA, USA
Tspan8	Tspan8_3	GTACCGGTTCTGAATGAAACG CTATATGCTCGAGCATATAGC GTTTCATTCAGAATTTTTTG	Mission TRC 1.0/TRC 1.5 mouse shRNA library, gift from A. Sweet- Cordero, Stanford, CA, USA
S100a6	S100a6_1	CCGGCACAAGTACTCTGGCAA GGAACTCGAGTTCCTTGCCAG AGTACTTGTGTTTTTG	Mission TRC 1.0/TRC 1.5 mouse shRNA library, gift from A. Sweet- Cordero, Stanford, CA, USA
S100a6	S100a6_2	CCGGTGATGGATGATCTGGAC CGTACTCGAGTACGGTCCAGA TCATCCATCATTTTTTG	Mission TRC 1.0/TRC 1.5 mouse shRNA library, gift from A. Sweet- Cordero, Stanford, CA, USA
S100a6	S100a6_3	CCGGCGTAACAAGGATCAGG AAGTACTCGAGTACTTCCTGAT CCTTGTTACGTTTTTG	Mission TRC 1.0/TRC 1.5 mouse shRNA library, gift from A. Sweet- Cordero, Stanford, CA, USA
Cdkn2a	Cdkn2a_1	CCGGGTGATGATGATGGGCA ACGTTCTCGAGAACGTTGCC ATCATCATCACTTTTTTG	Mission TRC 1.0/TRC 1.5 mouse shRNA library, gift from A. Sweet- Cordero, Stanford, CA, USA
Cdkn2a	Cdkn2a_2	CCGGCATCAAGACATCGTGCG ATATCTCGAGATATCGCACGA TGTCTTGATGTTTTTG	Mission TRC 1.0/TRC 1.5 mouse shRNA library, gift from A. Sweet- Cordero, Stanford, CA, USA
Cdkn2a	Cdkn2a_3	CCGGGCTCGGCTGGATGTGCG CGATCTCGAGATCGCGACAT CCAGCCGAGCTTTTTTG	Mission TRC 1.0/TRC 1.5 mouse shRNA library, gift from A. Sweet- Cordero, Stanford, CA, USA

Sox4	Sox4_1	CCGGTGAAGCGCGTCTACCTG TTTGCTCGAGCAAACAGGTAG ACGCGCTTCATTTTTG	Mission TRC 1.0/TRC 1.5 mouse shRNA library, gift from A. Sweet- Cordero, Stanford, CA, USA
Sox4	Sox4_2	CCGGCTGGAGTCCAGCATCTC TAACCTCGAGGTTAGAGATGC TGGACTCCAGTTTTTG	Mission TRC 1.0/TRC 1.5 mouse shRNA library, gift from A. Sweet- Cordero, Stanford, CA, USA
Sox4	Sox4_3	GTACCGGTAAAGACCGAAGG AATCTTTCCTCGAGGAAAGAT TCCTTCGGTCTTATTTTTG	Mission TRC 1.0/TRC 1.5 mouse shRNA library, gift from A. Sweet- Cordero, Stanford, CA, USA
Lgals2	Lgals2_1	CCGGCTTCCAAGATAAAGACT TCAACTCGAGTTGAAGTCTTTA TCTTGGAAAGTTTTTG	Mission TRC 1.0/TRC 1.5 mouse shRNA library, gift from A. Sweet- Cordero, Stanford, CA, USA
Lgals2	Lgals2_2	CCGGCCTGAACATGAAACCAG GGATCTCGAGATCCCTGGTTT CATGTTCAAGTTTTTG	Mission TRC 1.0/TRC 1.5 mouse shRNA library, gift from A. Sweet- Cordero, Stanford, CA, USA
Lgals2	Lgals2_3	CCGGGTCCCTGAAGATTAAG GCAACTCGAGTTGCCTTTAATC TTCAGGGACTTTTTG	Mission TRC 1.0/TRC 1.5 mouse shRNA library, gift from A. Sweet- Cordero, Stanford, CA, USA
Gkn2	Gkn2_1	CCGGCCATCAACTGGCTTCATC TTTCTCGAGAAAGATGAAGCC AGTTGATGGTTTTTTG	Mission TRC 1.0/TRC 1.5 mouse shRNA library, gift from A. Sweet- Cordero, Stanford, CA, USA
Gkn2	Gkn2_2	CCGGGAGAGCCTGTTACGTCA TCAACTCGAGTTGATGACGTA ACAGGCTCTTTTTTTG	Mission TRC 1.0/TRC 1.5 mouse shRNA library, gift from A. Sweet- Cordero, Stanford, CA, USA
Gkn2	Gkn2_3	CCGGGTCATCAAGATGGACCA CAAACCTCGAGTTTGTGGTCCA TCTTGATGACTTTTTTTG	Mission TRC 1.0/TRC 1.5 mouse shRNA library, gift from A. Sweet- Cordero, Stanford, CA, USA
Gkn2	Gkn2_4	CCGGCAAACCTCCAACGGTTCC TCTACTCGAGTAGAGGAACCG TTGGAGTTTGTTTTTTG	Mission TRC 1.0/TRC 1.5 mouse shRNA library, gift from A. Sweet- Cordero, Stanford, CA, USA

Gkn2	Gkn2_5	CCGGCTACGAGAAGCAGACA ATGAACTCGAGTTCATTGTCTG CTTCTCGTAGTTTTTTG	Mission TRC 1.0/TRC 1.5 mouse shRNA library, gift from A. Sweet- Cordero, Stanford, CA, USA
Cd24a	Cd24a_1	CCGGTGTTGCACCGTTTCCCG GTA ACTCGAGTTACCGGGAAA CGGTGCAACATTTTTG	Mission TRC 1.0/TRC 1.5 mouse shRNA library, gift from A. Sweet- Cordero, Stanford, CA, USA
Cd24a	Cd24a_2	CCGGTAGAGACTCAGGCCAG GAAACCTCGAGGTTTCCTGGC CTGAGTCTCTATTTTTG	Mission TRC 1.0/TRC 1.5 mouse shRNA library, gift from A. Sweet- Cordero, Stanford, CA, USA
Cd24a	Cd24a_3	CCGGCTCTTCTACATCTCTACT GTTCTCGAGAACAGTAGAGAT GTAGAAGAGTTTTTG	Mission TRC 1.0/TRC 1.5 mouse shRNA library, gift from A. Sweet- Cordero, Stanford, CA, USA
S100a4	S100a4_1	CCGGCCAGAAGGTGATGAGC AACTTCTCGAGAAGTTGCTCAT CACCTTCTGGTTTTT	Mission TRC 1.0/TRC 1.5 mouse shRNA library, gift from A. Sweet- Cordero, Stanford, CA, USA
S100a4	S100a4_2	CCGGGATGAGCAACTTGGACA GCAACTCGAGTTGCTGTCCAA GTTGCTCATCTTTTT	Mission TRC 1.0/TRC 1.5 mouse shRNA library, gift from A. Sweet- Cordero, Stanford, CA, USA
S100a4	S100a4_3	CCGGTGTGTCCACCTTCCACAA ATACTCGAGTATTTGTGGAAG GTGGACACATTTTT	Mission TRC 1.0/TRC 1.5 mouse shRNA library, gift from A. Sweet- Cordero, Stanford, CA, USA
S100a4	S100a4_4	CCGGCATGATGTGCAATGAAT TCTTCTCGAGAAGAATTCATTG CACATCATGTTTTT	Mission TRC 1.0/TRC 1.5 mouse shRNA library, gift from A. Sweet- Cordero, Stanford, CA, USA
S100a4	S100a4_5	CCGGCAGGGACAATGAAGTT GACTTCTCGAGAAGTCAACTT CATTGTCCCTGTTTTT	Mission TRC 1.0/TRC 1.5 mouse shRNA library, gift from A. Sweet- Cordero, Stanford, CA, USA
Cdh17	Cdh17_1	CCGGGCAGGATATGTCAAGAT CAA ACTCGAGTTTGATCTTGAC ATATCCTGCTTTTTG	Mission TRC 1.0/TRC 1.5 mouse shRNA library, gift from A. Sweet- Cordero, Stanford, CA, USA

Cdh17	Cdh17_2	CCGGCGGGAGAGACAGATGG TATATCTCGAGATATACCATCT GTCTCTCCCGTTTTTG	Mission TRC 1.0/TRC 1.5 mouse shRNA library, gift from A. Sweet- Cordero, Stanford, CA, USA
Cdh17	Cdh17_3	CCGGGCTAACAACATCAACAG TATTCTCGAGAATACTGTTGAT GTTGTTAGCTTTTTG	Mission TRC 1.0/TRC 1.5 mouse shRNA library, gift from A. Sweet- Cordero, Stanford, CA, USA
Tmsb10	Tmsb10_1	CCGGGATAAGGCCAAGCTGA AGAAACTCGAGTTTCTTCAGCT TGGCCTTATCTTTTTG	Mission TRC 1.0/TRC 1.5 mouse shRNA library, gift from A. Sweet- Cordero, Stanford, CA, USA
Tmsb10	Tmsb10_2	CCGGCTTCGATAAGGCCAAGC TGAACTCGAGTTCAGCTTGGC CTTATCGAAGTTTTTG	Mission TRC 1.0/TRC 1.5 mouse shRNA library, gift from A. Sweet- Cordero, Stanford, CA, USA
Tmsb10	Tmsb10_3	CCGGCGCCAGCTTCGATAAGG CCAACTCGAGTTGGCCTTATC GAAGCTGGCGTTTTTG	Mission TRC 1.0/TRC 1.5 mouse shRNA library, gift from A. Sweet- Cordero, Stanford, CA, USA
Tmsb10	Tmsb10_4	CCGGCCTGCCGACCAAAGAGA CCATCTCGAGATGGTCTCTTTG GTCGGCAGGTTTTTG	Mission TRC 1.0/TRC 1.5 mouse shRNA library, gift from A. Sweet- Cordero, Stanford, CA, USA
Cd44	Cd44_1	CCGGCCTCCCACTATGACACAT ATTCTCGAGAATATGTGCATA GTGGGAGGTTTTTG	Mission TRC 1.0/TRC 1.5 mouse shRNA library, gift from A. Sweet- Cordero, Stanford, CA, USA
Cd44	Cd44_2	CCGGCGACCCAATCTCACATC CAATCTCGAGATTGGATGTGA GATTGGGTCGTTTTTG	Mission TRC 1.0/TRC 1.5 mouse shRNA library, gift from A. Sweet- Cordero, Stanford, CA, USA
Cd44	Cd44_3	CCGGCCGAATTAGCTGGACAC TCAACTCGAGTTGAGTGTCCA GCTAATTCGGTTTTTG	Mission TRC 1.0/TRC 1.5 mouse shRNA library, gift from A. Sweet- Cordero, Stanford, CA, USA
Cd44	Cd44_4	CCGGGGACCGTTACCATAAC TATTCTCGAGAATAGTTATGGT AACCGTCTTTTTTG	Mission TRC 1.0/TRC 1.5 mouse shRNA library, gift from A. Sweet- Cordero, Stanford, CA, USA

Crisp1	Crisp1_1	CCGGCCCACCAAGAAAGTATA GATTCTCGAGAATCTATACTTT CTTGGTGGGTTTTTG	Mission TRC 1.0/TRC 1.5 mouse shRNA library, gift from A. Sweet- Cordero, Stanford, CA, USA
Crisp1	Crisp1_2	CCGGGTGGACATGAAGATAA GTATACTCGAGTATACTTATCT TCATGTCCACTTTTTG	Mission TRC 1.0/TRC 1.5 mouse shRNA library, gift from A. Sweet- Cordero, Stanford, CA, USA
Crisp1	Crisp1_3	CCGGCCTGATAGTGTGGTCGG ACATCTCGAGATGTCCGACCA CACTATCAGGTTTTTG	Mission TRC 1.0/TRC 1.5 mouse shRNA library, gift from A. Sweet- Cordero, Stanford, CA, USA
Crisp1	Crisp1_4	CCGGGATAGTGTGGTCGGACA TTATCTCGAGATAATGTCCGAC CACACTATCTTTTTG	Mission TRC 1.0/TRC 1.5 mouse shRNA library, gift from A. Sweet- Cordero, Stanford, CA, USA
Hmga2	Hmga2_1	CCGGCGGGAAATCTACACAGC CAAACCTCGAGTTTGGCTGTGT AGATTTCCCGTTTTTG	Mission TRC 1.0/TRC 1.5 mouse shRNA library, gift from A. Sweet- Cordero, Stanford, CA, USA
Hmga2	Hmga2_2	CCGGGCCACAACAAGTCGTTC AGAACTCGAGTTCTGAACGAC TTGTTGTGGCTTTTTG	Mission TRC 1.0/TRC 1.5 mouse shRNA library, gift from A. Sweet- Cordero, Stanford, CA, USA
Hmga2	Hmga2_3	CCGGCCCTCTCCTAAGAGACC CAGACTCGAGTCTGGGTCTCT TAGGAGAGGGTTTTTG	Mission TRC 1.0/TRC 1.5 mouse shRNA library, gift from A. Sweet- Cordero, Stanford, CA, USA
Hmga2	Hmga2_4	CCGGAGACCTAGGAAATGGCC ACAACCTCGAGTTGTGGCCATT TCCTAGGTCTTTTTTG	Mission TRC 1.0/TRC 1.5 mouse shRNA library, gift from A. Sweet- Cordero, Stanford, CA, USA
Hmga2	Hmga2_5	CCGGACTGAAGAGACATCCTC GCAACTCGAGTTGCGAGGATG TCTCTTCAGTTTTTTG	Mission TRC 1.0/TRC 1.5 mouse shRNA library, gift from A. Sweet- Cordero, Stanford, CA, USA
Reg3b	Reg3b_1	CCGGCTTGTCAAGAGCTTCTG GATTCTCGAGAATCCAGAAGC TCTTGACAAGTTTTTTG	Mission TRC 1.0/TRC 1.5 mouse shRNA library, gift from A. Sweet- Cordero, Stanford, CA, USA

Reg3b	Reg3b_2	CCGGCTGAAGAATATACCCTC CGCACTCGAGTGC GGAGGGT ATATTCTTCAGTTTTTTG	Mission TRC 1.0/TRC 1.5 mouse shRNA library, gift from A. Sweet- Cordero, Stanford, CA, USA
Foxg1	Foxg1_1	CCGGGCACTTTGAGTTACAAC GGGACTCGAGTCCCGTTGTAA CTCAAAGTGCTTTTTG	Mission TRC 1.0/TRC 1.5 mouse shRNA library, gift from A. Sweet- Cordero, Stanford, CA, USA
Foxg1	Foxg1_2	CCGGGTCTTCTCCAACCCTTT AATCTCGAGATTAAAGGGTTG GAAGAAGACTTTTTG	Mission TRC 1.0/TRC 1.5 mouse shRNA library, gift from A. Sweet- Cordero, Stanford, CA, USA
Foxg1	Foxg1_3	CCGGTCCAACCCTTTAATACA TTACTCGAGTAATGTATTTAA GGGTTGGAATTTTTG	Mission TRC 1.0/TRC 1.5 mouse shRNA library, gift from A. Sweet- Cordero, Stanford, CA, USA

4.5.1 Primers

Oligonucleotides were synthesized by Eurofins MWG GmbH (Ebersberg) and diluted in H₂O to a concentration of 10 μ M.

Table 10: PCR genotyping primers

PCR name	Primer name	Sequence (5' -> 3')
CreER	Cre347	CCTGGAAATGCTTCTGTCCG
	Cre349	CAGGGTGTTATAAGCAATCCC
	Cre Int forward	CAATGGTAGGCTCACTCTGG
	Cre Int reverse	AACACACACTGGCAGGACTG
<i>R26R</i> ^{LSL-YFP}	R26 common forward	AAAGTCGCTCTGAGTTGTTAT
	R26 WT reverse	GGAGCGGGAGAAATGGATATG
	R26-Tva-SA-mut-LP reverse	GCGAAGAGTTTGTCTCAACC
<i>Pdk1</i> ^{lox}	Pdk1 floxed forward	ATCCAAGTTACTGAGTTGTGTTGGAAG
	Pdk1 floxed reverse	TGTGGACAAACAGCAATGAACATACACGC
<i>LSL-Kras</i> ^{G12D}	LSL-Kras common forward	CACCAGCTTCGGCTTCCTATT
	LSL-Kras WT reverse	AGCTAATGGCTCTCAAAGGAATGTA
	LSL-Kras mut reverse	CCATGGCTTGAGTAAGTCTGC
<i>p53</i> ^{lox}	P53 Δ forward	CACAAAACAGGTTAAACCCAG

	P53Δ reverse	GAAGACAGAAAAGGGGAGGG
	P53lox reverse	AGCACATAGGAGGCAGAGAC
<i>Rb^{lox}</i>	RB lox/Δ forward	CTCTAGATCCTCTCATTCTTCCC
	RB lox reverse	GCAGGAGGCAAAAATCCACATAAC

Table 11: Primers for quantitative real time PCR

Gene	Primer name	Sequence (5' -> 3')	Origin
<i>Afp</i>	Afp forward	GTTCTGGCATGCTGCAAA	Mus musculus
	Afp reverse	CCTTTGCAATGGATGCTCTC	
<i>Alb</i>	Alb forward	TGACCCAGTGTGTGCAGAG	Mus musculus
	Alb reverse	TTCTCCTTCACACCATCAAGC	
<i>Gapdh</i>	Gapdh forward	TGCACCACCAACTG	Mus musculus
	Gapdh reverse	CCTGCTTCACCACCTTCTT	
<i>Dmbt1</i>	Dmbt1 forward	AATAGCCCATGGACTGAAGG	Mus musculus
	Dmbt1 reverse	CCGACTTTGACAATAACACCAC	
<i>Krt19</i> (CK19)	Krt19 forward	TGACTGGAGATGATGCAGATTG	Mus musculus
	Krt19 reverse	CCTCAGGGCAGTAATTCCTC	
<i>Lgals2</i>	Lgals2 forward	AGGCAAGATCCACAATGATGTGG	Mus musculus
	Lgals2 reverse	CCACCTTCACTGGTGTACAGAC	
<i>Reg3b</i>	Reg3b forward	TGGCTCCTACTGCTATGCCTTG	Mus musculus
	Reg3b reverse	CGCTATTGAGCACAGATACGAGG	

4.6 Cell culture

Table 12: Cell culture media and their components

Medium	Components
Cancer cell medium	DMEM 10% FCS 1% Penicillin/Streptomycin
Cancer cell medium	RPMI 10% FCS 1% Penicillin/Streptomycin

Freezing medium	DMEM 10% FCS 1% Penicillin/Streptomycin 10% DMSO
-----------------	---

Table 13: Reagents and kits for cell culture

Reagent / Kit	Source
Dimethylsulfoxide (DMSO)	Sigma-Aldrich Chemie GmbH, Munich
Dulbecco's modified Eagle medium (DMEM)	Invitrogen GmbH, Karlsruhe
Dulbecco's phosphate buffered saline (PBS)	Invitrogen GmbH, Karlsruhe
Fetal calf serum (FCS)	Biochrom AG, Berlin
MTT reagent	Sigma-Aldrich Chemie GmbH, Munich
Penicillin (10000 units/mL) / Streptomycin (10000 µg/mL) solution	Invitrogen GmbH, Karlsruhe
Puromycin dihydrochloride	Sigma-Aldrich Chemie GmbH, Munich
Roswell Park Memorial Institute medium (RPMI)	Invitrogen GmbH, Karlsruhe
0.25% Trypsin-EDTA (1x), phenol red	Invitrogen GmbH, Karlsruhe

4.7 Histology

Table 14: Reagents and kits for histological analysis

Reagent / Kit	Source
Acetic acid (glacial)	Merck KGaA, Darmstadt
Antigen unmasking solution, citric acid based	Vector Laboratories, Inc., Burlingame, CA, USA
Avidin/biotin blocking kit	Vector Laboratories, Inc., Burlingame, CA, USA
DAB peroxidase substrate kit, 3,3'-diaminobenzidine	Vector Laboratories, Inc., Burlingame, CA, USA
Donkey serum D9663	Sigma-Aldrich Chemie GmbH, Munich
Eosine	Waldeck GmbH & Co KG, Münster
Goat serum G9023	Sigma-Aldrich Chemie GmbH, Munich
Hematoxylin	Merck KGaA, Darmstadt

Hydrogen peroxide 30%	Merck KGaA, Darmstadt
Pertex mounting medium	Medite GmbH, Burgdorf
Rabbit serum R9133	Sigma-Aldrich Chemie GmbH, Munich
Roti® Histofix 4%	Carl Roth GmbH + Co. KG, Karlsruhe
Roti® Histol	Carl Roth GmbH + Co. KG, Karlsruhe
Sucrose (saccharose)	Merck KGaA, Darmstadt
Vectashield® mounting medium with DAPI	Vector Laboratories, Inc., Burlingame, CA, USA
Vectastain® elite ABC kit	Vector Laboratories, Inc., Burlingame, CA, USA

Table 15: Secondary antibodies for histological analysis

Antibody	Source
AlexaFluor® 488 goat anti-rabbit IgG	Thermo Fisher Scientific, Inc., Waltham, MA, USA
AlexaFluor® 555 goat anti-mouse IgG	Invitrogen GmbH, Karlsruhe
AlexaFluor® 555 goat anti-rabbit IgG	Thermo Fisher Scientific, Inc., Waltham, MA, USA
Biotinylated anti-goat IgG (H+L)	Vector Laboratories, Inc., Burlingame, CA, USA
Biotinylated anti-mouse IgG (H+L)	Vector Laboratories, Inc., Burlingame, CA, USA
Biotinylated anti-rabbit IgG (H+L)	Vector Laboratories, Inc., Burlingame, CA, USA
Biotinylated anti-rat IgG (H+L)	Vector Laboratories, Inc., Burlingame, CA, USA

4.8 Software

Table 16: Software

Software	Source
AxioVision 4.8	Carl Zeiss AG, Oberkochen
GraphPad Prism 5	La Jolla, CA, USA
ImageJ	Wayne Rasband, Public Domain
MATLAB	The MathWorks, Natick, MA, USA
MS Office	Microsoft Corporation, Redmont, WA, USA
Quantity One	Bio-Rad Laboratories GmbH, Munich
StepOne™ v2.3	Applied Biosystems, Inc., Carlsbad, CA, USA

5 Methods

5.1 Mouse experiments

All animal experiments were carried out in accordance with the German Animal Welfare Act (TierSchG) and in compliance with the protocols and withdrawal criteria set out in the animal test application. The approval for the execution of these tests by the local authority “Regierung von Oberbayern”. All mice in this study were bred in a mixed background.

5.1.1 Mouse strains

All mouse models used in this study were based on the conditional Cre/loxP system. The creation of conditional alleles is achieved by specific targeting of genes flanked by *loxP* or with interspaced *loxP-stop-loxP* (LSL) sites. Liver specific targeting was ensured by expression of inducible Cre recombinase under the control of a liver or cell type-specific promoter (Fig. 5) to conditionally inactivate genes or delete LSL cassettes to activate specific gene expression. Activation of an inducible Cre/loxP system where the Cre recombinase is fused to the tamoxifen-responsive estrogen receptor (CreER) enables the initiation of primary liver cancer in adult mice. All mice in this study were obtained by crossbreeding the different strains and are listed in Table 17. *Rosa26^{LSL-YFP/+}* was used as a recombination marker. TAM concentrations used for the specific mouse strains are listed at 5.1.3 “Tamoxifen treatment of mice” in Table 18.

Table 17: Mouse strains

Genetic background	Liver specific recombination by	Target cells
<i>RPK;Rosa26^{LSL-YFP/+}</i>	HTVI Transposon + 3x TAM i.p.	hepatocytes
<i>RPK;Rosa26^{LSL-YFP/+};Alb^{CreER/+}</i>	1x TAM i.p.	hepatocytes
<i>RPK;Rosa26^{LSL-YFP/+};Sox9-CreER</i>	1x TAM i.p.	cholangiocytes
<i>RPK;Rosa26^{LSL-YFP/+};Hnf1β-CreER</i>	1x TAM i.p.	cholangiocytes
<i>RPK;Rosa26^{LSL-YFP/+};Pdk1^{lox/lox}</i>	HTVI Transposon + 3x TAM i.p.	hepatocytes
<i>RPK;Rosa26^{LSL-YFP/+};Pdk1^{lox/lox};Alb^{CreER}</i>	1x TAM i.p.	hepatocytes

5.1.2 Genotyping

About 3 weeks after the mice were born, they were numbered with an assigned ear punch and a 3 mm tail biopsy was taken for genotyping with a sterile scalpel. The wound was disinfected and the bleeding stopped. The DNA from those tail biopsies was extracted as described in 5.4.1 “Isolation of genomic DNA”.

5.1.3 Tamoxifen treatment of mice

The amount of TAM is different per mouse line and is listed in Table 18. In general, the specific amount of TAM was dissolved in 40 µl 100% EtOH and incubated at 55°C for around 10 min till TAM was completely solved. Corn oil was added to a total amount of 1 ml solution and incubated for another 10 min at 55°C to make sure there are no unsolved TAM residues left. 100 µl per mouse were injected intraperitoneal in the lower left quadrant of the abdomen once for mice carrying a *CreER* recombinase allele or on 3 consecutive days after HTVI (Table 18).

Table 18: TAM concentration per strain

mouse strain	TAM concentration per mouse
<i>RPK;Rosa26^{LSL-YFP/+} + CreER</i> transposon	1 mg TAM (each day for 3 days)
<i>RPK;Alb^{CreER/+};Rosa26^{LSL-YFP/+}</i>	100 ng TAM once
<i>RPK;Sox9-CreER;Rosa26^{LSL-YFP/+}</i>	1 mg TAM once
<i>RPK;Hnf1β-CreER;Rosa26^{LSL-YFP/+}</i>	1 mg TAM once
<i>RPK;Alb^{CreER/+};Pdk1^{lox/lox};Rosa26^{LSL-YFP}</i>	100 ng TAM once

5.1.4 Hydrodynamic tail vein injection

RPK mice at the age of 8 - 12 weeks were injected by either a transposon construct containing an ApoE-TBG-CreER only (pTA-Cre) or a construct that also contained a doxycycline-inducible shRNA (pTC ApoE-Tet). For this purpose, 20 µg pTA-Cre or 30 µg for pTC ApoE-Tet (containing shRNA) and 2 µg pc-HSB5 were dissolved in 2 mL of isotonic 0.9% saline solution per mouse [98, 123]. The animals were placed in a restrainer for intravenous injection and then the tail was warmed for 30-60 seconds under red light to dilate the veins under constant control of

the animals. After disinfecting and cleaning the injection site with 70% EtOH, 2 ml of the injection solution was injected within 5-10s.

5.1.5 Doxycycline treatment of mice

Mice injected by HTVI with a CreER construct containing an inducible shRNA (*shDmbt1* or control *shScrambled*) were fed with DOXY chow (625 mg per kg Doxycycline hyclate diet; daily Doxycycline 1.6 - 2.7 mg in 3-5 g diet) from the day on of the first TAM injection till the day of dissection of the mouse.

5.1.6 Mouse dissection and fixation of organs

Before tissue and organ harvesting, the mice were anesthetized with isoflurane and euthanized by cervical dislocation. Mice were fixed, disinfected with 70% EtOH and the abdomen was opened by a longitudinal incision. For retrograde perfusion of the liver, phosphate buffered saline (used if frozen tissue was obtained) or 4% phosphate buffered formaldehyde solution (for paraffin embedding only) was injected in the inferior vena cava. The vena portae was transected and finally the liver was completely irrigated. Liver, lung, intestine, tumors, and metastasis samples were fixed for 2 nights in 4% Roti® Histofix to be processed to histological analysis. In addition, micro dissected tumors and metastases were snap-frozen in liquid nitrogen.

5.2 Histological analysis

5.2.1 Paraffin sections

After fixation the samples were stored in 70% EtOH till dehydration in the tissue processing unit ASP300 overnight and finally embedded in paraffin. The paraffin block was cut for stainings with the microtome Microm HM355S in sections of 2-2.5 µm thickness.

5.2.2 Hematoxylin and eosin (H&E) staining of tissue sections

For H&E staining, paraffin-embedded tissue sections were processed as described below.

2 x 5 min	Roti® Histol
2 x 5 min	99% EtOH

2 x 5 min	96% EtOH
2 x 5 min	80% EtOH
10 sec	Distilled water
2 sec	Hematoxylin
5 – 10 min	Tap water
20 sec	Eosin 0.33%
10 sec	Distilled water
2 x 5 min	80% EtOH
2 x 5 min	96% EtOH
2 x 5 min	99% EtOH
2 x 5 min	Roti® Histol

After the staining slides were enclosed with Pertex and a coverslip.

5.2.3 Immunohistochemistry (IHC)

Paraffin-embedded tissue sections were processed as described below for dewaxing and rehydration.

2 x 5 min	Roti® Histol
2 x 5 min	99% EtOH
2 x 5 min	96% EtOH
2 x 5 min	80% EtOH
10 sec	Distilled water

Unmasking solution was prepared by dilution of 9.4 ml of unmasking stock solution in 1000 ml distilled water and the sections were boiled in a microwave 3 min at 300 W and then 16 min at 150 W. After cooling, the sections were removed from the solution, remaining unmasking solution was aspirated, the tissue fields were edged with the ImmEdge pen and the sections wetted with PBS-T. Thereafter, the sections were washed 3 times with PBS-T for 5 minutes each. Blocking of the endogene peroxidase activity was done by 10 min treatment in the dark with 3% H₂O₂ solution. Again, they were washed 3 times with PBS-T for 5 minutes each, before the blocking solution containing 5% serum blocking solution was applied for 1 h at RT. After

another washing step 3 times with PBS-T for 5 minutes each, 100 µl of the diluent solution containing the antibody or without the diluent solution as a negative control were incubated at initial 30 min at 37°C then over night at 4°C. The following day the sections were washed 3 times with PBS-T for 5 minutes each and the sections were incubated with the second antibody for 1 h at RT. The sections were washed as described before and ABC reagent was applied for 30 min at RT. After a washing step, 100 µl of DAB solution was applied. The duration of DAB solution treatment was individually assessed by microscopic control of the slides. Counterstain was performed as follows.

2 sec	Hematoxylin
5 – 10 min	Tap water
20 sec	Eosin
10 sec	Distilled water
2 x 5 min	80% EtOH
2 x 5 min	96% EtOH
2 x 5 min	99% EtOH
2 x 5 min	Roti® Histol

After staining, slides were enclosed with Pertex and a coverslip.

5.2.4 Immunofluorescence (IF)

Tissue sections were dewaxed and rehydrated as described in 5.2.3. Sections were removed from the distilled water, excess water aspirated, the tissue wells bordered with the ImmEdge pen, and the sections wetted with PBS-T. After a washing step 3 times with PBS-T for 5 minutes each, sections were blocked by 5% serum blocking solution for 30-60 min. Subsequently, 75 µl of the blocking solution with the first antibody was added to the positive control. The sections were incubated with the first antibody at 37°C for 30 min and then overnight at 4°C. The next day, sections were washed 3 times with PBS-T for 5 minutes each. Then 75 µl of the blocking solution with the second antibody were applied to all positive and negative controls. The sections were incubated for 45-60 min with the secondary antibody at RT. Thereafter, they were washed 3 times with PBS-T for 20 min each. Covering was done with fluoroshield and coverslips.

5.2.5 Analysis of stainings

Documentation and analysis of H&E and IHC stainings have been done by using the microscope Axio Imager. A1 with AxioCam HRc and software AxioVision 4. Documentation, quantification and analysis of IF stainings has been carried out with the Zeiss Axiovert 200M. For quantification of Ki67-positive cells images in 200x magnification and of five to ten visual fields were used. Ki67-positive cells were counted by ImageJ. The statistical evaluation was made with a two-tailed Student T-Test, and the result was considered statistically significant at $p < 0.05$. Charts display the mean; error bars the standard deviation.

5.3 Cell Culture

RPK cancer cells established from tumor mice, TKO2.1 liver cancer cells derived from *Rb^{lox/lox};p130^{lox/lox};p107^{-/-}* mice and human A549, HCT-116, HepG2, HeLa, SNU449, CaCo-2 cells were maintained in DMEM supplemented with 10% FCS and 1% penicillin/streptomycin cancer cell medium. TKO1.1 cancer cells derived from *Rb^{lox/lox};p130^{lox/lox};p107^{-/-}* mice [2] were cultivated in RPMI supplemented with 10% FCS and 1% penicillin/streptomycin. All cell lines were incubated at 37°C, 5% CO₂ and 100% humidity.

5.3.1 Cryopreservation of cell lines

For cryopreservation, trypsinized cells were diluted in cancer cell medium and centrifuged at 1000 rpm for 5 min. The pellet was resuspended in cold freezing medium and transferred to CryoPure tubes. The samples were frozen at -80°C for 24 h and for long time storage stored in liquid nitrogen until further use.

5.3.2 Transfection of RPK cells lines with shRNA constructs

HEK293T cells were seeded in 10 cm² dishes at a density that results in a confluence of 60 - 70% the next day in DMEM supplemented with 10% FCS and 1% penicillin/streptomycin. When the plate reached the desired confluency the media was changed by fresh pre-warmed DMEM cancer cell media. Transfection mix was prepared as listed in Table 19.

Table 19: Transfection mix

transfection ingredients	amount for 1 plate of 10 cm ²
pLKO.1 vector	8 µg
PAX vector	4 µg
PMD vector	4 µg
CaCl ₂	50 µl
distilled H ₂ O	adjusted to 500 µl

After the preparation of a 500 µl transfection mix, the mix was slowly and as carefully as possible pipetted into 2x HBS. The HBS/transfection mix then was incubated for 20 min at RT. The formed complex was added dropwise to the HEK293T cells and left in the incubator overnight at 37°C. The day after the transfection, the medium was changed and *RPK* cell lines were seeded to result in 70 – 80% confluence at the time of infection. The following day, the supernatant containing the desired lentivirus was taken off HEK293T cells, centrifuged for 7 min at 2000 rpm and added without any cell debris to the *RPK* cells plated the day before. Fresh media was added to HEK293T cells immediately after collection of the supernatant. 12 h later the supernatant was collected again, centrifuged as described above, and added to *RPK* cells after removal of the old infection medium. This step was repeated a third time the next day, after that HEK293T cells were discarded. 12 h later, the infection medium of *RPK* cells was replaced with fresh growth medium to let the cells recover overnight. The following day, DMEM medium containing the selection marker puromycin was applied. The amount of puromycin needed differed in each *RPK* cell line and was tested before.

5.3.3 MTT assay

3-(4,5-dimethyl-2-thiazolyl)-2,5-diphenyl-tetrazolium bromide (MTT) is a yellow reagent that is reduced by mitochondria of living cells to insoluble purple colored formazan. The optical density (OD) value of the purple stain reveals the content of living cells in solution after treatment. The relative amount of the cell viability compared to the control can be measured and the impact of the treatment on the cell viability, respectively. Between 500 and 15000 cells were seeded in 10 ml of DMEM or RPMI supplemented with 10% FCS and 1% penicillin/streptomycin. The right number of cells for seeding was tested individually before, based on the division rate of each cell line. Cell number was determined by a Neubauer

hemacytometer. The cells were seeded in 96-well plates. One day after seeding, cells were treated with GDC0941 (PI3K) and PD0325901 (MEK) inhibitors in 100 μ L DMEM or RPMI media. In the case of shRNA transfected cell lines, DMEM media was changed, no further treatment by inhibitors was undertaken. The cells were left in the incubator 37°C, 5% CO₂ and 100% humidity for 3 more days. MTT was added to a final concentration of 0.5 mg/mL MTT reagent in the medium (10 μ L MTT in 100 μ L medium). The cells were put in the incubator for 4 h at 37°C. The media was removed and 200 μ L EtOH/DMSO mix (1:1, v/v) was added to each well to solve formazan. The plate then was shaken for 10 min at RT and the OD was measured at 595 nm. The MTT assay was carried out on 5 consecutive days to quantify the cell proliferation.

5.3.4 Clonogenic assay

2000 cells/well were seeded on a 6-well plate. Cell number was determined by a Neubauer hemacytometer. It was assured to get a single cell suspension. The next day treatment by GDC0941 (PI3K) and PD0325901 (MEK) inhibitors was performed. In the case of transfected RPK cell lines by shRNA no further treatment was done, only fresh medium was applied to all cells. Cells were put in an incubator at 37°C for 10 days after seeding. On the day of fixation every well was washed 3 times with PBS and stained for 20 – 30 minutes with crystal violet solution. The solution was removed, and the wells washed with H₂O till excessive crystal violet was removed. The plate was scanned and analyzed using ImageJ.

5.4 Molecular biology

5.4.1 Isolation of genomic DNA

For genotyping PCRs, 30 – 50 μ L of tail lysis solution containing 0.7 – 0.9 μ L proteinase K was added to the tail biopsy of mice. Lysis was performed in a thermocycler at 55 °C overnight. Proteinase K was heat inactivated for 50 min at 85°C. Samples were vortexed and the DNA-containing supernatant was separated from the debris by centrifugation at 15000 rpm and 4°C for 10 min. The DNA solution was used immediately or was stored at 4°C for short or at -20°C for long time storage.

5.4.2 Polymerase chain reaction

Polymerase chain reaction (PCR) is a standard technique to amplify desired DNA segments by specific primers. For genotyping we used 2 different Taq polymerases. Which Taq polymerase is best suited for which primer has been tested. REDTaq® and GREENTaq® were used. The composition of the respective PCR mixes is shown in Table 20, volumes are listed for one reaction. Isolated DNA from mouse tails as described in 5.4.1 “Isolation of genomic DNA” were used for genotyping. For each allele, specific primers were designed (Table 10). Annealing temperatures and time, Taq and PCR products are shown in the Tables 21 and 22.

Table 20: Composition of PCR.

	GREENTaq®	REDTaq®
Polymerase mix	10 µl	10 µl
Primer Mix	1 µl	1 µl
distilled H ₂ O	8 µl	8 µl
DNA	1 µl	1 µl

Table 21: Conditions for standard PCR.

temperature	time	cycle repetition
94°C	5 min	1x
94°C	1 min	40x
Annealing temperature (see Table 22)		
72°C	1 min	
72°C	7 min	1x
4°C	∞	hold

Table 22: Annealing temperatures and PCR products.

gene	annealing temperature	annealing time per cycle	PCR products (bp) mut = mutant allele; WT = wild type allele.	Taq
<i>Pdk1</i>	63°C	1:00 min	280 (mut) / 200 (WT)	red Taq

<i>Kras</i> ^{G12D}	55°C	0:45 min	170 (mut) / 270 (WT)	red Taq
<i>Rb</i>	56°C	0:45 min	260 (mut) / 308 (WT)	red Taq
<i>p53</i>	56°C	0:45 min	350 (mut) / 450 (WT)	red Taq
<i>Rosa26</i> ^{LSL-YFP}	60°C	0:45 min	250 (mut) / 500 (WT)	green Taq
<i>Alb</i> ^{CreER} , <i>Sox9-CreER</i> , <i>Hnf1β-CreER</i>	60°C	0:30 min	400 (mut) / 300 (WT)	red Taq

5.4.3 Separation of DNA by agarose gel electrophoresis

PCR products were applied to a 2% agarose gel and separated by electrophoresis. The agarose powder was mixed with 150 ml of 1x TAE buffer and dissolved by boiling in the microwave at max W for 3 min. The liquid agarose then was stirred for 20 min at RT. 5 -7 µl of Ethidium bromide solution was added and the gel was poured on a tray. After the gel became firm. DNA samples were pipetted into the gel pockets and separated at 100 – 120 V. The nucleic acid bands were visualized by UV light.

5.4.4 RNA isolation and cDNA synthesis

Cells were cultured on 10 cm² dishes till they reached a confluency of 70 – 90%. Cells were trypsinized and centrifuged for 5 min at 2000 rpm at 4°C. The pellet was resuspended in PBS and centrifuged for 10 min at 15000 rpm at 4°C. The supernatant was aspirated and the pellet was frozen for at least 24 h at -80°C. RNA extraction was carried out by using the Maxwell 16 LEV simply RNA Cells Kit (Promega) according to manufacturer's protocol. RNA concentration was measured with the spectrophotometer NanoDrop 2000 and samples were stored at -80°C or directly used for cDNA synthesis. cDNA synthesis was performed using SuperScript II Reverse Transcriptase following the manufacturer's instructions. Generally, 1 µg of RNA were used for generation of cDNA, which was stored at -20°C.

5.4.5 Quantitative real time PCR

Quantitative real time PCR (qPCR) was performed with the StepOnePlus™ real time PCR system, the QuantiFast® SYBR® green PCR master mix as fluorescent DNA binding dye. Target mRNA expression was normalized to ubiquitously expressed endogenous housekeeping gene

GAPDH and quantified by the $2^{-\Delta\Delta C_t}$ method ($2^{\Delta C_t(\text{GAPDH}) - \Delta C_t(\text{target gene})}$) by StepOne™ software and Excel. qPCR primers are listed in Table 11. To exclude unwanted primer dimerization, a melt curve was performed after the run.

5.5 Protein biochemistry

5.5.1 Protein extraction

Cells were harvested when they reached about 80–90% confluency, trypsinized, and centrifuged for 5 min at 2000 rpm at 4°C, then washed once by PBS and centrifuged again. The pellet was resuspended in PBS and centrifuged for 10 min at 15000 rpm at 4°C. The supernatant was aspirated, and the pellet was frozen for at least 24 h at -80°C. 500 µl of TENS buffer including complied protease inhibitor was put to the pellet, then put on ice for 20 min. The solution was vortexed every 5 min, till the pellet was dissolved. After the 20 min, the samples were centrifuged for 10 – 20 min at 15000 rpm at 4°C. Supernatant was transferred in a new tube and was instantly used or stored at -80°C.

5.5.2 Protein concentration estimation

Protein concentration was measured by the Pierce™ BCA Protein Assay Kit according to manufacturer's protocol. A defined BSA standard curve is used to determine the protein concentration of the samples. Samples usually had to be diluted 1:10. After incubation of the BCA working reagents for 1 h at 37°C or 2 h at RT, samples were measured by Multiskan™ FC microtiter plate – photometer at 562 nm. Each sample was measured in triplicates. Protein concentrations were adjusted by Laemmli buffer with 2-mercaptoethanol and TENS buffer including complied protease inhibitor. Protein samples with Laemmli were denatured at 95°C for 5 min before use and stored at -20°C.

5.5.3 SDS polyacrylamide gel electrophoresis (SDS-PAGE)

The percentage of gels was decided based on the size of the protein of interest and varied between 7.5 and 12.5%. The composition of the gels used is listed in Table 23. After pouring the running gel between the glass plates, the gel was covered by 1 mL 2-propanol to ensure an equal distribution of the gel and to get an even surface. After polymerization and removing of 2-propanol, the stacking gel was poured on the running gel und polymerized. 30 µL protein

solution containing 60 µg of the protein were loaded onto the gel. Initially the protein samples were run at 90 V till crossing the stacking gel and then separated at 130 V.

Table 23: Composition of running and stacking gel

Running gel			
end concentration of Acrylamide	7.5%	10%	12.5%
30% Acrylamide	2.5 ml	3.3 ml	4.3 ml
TRIS (pH8.8, 1.5M)	2.5 ml	2.5 ml	2.5 ml
10% SDS	100 µl	100 µl	100 µl
TEMED	10 µl	10 µl	10 µl
10% APS	50 µl	50 µl	50 µl
distilled H ₂ O	4.84 ml	4.0 ml	3.0 ml

Stacking gel	
30% Acrylamide	1.6 ml
TRIS (pH6.8, 1M)	1.3 ml
10% SDS	100 µl
TEMED	5 µl
10% APS	75 µl
distilled H ₂ O	6.9 ml

5.5.4 Immunoblot

Before transfer of the separated SDS-PAGE onto a PVDF membrane, the membrane was activated in 100% methanol. Transfer was carried out in a blotting tank either immediately (100 V, 4°C, 2 h) or overnight (30 V, 4°C, 16 h). After that unspecific binding was blocked by 5% milk at RT for 30 – 60 min on the membrane, the membrane was washed 3 times with TBS-T for 10 min each, and the primary antibody was put on the membrane and incubated overnight at 4°C. The membrane was washed again 3 times with TBS-T for 15 - 20 min each and the secondary antibody in a concentration of 1:5000 was applied. All secondary antibodies were diluted in 5% milk and the membrane incubated for 1 h at RT. Thereafter, membranes were washed again 3 times with TBS-T for 15 - 20 min each. Hrp-conjugated secondary

antibodies were detected on CL-XPosure™ Film by Pierce™ ECL Western Blotting Substrate or ECL prime for low-abundance proteins. Developed autoradiography films were digitalized with a flatbed scanner and analyzed with ImageJ. Rab11, α -tubulin, HSP90 and β -actin served as loading control and for normalization of protein expression.

5.6 Statistical analysis

Graphical depiction, data correlation and statistical analysis were executed with GraphPad Prism 5. If not indicated otherwise, data were obtained from at least three independent experiments and expressed as mean values \pm standard deviation (SD). Cell culture-based assays were generally performed in triplicates. To calculate statistical differences between certain data sets, normality and variance were analyzed and a two-tailed Student's t test was employed. For survival analysis, Kaplan-Meier estimator was used. Log rank test was done for statistical analysis of survival curves. $p < 0.05$ was considered to be statistically significant.

6 Results

6.1 Novel mouse model for the development of primary liver cancer

In order to mimic the molecular changes that occur in human hepatocarcinogenesis, we genetically targeted three pathways that are commonly altered in human primary liver cancer. The RB and p53 pathways function as well-known tumor suppressors and are closely associated with promotion of human HCC [50]. Oncogenic Ras signaling is activated in liver tumors either by mutation of the *RAS* genes (*KRAS/NRAS*, more common in ICC) or by activation of the Ras signaling cascade through other molecular mechanisms such as activation of receptor tyrosine kinase EGFR signaling upstream of Ras, which is more common in HCC [124]. To achieve hepatic deletion of *Rb* and *p53* genes together with expression of oncogenic *Kras*, we injected adult *Rb^{lox/lox};p53^{lox/lox};Kras/IsI-Kras^{G12D}* (*RPK*) mice intravenously with a liver-specific adeno-associated virus (AAV2/8-TBG-Cre, AAV-Cre) to express Cre recombinase in hepatocytes, which leads to a rapid formation of large liver tumors with characteristics of HCC and ICC (Fig. 6A + B). By histomorphology, hepatic tumor lesions resembled poorly-differentiated human hepatocellular carcinoma (Fig. 6A) or were composed of biliary structures resembling cholangiocarcinoma. Additionally, a number of tumors contained both hepatocellular and biliary structures – indicating for mixed hepatic/biliary differentiation. Of note, some tumors were highly pleomorphic with small sarcomatoid cells and few poorly differentiated hepatocytes and cholangiocytes. These lesions were classified as undifferentiated tumors. The second system used was the *RPK* Transposon-CreER system, with a CreER under the control of a liver specific TBG promotor that was injected hydrodynamic tail vein injection. Both alternative models contained a *Rosa26^{LSL-YFP}* reporter gene to verify cell type-specific Cre expression in targeted cells by visualizing reporter gene expression and therefore targeting efficiency. In the transposon model, mice were injected intraperitoneally with TAM 2 weeks after tail vein injection to activate Cre-mediated recombination. Mice were sacrificed after 4 weeks or were aged until their health deteriorated due to tumor development. Adult *RPK;Alb^{CreER};Rosa26^{LSL-YFP}* were injected once with TAM, and analyzed 4 weeks after TAM injection or aged till tumor development. While tumors in both models developed within few months, *RPK* Transposon-CreER mice have a lower targeting of hepatocytes compared to *RPK;Alb^{CreER}*, which might explain the higher variability of time to tumor development after TAM injection possibly depending on the targeting efficiency.

Median survival was not significantly different between those three groups (Fig. 6C). Although *RPK* Transposon-*CreER* have a lower targeting efficiency than *RPK Alb^{CreER}*, the median survival shows no significant difference between the groups. After 1 to up to 5 months, large solid liver tumors were observed with all 3 treatments with comparable histomorphology (data not shown).

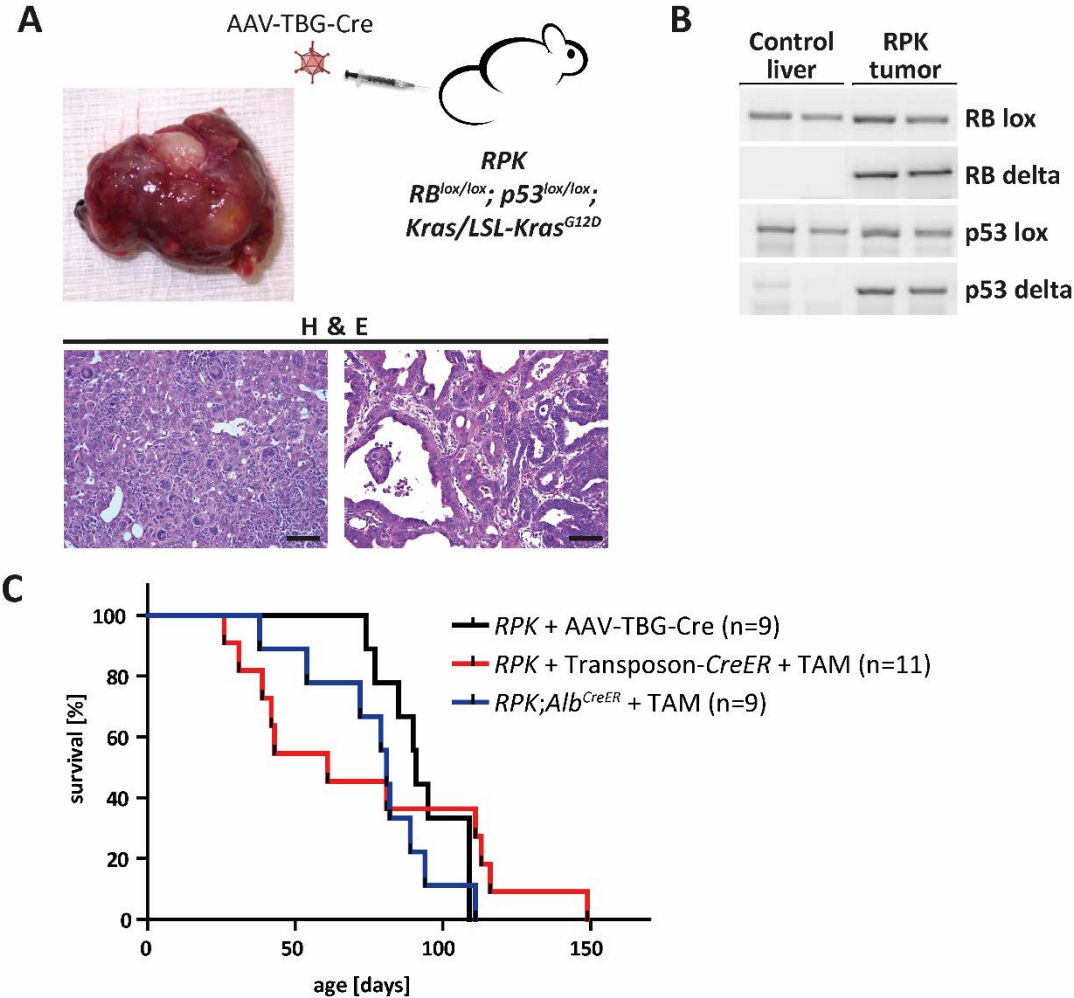


Figure 6: Liver tumor development in *RPK* mice
 (A) Liver-specific gene mutation by tail vein injection of AAV-TBG-Cre into *RPK* mice and macroscopic appearance of liver tumors in *RPK* mice (top). Liver tumors in *RPK* mice show characteristics of hepatic and biliary differentiation by histomorphology (bottom). Scale bars equal 100 μ m.
 (B) PCR analysis of non-recombined $p53^{lox}$ and Rb^{lox} and recombined $p53^{delta}$ and Rb^{delta} DNA from the liver of *RPK* control mice not injected with AAV-TBG-Cre compared to Cre-induced liver tumors in *RPK* mice.
 (C) Kaplan-Meier survival analysis of indicated genotypes and treatments in male *RPK* mice. Survival between groups was not significantly different.

6.2 Liver tumors in RPK mice show characteristics of hepatocyte and biliary differentiation

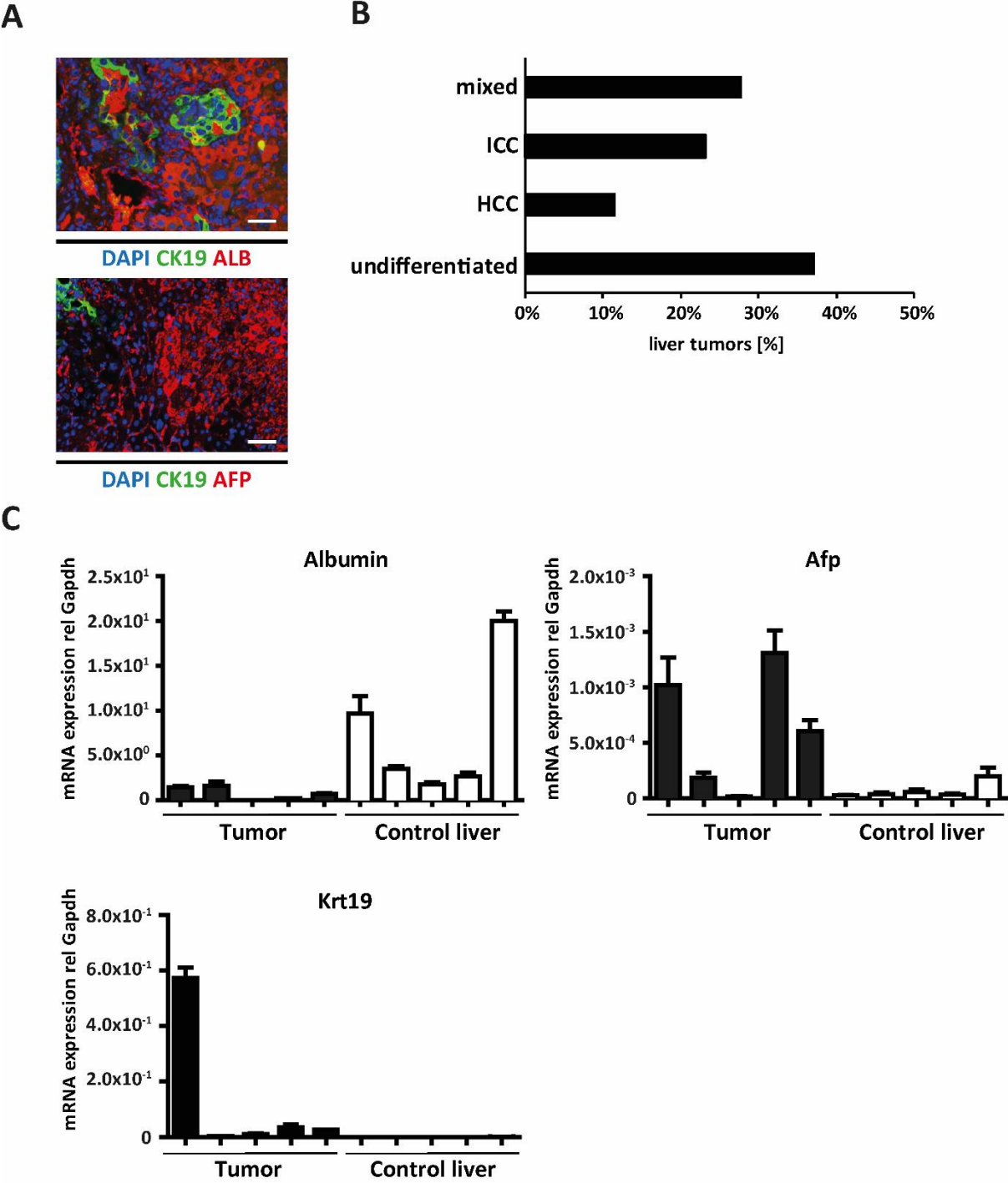


Figure 7: Liver tumors in *RPK* mice show characteristics of mixed hepatocyte and biliary differentiation
 (A) Immunostaining for biliary (CK19) and hepatocyte (ALB and AFP) differentiation markers in *RPK* tumors. Scale bars equal 100 μ m.
 (B) Analysis of differentiation of liver tumors in *RPK* mice after AAV-TBG-Cre injection by histomorphology and immunostaining (43 tumors, 11 mice).
 (C) mRNA analysis for expression of *Krt19* (CK19), *Afp*, and *Alb* in tumor samples in comparison to control liver.

As histomorphology suggested the tumors in RPK mice contain cells with characteristics of hepatocytes and cholangiocytes, we analyzed tumor tissue for expression of alpha-fetoprotein (AFP). Expression of *Afp*, an early differentiation marker of developing hepatocytes that is nearly undetectable in the adult liver, was elevated in tumor samples (Fig. 7C). Additionally, areas that were characterized by biliary histomorphology stained positive for the bile duct differentiation marker CK19, which correlated with elevated *Krt19* (*CK19*) RNA levels in whole tumor lysates (Fig. 7A and C). Quantification and classification of tumors according to histopathology and immunohistochemical markers revealed a relatively high percentage of tumors with ICC and mixed HCC-ICC differentiation (Fig. 7B). In summary, the analysis of liver tumors derived from RPK AAV-TBG-Cre treated mice showed a variable expression of hepatocyte and bile duct markers on the mRNA level and by immunostaining. Interestingly, the individual tumor cells displayed either biliary or hepatocyte specific markers – indicating that they were still committed to one of the two differentiation lineages.

6.3 Tumors in RPK mice develop from hepatocytes

In primary liver cancer, several hepatic cell types have been discussed as tumor initiating cells, including hepatocytes, liver progenitor cells, and bile duct cells. Recent studies in animal models of liver cancer indicate that hepatocellular carcinoma and as well as intrahepatic cholangiocarcinoma both arise primarily from hepatocytes, while liver progenitor cells or oval cells do not seem to play a relevant role in the development of HCCs [30]. It is not completely clear if ICCs can directly arise from hepatocytes or if an activation of biliary signaling pathways is required for cholangiocyte differentiation necessary, for example via induction of notch signaling in genetic models [125]. The occurrence of cells with characteristics of hepatocytes and cholangiocytes within the same tumor in the RPK model suggests that the tumors in this model arise from the same cell of origin in the liver. To identify the cell of origin of hepatic tumors in the RPK mouse model, we used the RPK;*Alb*^{CreER} and RPK transposon model to specifically target hepatocytes. One of the systems was generated by crossing mice harboring a *CreER* driven by the Albumin promotor (*Alb*^{CreER}) with RPK mice to target hepatocytes [126]. Specific targeting of putative liver progenitor and bile duct cells was achieved by breeding RPK mice with mice containing either a *Hnf1β*-*CreER* or a *Sox9*-*CreER*, respectively [105]. Mice were injected with TAM 8 weeks of age 1 time (Fig. 8C). In all hepatocyte-specific Cre models we could observe hepatic tumors comparable to the AAV-TBG-Cre model.

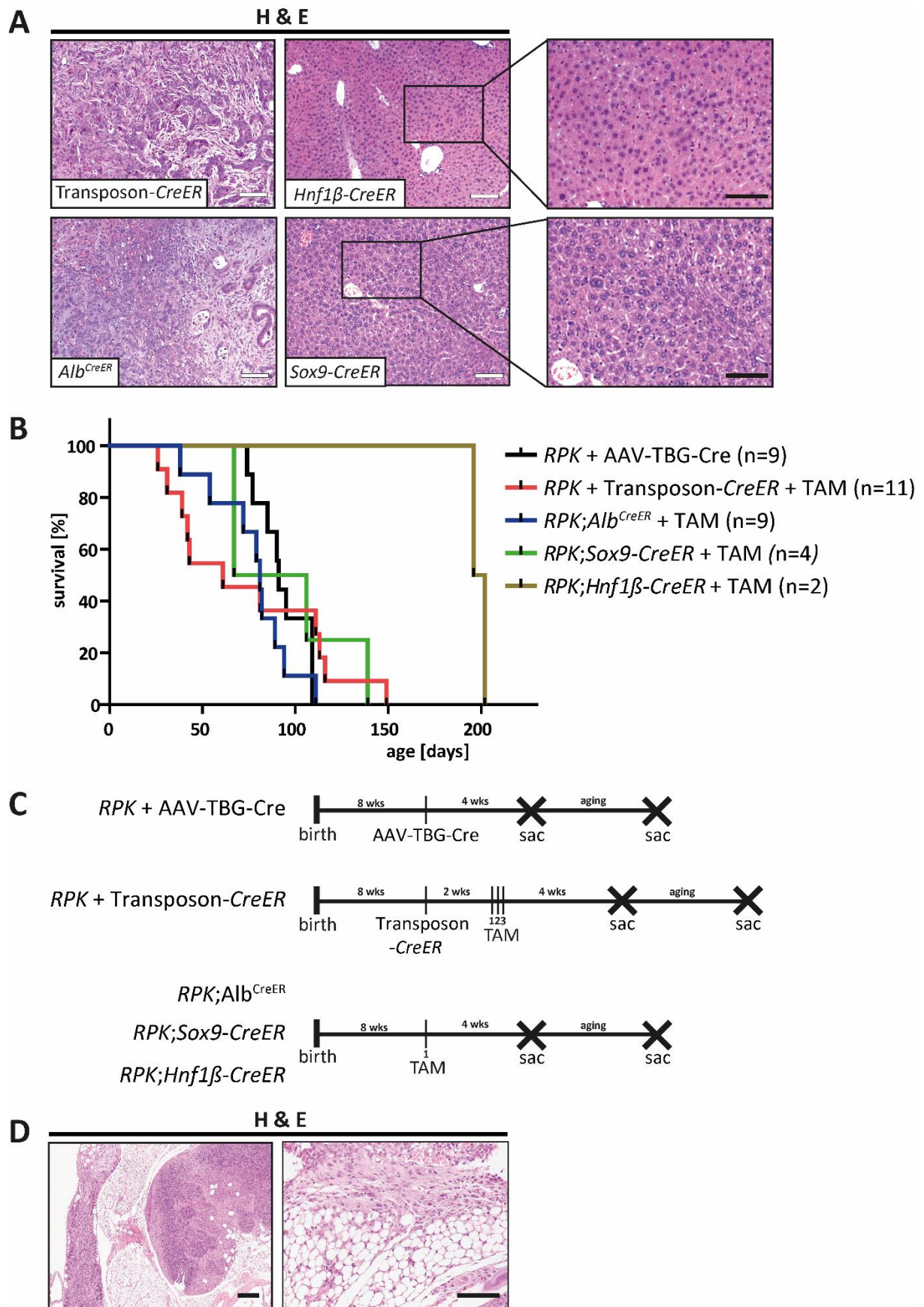


Figure 8: Tumors in *RPK* mice develop from hepatocytes
 (A) Tumor development after hepatocyte specific (left) or bile duct/oval cell specific (right) targeting after *CreER*-transposon + TAM in male *RPK* mice or TAM treatment in male *RPK*; *Alb*^{*CreER*} mice. Scale bars equal 200 μ m.

(B) Kaplan-Meier survival analysis of indicated genotypes and treatments. Early death in male *RPK;Sox9-CreER* mice was due to multiple lung tumors without any histological liver lesions at the time of death.

(C) Scheme illustrating induction of Cre-recombinase expression in adult 8-week old RPK mice by either AAV-TBG-Cre, Transposon-*CreER* + 3 times TAM on 3 consecutive days, or Alb^{CreER}, *Sox9-CreER*, *Hnf1β-CreER* + 1-time TAM treatment. Mice were sacrificed at 4 weeks after TAM or AAV-TBG-Cre injection or were aged till a termination criterion of the animal protection act appeared.

(D) Lung tumors in male *RPK;Sox9-CreER* mice. Scale bars equal 200 μm.

Histological analysis of liver tumors in these mice showed continued proliferation of dysmorphic tumor cells as well as nuclear and cellular pleomorphism. In contrast at the point of sacrifice, *RPK;Hnf1β-CreER* mice were in a healthy and unremarkable condition and showed no overt pathology of the liver (Fig. 8A). In *Sox9-CreER* animals we detected primary lung tumors (Fig. 8D), that shortened the life span of the animals independent of their liver pathology (Fig. 8B). In conclusion, lineage tracing by hepatocyte-specific targeting in RPK tumors showed that hepatocytes present the cell of origin in RPK liver tumors with hepatocyte, cholangiocyte and mixed HCC/ICC differentiation. In contrast, bile duct and liver progenitor cell specific targeting by Sox9- and Hnf1β-driven *CreER* did not rise to primary liver cancer. Importantly, the targeting of two important tumor suppressor pathway as well as activation of oncogenic Kras did not result in any tumor formation in the liver or even an expansion of the targeted cell population.

6.4 Microarray and KEGG pathway analysis

Our findings from lineage specific Cre models show that transformed livers cells in *RPK* mice give rise to hepatic tumors of mixed differentiation. To test if these liver tumors represented a good model of human liver cancer as suggested by histopathology, we performed microarray analysis on macro-dissected tumor tissue and control livers. Comparison of our expression data with publicly available data sets from human patients [25, 127] revealed clustering of *RPK* tumors with a subset of undifferentiated HCC, as well as ICC and liver tumors of mixed differentiation (data not shown). To gain insight into the mechanisms that drive hepatocarcinogenesis in our model, we then analyzed differently expressed genes in *RPK* tumors *versus* control livers. Strikingly, genes that were significantly up-regulated in our model showed strong enrichment for a multitude of different pathways associated with carcinogenesis in the liver and other tissues, such as MAPK, Wnt, TGF-β and p53 signaling pathways (Fig. 9A). MAPK signaling, which is one of the major downstream effectors of Ras signaling, was among the top enriched oncogenic pathways in *RPK* tumors. The

Ras/Raf/MEK/ERK and PI3K/AKT signaling pathways are the cell's major mechanisms for controlling cell survival, differentiation, proliferation, metabolism, and motility (Fig. 9C).

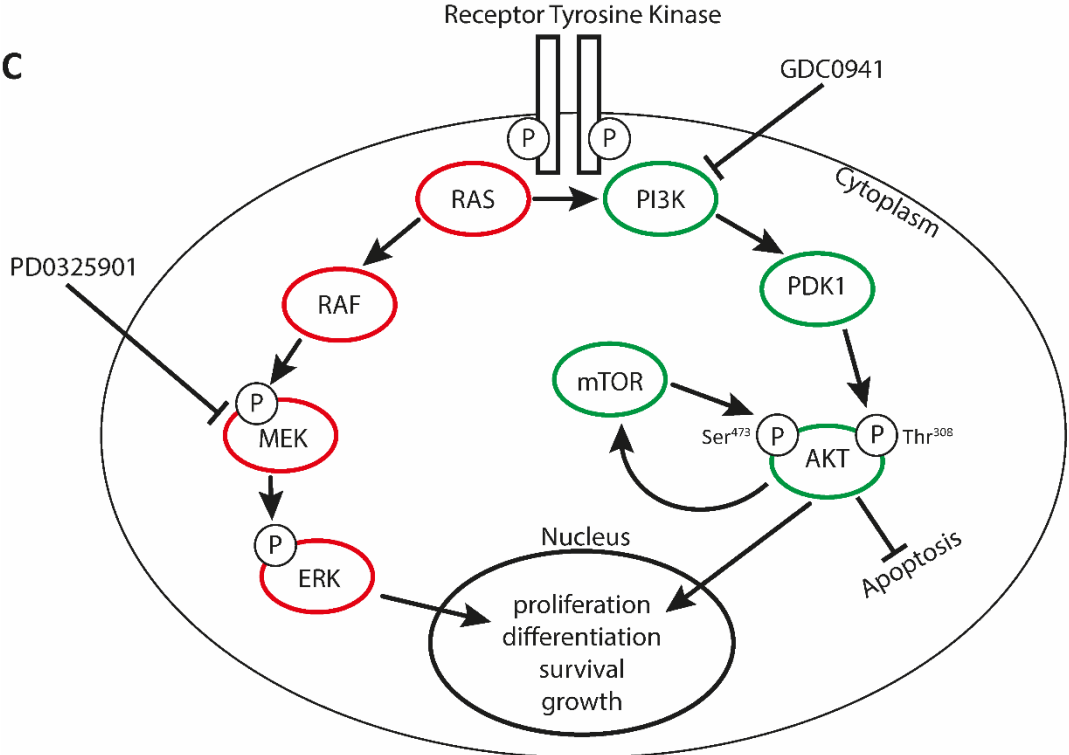
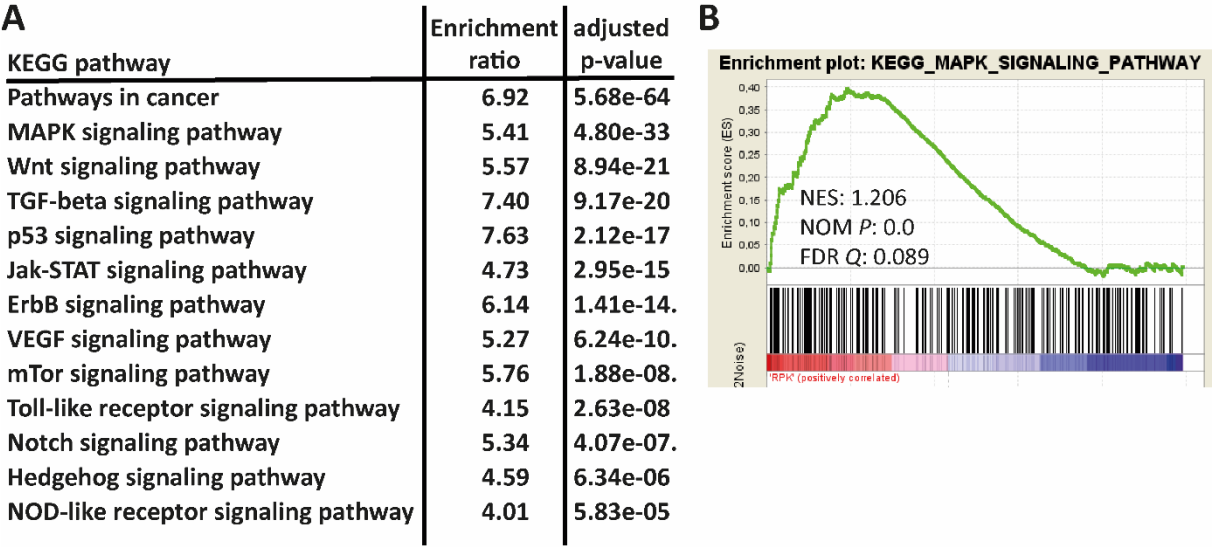
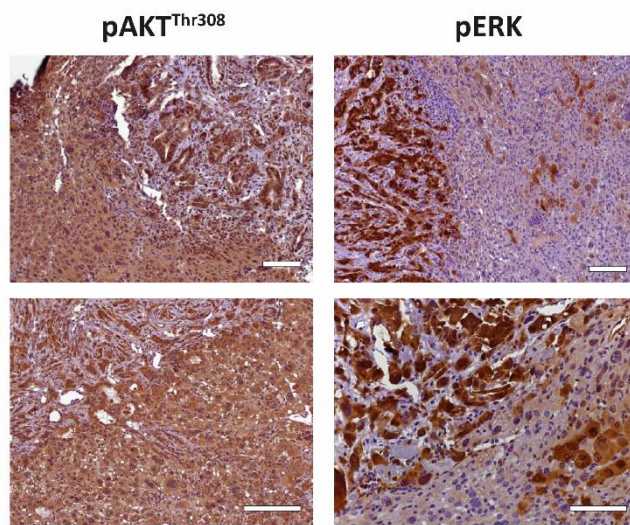


Figure 9: Microarray and KEGG pathway analysis
 (A) Microarray analysis shows differently enriched KEGG pathways among genes significantly up-regulated in RPK tumors in comparison to control livers.
 (B) Gene-set enrichment analysis against the KEGG database for the MAPK signaling pathways of RPK tumors in comparison to control livers.
 (C) Signaling pathway of the MEK/ERK and PI3K/AKT/mTOR pathways, including the inhibitors GDC0941 (PI3K/AKT/mTOR) and PD0325901 (MEK/ERK).

6.5 Activation of ERK and PI3K-dependent AKT activation in RPK liver tumors *in vivo*

A



B

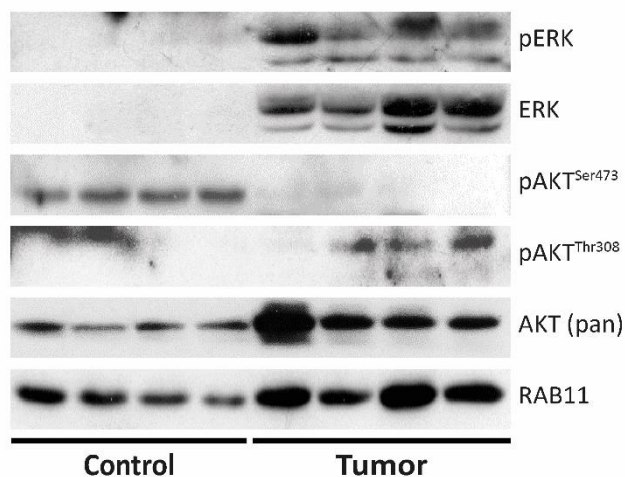


Figure 10: Activation of ERK and PI3K-dependent AKT activation in *RPK* liver tumors *in vivo*

(A) IHC stainings of pAKT^{Thr308} (left) and pERK (right) of tumors from *RPK* mice. Scale bars equal 200 μ m.

(B) Immunoblot analysis of activated AKT and ERK proteins in protein lysates of tumors of *RPK* mice comparison to livers from control mice. Rab11 was used as loading control.

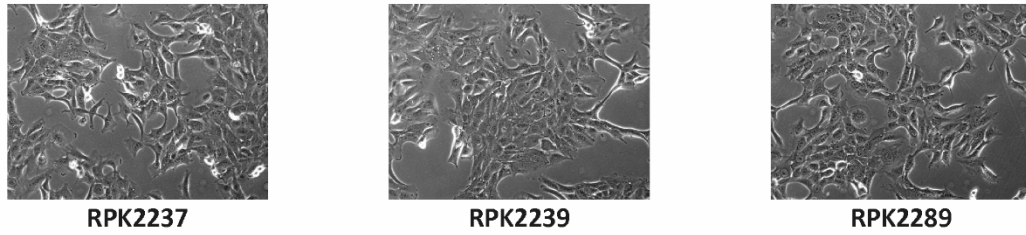
The tumor development in the RPK model is dependent of the activation of oncogenic KRAS, hepatic tumors show an activation Ras-dependent signaling pathways like MEK/ERK-or PI3K/AKT signaling. In human primary liver tumors *RAS* mutations are mainly found in ICCs, but less common in HCCs [1, 42]. However, in a majority of human HCCs an activation of the Ras-signaling pathway independent of activating *RAS*-mutations, this pathway plays also a crucial role in HCC formation [128]. Confirmation of the relevance of the microarray analysis was performed by IHC staining of *RPK* tumors for the activated form of pAKT^{Thr308}, which gets phosphorylated at threonine 308 (Thr308) in a PI3K-dependent manner and for activated

pERK. Testing for activation of components of the Ras/ERK signaling revealed high levels of activated pERK in tumor tissue, (Fig. 10A), suggesting that activation of ERK signaling downstream of oncogenic Kras contributed to transformation and carcinogenesis in our liver cancer model. Advanced *RPK* tumors also displayed considerable levels of pAKT^{Thr308}, another major effector of activated Ras signaling. However, comparable levels of AKT activation were also observed in the surrounding liver tissue (Fig. 10A). Immunoblot analysis of control livers compared to *RPK* tumors revealed an upregulation of ERK, activated pERK and pAKT^{Thr308}. Interestingly, downregulation of Ras-independent AKT activation (pAKT^{Ser473}) on the protein level was observed in all tumor samples when compared to control liver (Fig. 10B). Therefore, our data indicate for strong activation of several RAS downstream targets.

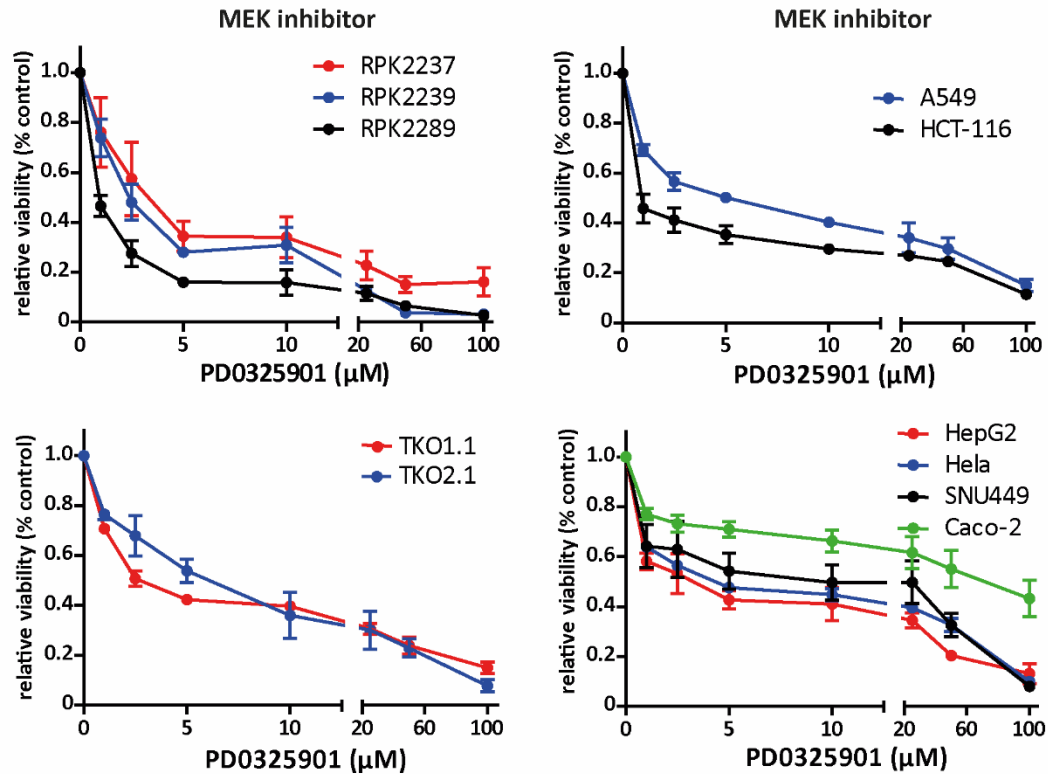
6.6 Inhibition of MEK activity in *RPK* liver tumor cell lines *in vitro*

MAPK and mTOR signaling pathway belonged to the top upregulated pathways in our microarray analysis (Fig. 11A). Underlining the importance of these pathways, in the human situation amongst other signaling pathway, the MEK/ERK and PI3K/AKT/mTOR pathways plays a critical role in a majority of poor prognosis human HCCs [129]. In our model, both pathways are likely activated by oncogenic RAS. To investigate the impact of these signaling pathways in our *RPK* model, we used specific pathway inhibitors in cell lines derived from *RPK* liver tumors (Fig. 11A). The effect of pathway inhibition was assessed by MTT assay which allows relative determination of the viable cell number after treatment. In the MTT assay we compared the cell viability of a vehicle-treated control cell line with cells treated with specific pathway inhibitors, including different concentrations of the MEK (PD0325901) inhibitor to specifically inhibit Ras-dependent MEK/ERK-signaling *in vitro*. We analyzed different mouse hepatoma cell lines as well as human cancer cell lines from hepatocellular and other carcinomas. Different concentrations of the MEK inhibitor revealed a high sensitivity of *RPK* cell lines in comparison to mouse cell lines without continuously activated Kras (TKO) and human cancer cell lines from liver (HepG2, SNU-449), cervix (Hela), and from the colon (Caco-2) (Fig. 11B).

A



B



C

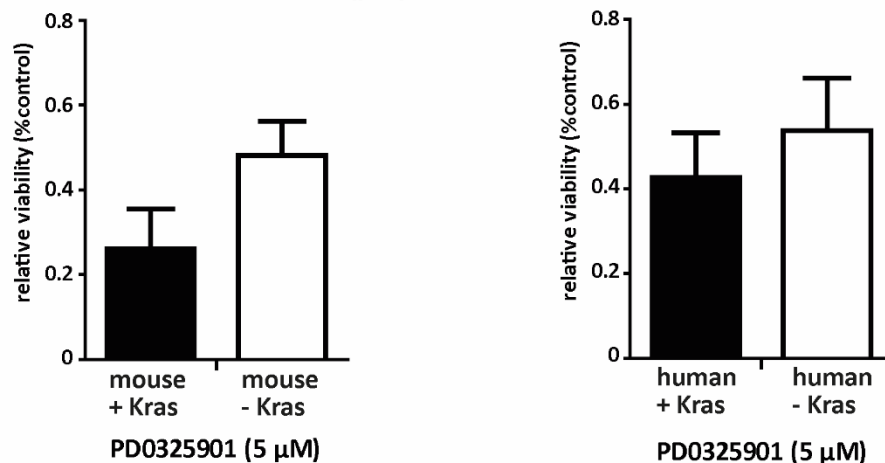


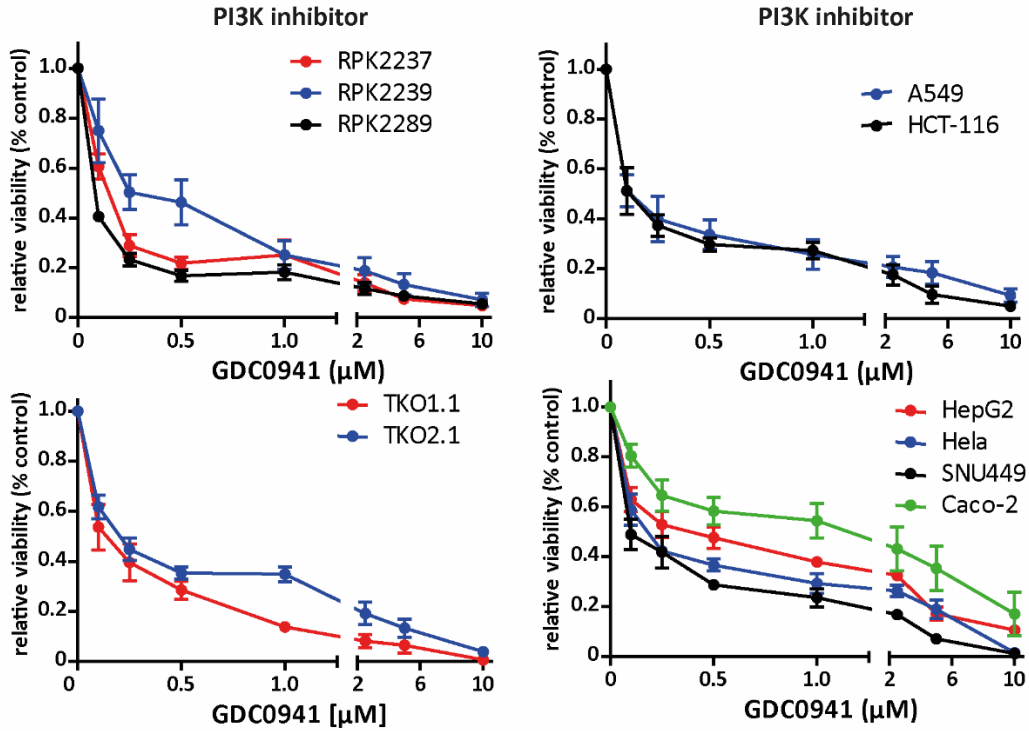
Figure 11: Inhibition of MEK activity in *RPK* liver tumor and mouse and human cancer cell lines *in vitro*
 (A) Pictures of primary tumor cell lines isolated from *RPK* tumors.
 (B) MTT assay of *RPK*, TKO and 6 human cell lines treated with the MEK inhibitor PD0325901. Data is shown as mean \pm SD; n = 3 replicates.
 (C) MTT assay analysis of cell number in of human or mouse cell lines with or without activated Kras after MEK inhibition by PD0325901. Inhibitor concentrations listed in μ M. Mouse Kras-activated cell lines include RPK2237, RPK2239 and RPK2289. Mouse Kras wild type cell lines include TKO1.1 and TKO2.1 isolated from mouse liver tumors in Retinoblastoma triple-KO mice Ehmer, Zmoos, Auerbach, Vaka, Butte, Kay and Sage [2]. Human Kras-activated cell lines include A549 and HCT-116. Human Kras wild type cell lines include Caco-2, HepG2, SNU449 and Hela. Data is shown as mean \pm SD; N = 3 replicates.

Interestingly, when cell lines were analyzed according to the presence of activating mutations in the Ras signaling pathway, the sensitivity towards pathway inhibition seemed to be higher in Ras-mutated cell lines of mouse and human origin (Fig. 11C).

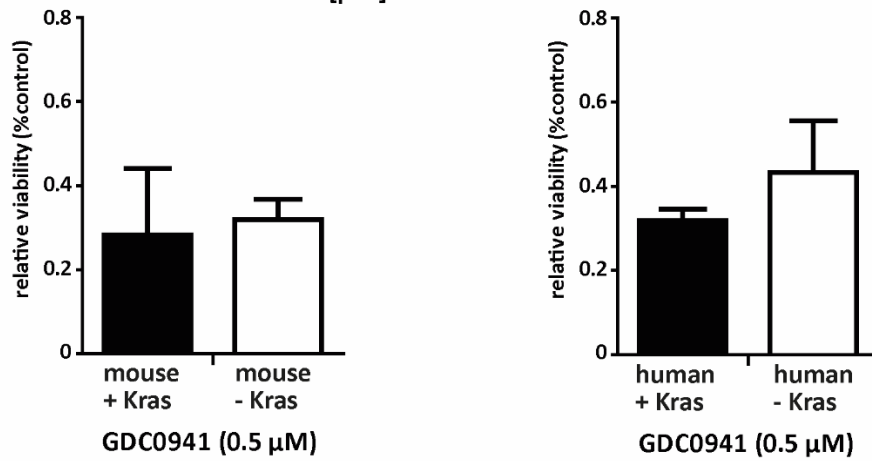
6.7 Inhibition of PI3K activity in *RPK* liver tumor cell lines *in vitro*

Another effector pathway of Ras signaling is the PI3K/AKT/mTOR pathway. As investigated with the MEK inhibitor we tested our cell lines derived from RPK livers with a specific PI3K (GDC0941) inhibitor to specifically inhibit Ras-dependent AKT-signaling *in vitro*. We compared the viability change by PI3K inhibition in different mouse hepatoma cell lines as well as human cancer cell lines from hepatocellular and other carcinomas. Increasing PI3K inhibitor concentrations showed a high efficiency in activated Kras cell lines derived from mouse and human, but also in mouse cell lines without continuous RAS activation (Fig. 12A). According to our results, PI3K inhibition results in a viability decrease in liver mouse cell lines with or without steady Ras signaling, whereas in human cell lines the inhibition of PI3K only shows a great effect in cell lines containing activated Ras (Fig. 12B). These results indicate that activation of Ras signaling is a predictor of response to inhibitors of MEK/ERK and also PI3K/AKT signaling. To test if inhibition of MEK/ERK and PI3K/AKT pathways does work synergistically to inhibit tumor cell proliferation, combinations of the IC50 concentration was tested by MTT assay in 3 *RPK* cell lines. Interestingly, inhibitors of both signaling pathways have an additive effect regarding the inhibition of the proliferation in comparison to the single substances (Fig. 12C), underlining the importance of both sub-pathways for *RPK* tumor cell viability *in vitro*.

A



B



C

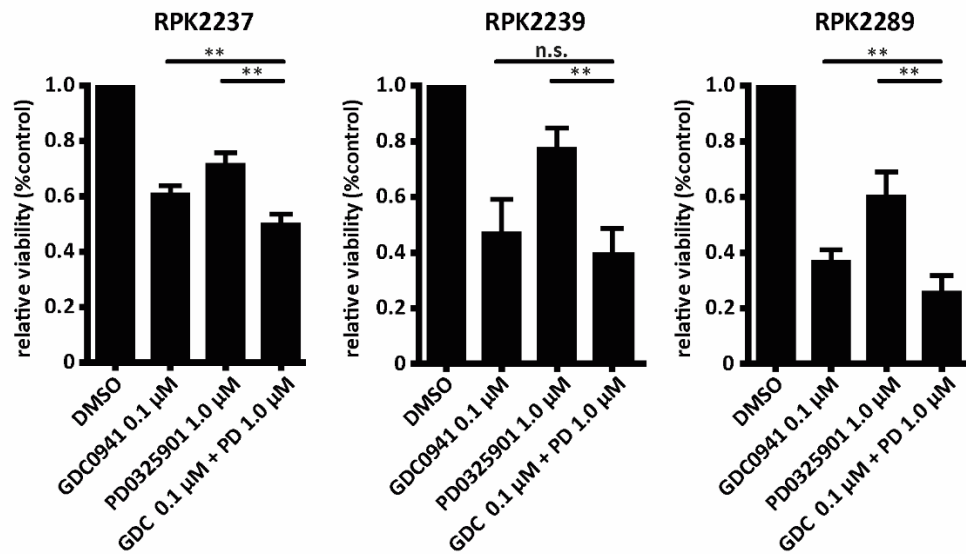


Figure 12: Inhibition of PI3K activity in *RPK* liver tumor cells and mouse and human cancer cell lines *in vitro* (A) MTT assay of *RPK*, *TKO* and 6 human cell lines treated with the PI3K inhibitor GDC0941. Data is shown as mean \pm SD; n = 3 replicates.

(B) MTT assay analysis of cell number in of human or mouse cell lines with or without activated Kras after PI3K inhibition by GDC0941. Inhibitor concentrations listed in μM . Mouse Kras-activated cell lines include RPK2237, RPK2239 and RPK2289. Mouse Kras wild type cell lines include TKO1.1 and TKO2.1 isolated from mouse liver tumors in Retinoblastoma triple-KO mice [2]. Human Kras-activated cell lines include A549 and HCT-116. Human Kras wild type cell lines include Caco-2, HepG2, SNU449 and Hela. Data is shown as mean \pm SD; N = 3 replicates. (C) Single and combined GDC0941 and PD0325901 inhibition for 3 cell lines derived from *RPK* tumors. Data is shown as mean normalized to the control \pm SD; N = 3 replicates. ** $p < 0.01$, n.s. = not significant, Student's test.

6.8 Genetic inactivation of *Pdk1* increases the survival of *RPK* mice

Next, we aimed to confirm the relevance of Ras-dependent AKT signaling for tumor development *in vivo* in our RPK model. To this aim, we induced genetic knockout of PDK1 in our mice. PDK1 is an effector kinase of Ras signaling, which gets activated by PI3K and in turn phosphorylates and activates $\text{pAKT}^{\text{Thr308}}$ [130] (Fig. 9C). Therefore, we bred *RPK;Alb^{CreER}* to *Pdk1^{lox/lox}* mice to generate *RPK;Alb^{CreER};Pdk1^{lox/lox}* mice. Additionally, we generated *RPK;Pdk1^{lox/lox}* mice and injected them with our *CreER* transposon. Looking at the overall survival rate after TAM injection, we observed a significant increase in survival in mice with conditional knock-out of *Pdk1* and therefore inactivation of the PI3K-PDK1-AKT cascade with no activated $\text{pAKT}^{\text{Thr308}}$ (Fig. 13A). From *RPK;Pdk1^{lox/lox}* + Transposon-*CreER* mice we quantified

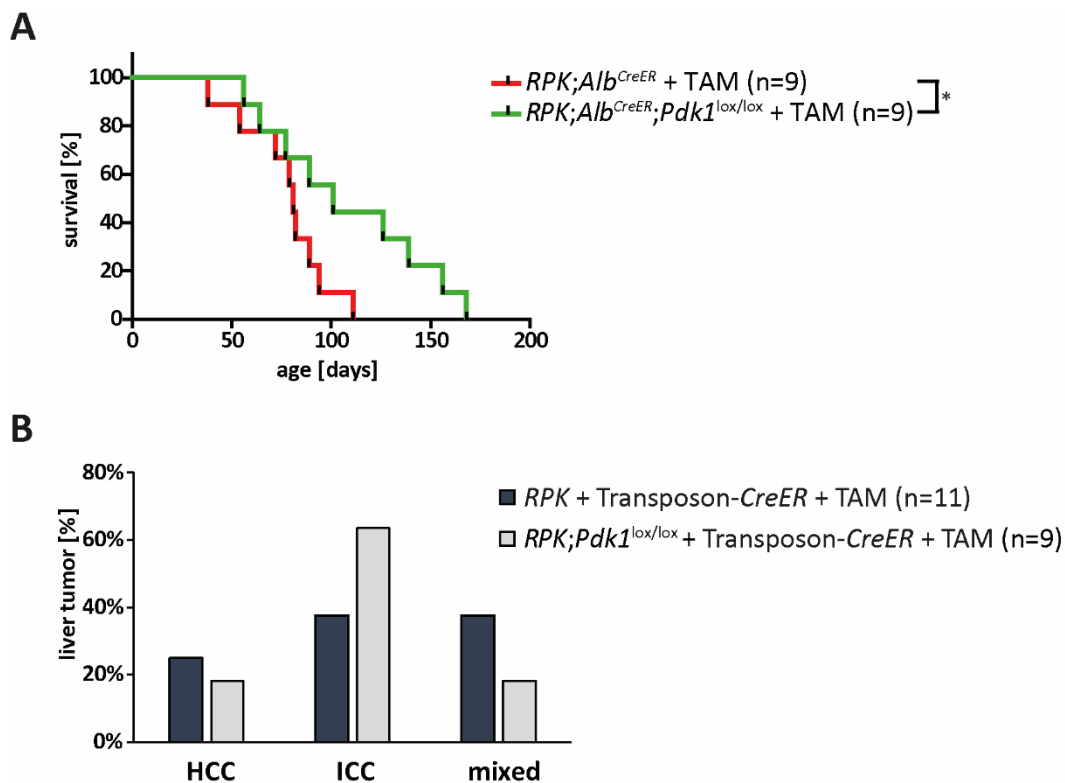


Figure 13: Genetic inactivation of *Pdk1* increases median survival of *RPK* mice

(A) Kaplan-Meier survival analysis of *RPK;Alb^{CreER}* and *RPK;Alb^{CreER};Pdk1^{lox/lox}* mice. * $p < 0.05$, Log-rank (Mantel-Cox) Test.

(B) Differentiation of hepatic tumors in *RPK* + Transposon-*CreER* and *RPK;Pdk1^{lox/lox}* + Transposon-*CreER* mice after Transposon-*CreER* injection and TAM treatment. n = number of tumors

the tumor differentiation of HCC, ICC, and mixed differentiation and compared these with the differentiation found in *RPK* Transposon-*CreER* mice and showed a trend towards a more bile duct-like phenotype in comparison to tumors from *RPK* mice (Fig. 13B).

6.9 Genetic inactivation of *Pdk1* decreases proliferation in *RPK* livers

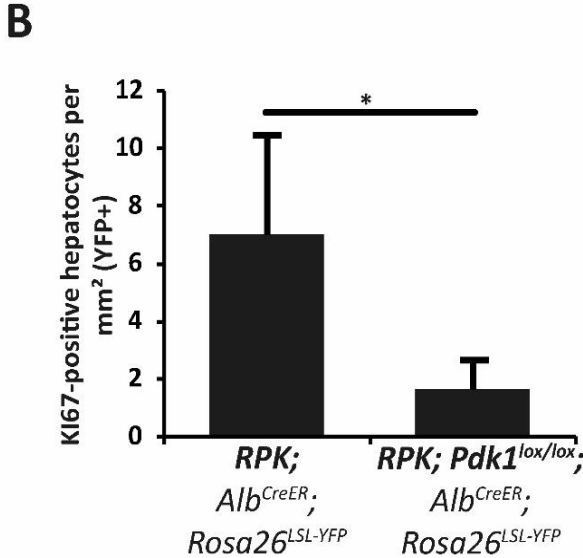
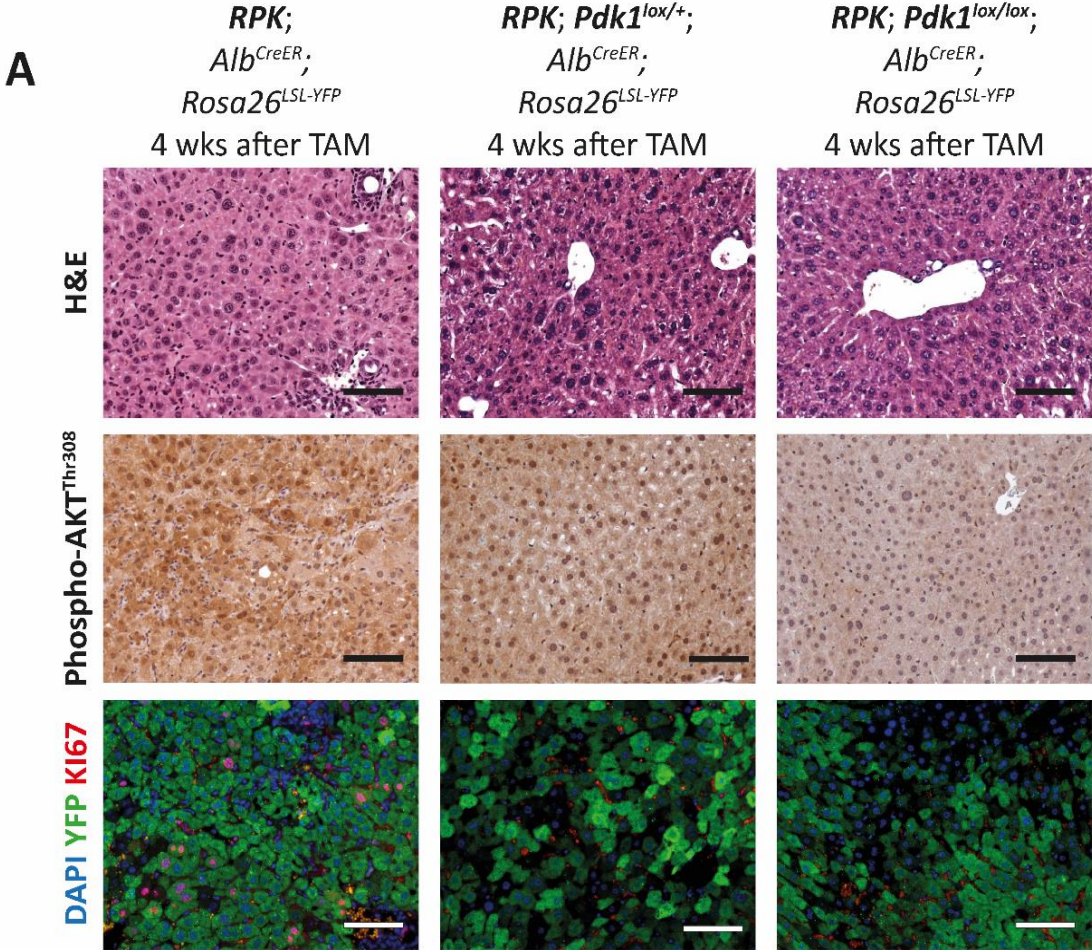


Figure 14: Genetic inactivation of PDK1 decreases proliferation in *RPK* livers

(A) IF, H&E and IHC staining for *RPK;Alb^{CreER}*, *RPK;Alb^{CreER};Pdk1^{lox/+}* and *RPK;Alb^{CreER};Pdk1^{lox/lox}* male mice 4 weeks after TAM-induced gene recombination. IHC staining for pAKT^{Thr308} and IF staining for DAPI, YFP and Ki67. Scale bars equal 200 μ m.

(B) Quantification of proliferating cells by IF staining of *RPK;Alb^{CreER};Rosa26^{LSL-YFP}* and *RPK;Alb^{CreER};Pdk1^{lox/lox};Rosa26^{LSL-YFP}* mice, by counting the Ki-67 positive hepatocytes per mm² of recombined hepatocytes (YFP+). *p<0.05, Student's test.

RPK;Alb^{CreER} mice 4 weeks after TAM-induced gene recombination show proliferation of dysmorphic hepatocytes as well as nuclear and cellular pleomorphism associated with positive staining for pAKT^{Thr308} (Fig. 14A). Interestingly, livers of *RPK;Alb^{CreER};Pdk1^{lox/+}* and *RPK;Alb^{CreER};Pdk1^{lox/lox}* mice were less proliferative, which correlated with a decreased activation of pAKT^(Thr308) by immunostaining (Fig. 14A). To quantify differences of proliferating hepatocytes in our model, we counted the Ki-67 positive hepatocytes per mm² of recombined, YFP-positive hepatocytes and observed a significant decrease of proliferating cells in *RPK;Alb^{CreER};Pdk1^{lox/lox}* compared to *RPK;Alb^{CreER}* mice (Fig. 14B). This finding indicates that activation of AKT is crucial for early proliferation in *RPK* livers and likely contributes to the increased time to tumor development in *Pdk1*-deficient *RPK* mice.

6.10 Screening of cancer associated genes

Microarray analysis of gene expression data from *RPK* liver tumors revealed significant up-regulation of numerous genes that are related to cancer and metastasis. For further analysis, we chose a subset of top up-regulated genes that were highly expressed in *RPK* liver tumors but not in control livers. We used quantitative real time polymerase chain reaction (qRT-PCR) to verify the significant up-regulation of curated genes from microarray data in *RPK* tumor samples. Using the pLKO.1 lentiviral vector system, we established stable cell lines from *RPK* liver tumors that harbor shRNA constructs to specifically target the mRNA of corresponding genes or "scrambled" shRNA as control to test the functional impact of selected gene knock-down. We transfected *RPK* cells (RPK2289) with pLKO.1 shRNA vectors and analyzed the effect of the transfected shRNA on the cell viability by MTT assay. For further analysis, we chose shRNA constructs that led to a cell viability reduction of 50% or more (Fig. 15A). From the transfected cell lines, those transfected with shRNA against *Dmbt1*, *Lgals2* and *Reg3b* met these requirements. To confirm downregulation of targeted genes, we analyzed mRNA levels. An mRNA reduction of a minimum of 50% was considered as an effective knock-down. Of note,

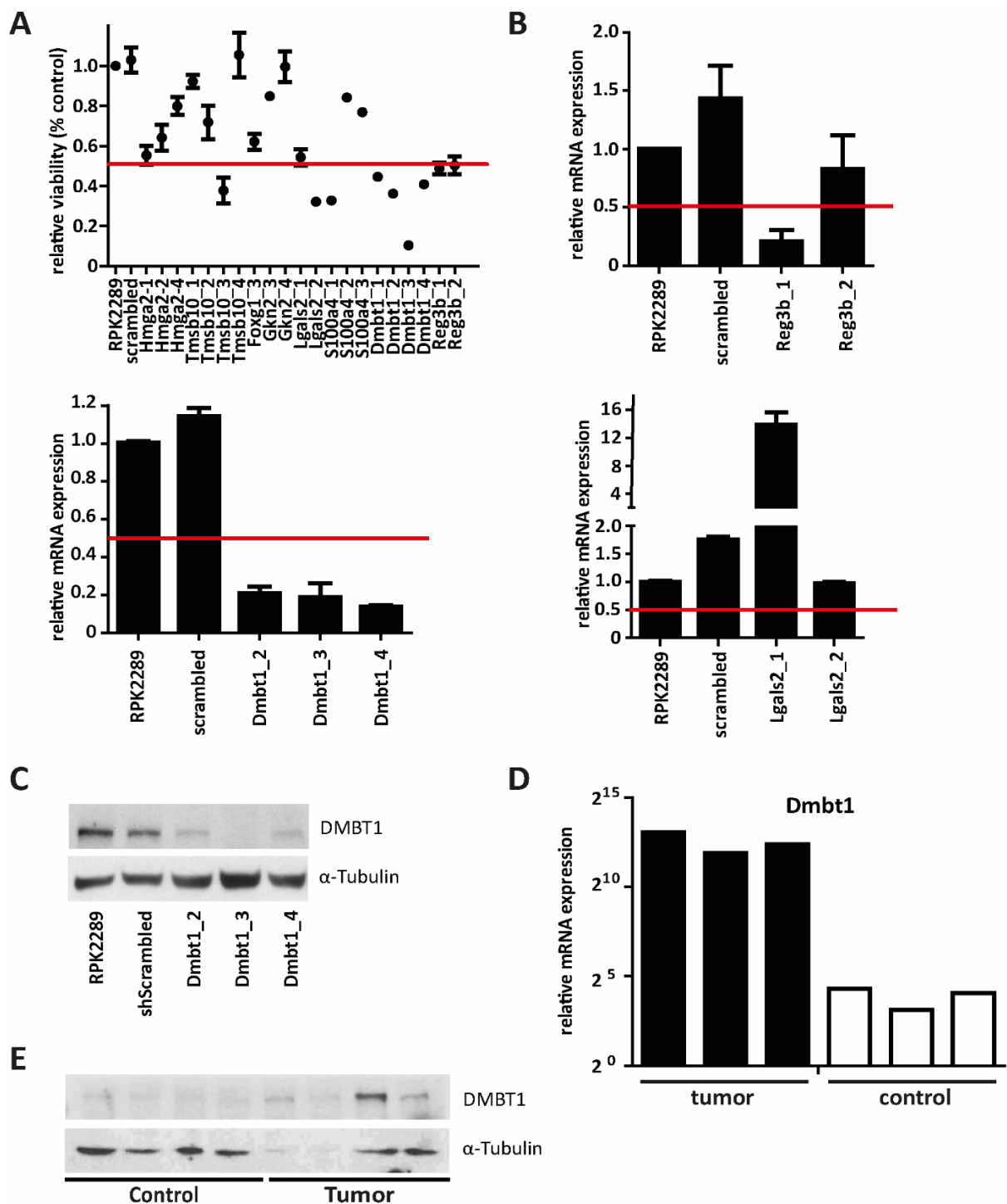


Figure 15: Screening of cancer associated genes

(A) MTT assay of RPK cells infected with specific shRNA compared to controls (shScrambled and non-transfected). Cut-off was made at viability of a max of 50% compared to the control. Data is shown as mean normalized to RPK2289 \pm SD; n = 3 replicates.

(B) qRT-PCR of RPK2289 cells transfected with shRNAs for candidate genes. Data is shown as mean normalized to RPK2289 \pm SD; n = 3 replicates.

(C) Immunoblot analysis of DMBT1 protein levels in protein lysates of transfected RPK2289 cells with 3 different shRNA constructs against *Dmbt1* compared to shScrambled. α -Tubulin was used as a loading control.

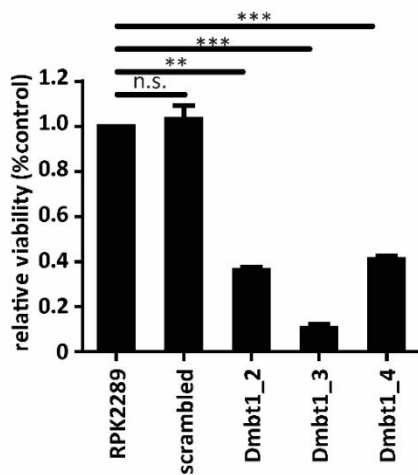
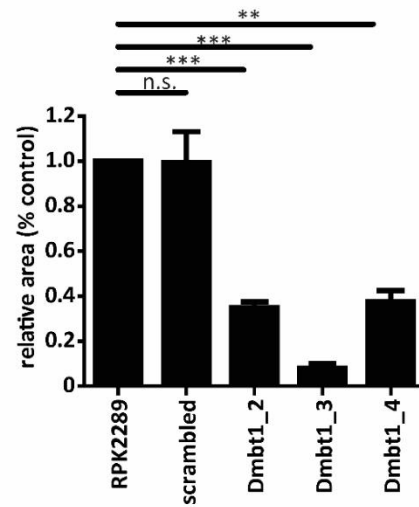
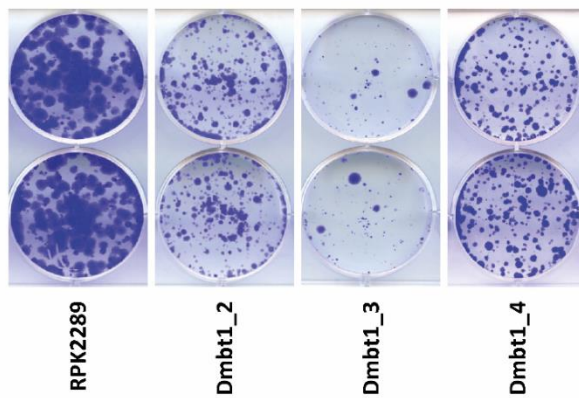
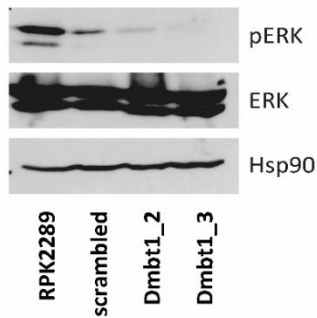
(D) Microarray data of 3 independent tumor samples derived from *RPK* mice injected with AAV-TBG-Cre in comparison to control liver.

(E) Immunoblot analysis of DMBT1 protein in lysates of tumors derived from *RPK* mice injected with AAV-TBG-Cre in compared to normal control liver. α -Tubulin was used as a loading control.

only shRNA against *Dmbt1* (shDmbt1) showed an effective knock-down of mRNA for 3 different shRNAs. In contrast, shRNAs against *Lgals2* (shLgals2) did not have an effect on *Lgals2* mRNA levels, and shRNA against *Reg3b* (shReg3B) had only one good candidate that led to efficient mRNA downregulation (Fig. 15B), suggesting that cell viability reduction for the two latter genes is not dependent on gene knock-down, but rather on off-target effect. We confirmed that the mRNA downregulation of our best candidate *Dmbt1* by immunoblot analysis, also is visible on the protein level (Fig. 15C). Microarray data of *RPK* AAV-TBG-Cre tumor mice compared to control samples showed an upregulation of *Dmbt1* mRNA in tumors (Fig. 15D). Immunoblot analysis revealed an increase of DMBT1 protein in tumors derived from *RPK* mice injected with AAV-TBG-Cre (Fig. 15E). As *shDmbt1* cells showed a decrease in the vitality and a potent reduction of mRNA and protein levels, we chose *Dmbt1* for further analysis.

6.11 shDMBT1 expression decreases cell viability *in vitro*

DMBT1 („Deleted in malignant brain tumors 1“) was described as a tumor suppressor in glioblastoma, in lung, and in the gastrointestinal tract [108, 112, 117]. In contrary, in the liver and biliary tract DMBT1 seems to have a pro-proliferative role, and the function in primary liver tumors up to date has not been clarified [122, 131]. According to earlier studies, the DMBT1 protein is primarily secreted into the extracellular compartment and the tumor suppressive function is mainly attributed to modulation of the tumor specific immune response [132]. Further screening of candidate *shDmbt1* cells by proliferation and clonogenic assay analysis to confirm cell viability reduction and a profound impact on clonogenic capacity. Knock-down of *Dmbt1* in *RPK* cell lines shows a significant reduction of the cell proliferation (Fig. 16A) and a partial loss of clonogenic capacity of the tumor cells (Fig. 16B). Functionally, we showed a reduced activation of the MEK/ERK signaling pathway after *Dmbt1* knockdown (Fig. 16C). To summarize, we showed that knock-down of the candidate gene reduced tumor cell proliferation and the capacity to form colonies – by a mechanism that possibly functions through influencing ERK activation. An interaction with the MEK/ERK signaling pathway provides a plausible explanation for the oncogenic impact of DMBT1 in our model.

A**B****C****Figure 16:** shDMBT1 expression decreases cell viability *in vitro*

(A) MTT assay of RPK2289 cells transfected with 3 different shRNAs against *Dmbt1* compared to “scrambled” shRNA and normalized to untransfected RPK2289 cells as control. Data is shown as mean normalized to control RPK2289 \pm SD; n = 3 replicates. ***p<0.001, **p<0.01, n.s. = not significant, student’s test.

(B) Clonogenic assay in RPK2289 controls and RPK2289 cells transfected with the indicated shRNAs for 10 d (left) and quantification of the area coverage compared to the control (right). Data is shown as mean normalized to control RPK2289 \pm SD; n = 3 replicates. ***p<0.001, **p<0.01, n.s. = not significant, student’s test.

(C) Immunoblot analysis of ERK signaling in protein lysates of transfected RPK2289 cell line with 2 different shRNA against *Dmbt1*. Hsp90 was used as a loading control.

6.12 Injection of shDmbt1 increases survival compared to control *RPK* mice

To answer the question of an *in vivo* relevance of DMBT1, *RPK* mice were injected via hydrodynamic tail vein injection with a CreER/shRNA construct, that was developed in our laboratory [98]. The transposon construct allowed stable integration of a CreER construct together with a DOXY inducible shRNA in hepatocytes. After activation of CreER by TAM injection and induction of the shRNA expression by DOXY (Fig. 17A), shDmbt1 injected *RPK* mice show a significantly longer survival compared to animals injected with control shRNA (shScrambled) or control *RPK* mice injected with *CreER* only (Fig. 17B). shScrambled-injected animals had a lower or equal transfection efficiency compared to shDmbt1-injected mice, determined by YFP reporter-gene staining (Fig. 17C). Quantification of GFP positive cells compared to the total cell number, had a mean of 1.55% GFP positive cells for shScrambled-injected animals and a mean of 4.35% GFP positive cells in shDmbt1-injected mice. IHC stainings of shDmbt1 injected *RPK* mice reveal presence of Dmbt1 in tumorous tissue comparable to tumors from control animals injected with shScrambled, suggesting that Dmbt1 expression does get re-activated during tumor development or that incomplete inactivation of Dmbt1 in a subset of targeted hepatocytes might predispose them to tumor development (Fig 17D). Finally, we showed that knock-down of *Dmbt1* increased survival in *RPK* mice. This finding underlines our thesis that Dmbt1 is important for the initial tumor formation and growth and could present a novel prognostic marker – and potential target – in liver cancer.

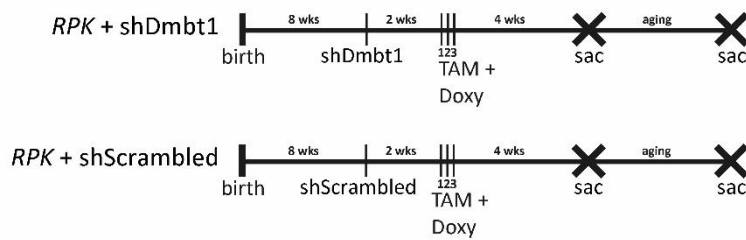
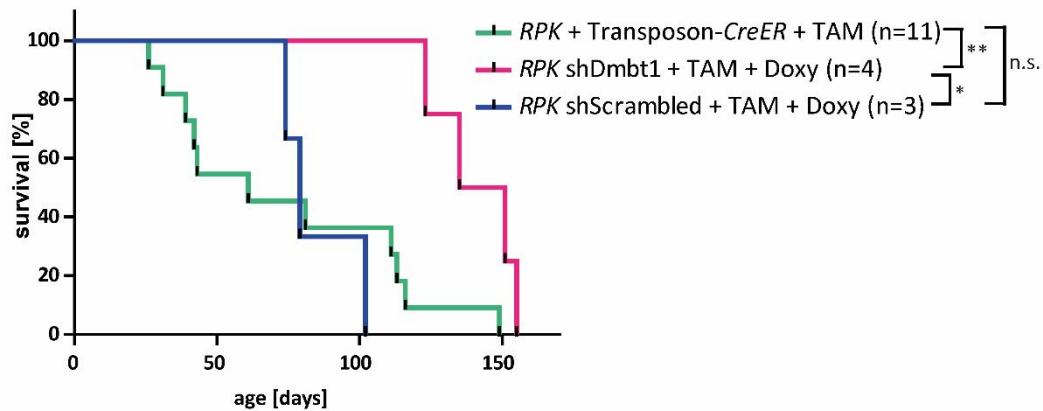
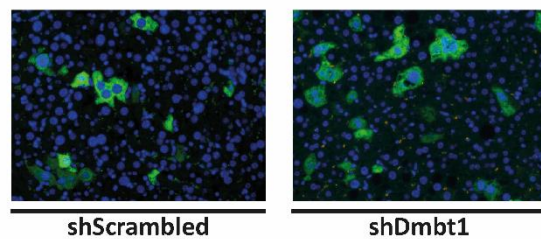
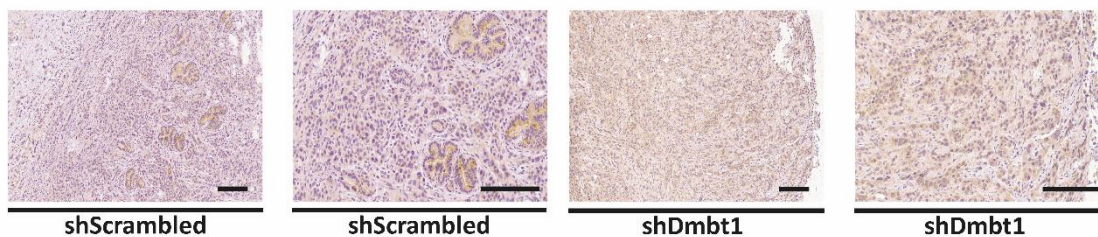
A**B****C****D**

Figure 17: Injection of shDMBT1 increases survival compared to non-treated *RPK* mice *in vivo*

(A) Scheme illustrating injection in adult 8-week old *RPK* mice by either shDmbt1 or shScrambled. Induction of Cre-recombinase expression by 3 times TAM on 3 consecutive days 2 weeks later. Activation and expression of shRNA by DOXY chow. Mice were sacrificed at 4 weeks after TAM/DOXY or were aged till a termination criterion of the animal protection act appeared.

(B) Kaplan-Meier survival analysis of *RPK + Transposon-CreER*, *RPK shDmbt1* and *RPK shScrambled* male mice. ** $p < 0.01$, * $p < 0.05$, n.s. = not significant, Log-rank (Mantel-Cox) Test.

(C) IF staining for DAPI, and YFP to test for target efficiency of transfected hepatocytes of shDmbt1 or shScrambled in *RPK; Rosa26LSL-YFP* mice by counting the GFP positive hepatocytes per mm^2 .

(D) IHC DMBT1 staining in shDmbt1- and shScrambled-injected aged *RPK* mice. Size bars equal 200 μm .

7 Discussion and outlook

Genetically engineered mouse models (GEMM) are a valuable tool for investigating severe and complex dysfunctions of the body. Basic research in animal models is essential for the understanding of molecular changes undergoing in a diseased body. In contrast to *in vitro* work, GEMM can be used to investigate initiation, development and the different stages of the disease, as well the role of endogenous defense mechanisms like the immune system. Although primary liver cancer is heterogeneous at the genetic level, recurring genetic patterns found in human hepatic tumor samples can be used to mimic the main events leading to primary liver cancer. The prognosis of primary liver cancer in the advanced stage of the disease remains poor despite new therapeutic approaches. Due to the ineffectiveness of conventional chemotherapies, all hopes were placed in targeted tumor therapy [15]. Various approaches to targeted therapy were either not or only partially successful. The reasons are not completely clarified, but the heterogeneity of primary liver cancer in different patients and different resistance mechanisms to the treatments seem to be the main reasons for nearly no tumor specific therapy. Before the development of immunotherapies, the most promising approach in the treatment of HCC was treatment with multi-tyrosine kinase inhibitors such as Sorafenib, which achieves a moderate increase in overall survival [66, 152]. Sorafenib targets several oncogenic pathways including Raf signaling, leading to reduced cell division and proliferation and also targets VEGF signaling, resulting in reduced tumor angiogenesis [133]. The choice and the success of therapy strategies most likely depends largely on the expression of certain markers or activated signaling pathways. In primary liver cancer multiple oncogenic signaling pathways are altered [1] and a targeted inhibition of a single signaling pathway can lead to the activation of further oncogenic pathways which acts as a resistance mechanism that prevents a lasting response to therapy [134]. Combination of pharmacotherapies to influence and target multiple signaling pathways can potentially lead to a disruption of tumor intrinsic resistance mechanisms and to an improved response to therapy [153, 154]. The effectiveness of such combination therapies depends on one hand on the relevance of the corresponding signaling pathways in primary liver cancer, on the other hand on the dependence of these signaling pathways on each other. Especially regarding the heterogeneity of primary liver cancer, combined pharmacotherapies have to consider the individual tumor biology. In addition to genetic tumor analyzes and bioinformatic algorithms for the identification of suitable combination therapies [153], *in vitro* validation and animal model analysis remain

essential components for the development of rational and calculated therapeutic approaches. In particular, the identification of relevant oncogenic signaling structures and resistance mechanisms continues to depend on the analysis of representative animal models.

The *RPK* mouse model of primary liver cancer

The *RPK* mouse model with genetically inactivated RB and p53 signaling and continuously activated Kras mimics molecular changes occurring in many human primary liver cancers. This mouse model is a tool to investigate on critical mechanisms in liver carcinogenesis to mimic continuously activated Ras signaling found in the majority of human HCCs and ICCs. The *Rb* gene itself is only relatively rarely mutated in HCC, but inactive mechanisms of retinoblastoma signaling in the majority of hepatocellular carcinomas are observed by alternative mechanisms [49]. Functionally, the relevance of the RB signaling pathway in the liver is not only evident in the control of cell cycle initiation, but also in the regulation of mitosis. The loss of *Rb* gene function alone is not suitable to induce primary liver cancer, but the complete inactivation of the RB signaling pathway leads to tumor formation in the liver and is constantly mutated in human HCC [2, 135]. p53 is commonly altered in a multitude of cancers and its inactivation is essential for the formation of the majority of human tumors [136]. Interestingly the rate of p53 mutations is depending on the underlying disease leading to HCC development. In HBV-related HCC, p53 is mutated in 45% of the patients, while in HCV-related HCC, p53 is only mutated in 13% of cases [137]. Homozygous genetic deletion of p53 and Rb together by liver-specific *Alb^{CreER}* leads to tumor formation after 13 up to 26 months with an incidence rate of 63% [138]. Considering the mean lifespan of the WT control mice of around 24 months, liver cancer developed very late and needs more than a deleted Rb/p53 signaling pathway to initiate and progress. For a faster and more aggressive progression we used induced and continuously activated Kras signaling, as a strong driver of tumor formation in many tissues like biliary tract cancer, colon, lung, pancreas [139]. *RAS* mutations are non-druggable with current methods, blocking of all mutated RAS isoforms will lead to cell toxicity, blocking of more than 2 isoforms is lethal to the embryo [140]. Uncontrolled activation of KRAS leads to proliferation and finally to tumor formation. Our goal was to create a mouse model that mimics the human situation of bad prognosis primary liver cancer. On the molecular level, our tumors show elevated levels of AFP which is seen as a strong prognostic factor for poorer overall survival in HCC patients [141]. The pathological analysis of differentiation of liver

tumors in *RPK* mice after AAV-TBG-Cre injection revealed that the *RPK* mouse model gives rise to tumors with varying differentiation. The appearance of undifferentiated tumors, mixed ICC/HCC and ICCs range from 25 to 38% of the tumors. Interestingly only around 10% of the tumors were HCC. This mouse model mimics the human situation of bad prognosis primary liver cancer, which results in a rapid tumor formation and tumors histology similar to poorly differentiated human HCC, ICC, and tumors of mixed differentiation.

***RPK* tumors arise from hepatocytes**

Tumors arise from normal cells that develop into cancer cells through genetic alteration. The liver consists of various cell populations, for the most part it consists of hepatocytes which take about three-quarters of the liver volume, other parenchymal cell populations found are oval or liver progenitor cells – that are only observed under certain conditions – and bile duct cells. Which of these cells give rise to the different entities of primary liver cancer is still debated. The tumor phenotype is determined by genetic alterations in the cell of origin which leads to initiation and transformation to cancer. The identification and characterization of the cell of origin could deliver important information about the genetic background of the tumor initiating cell. This information can be used to detect malignancies, to identify patients at risk, for prevention of tumor initiation and prediction of cell responses to therapy [142, 143]. The two major cells found in the liver express different markers, Albumin is mainly expressed in hepatocytes, SOX9 and HNF1 β are both expressed in bile duct cells/cholangiocytes. By using cell-type specific promoters to drive CreER expression, recombination is limited to the specific cell compartment. However, Alb^{CreER} is not strictly limited to the targeting of hepatocytes and therefore also the bile duct/cholangiocyte compartment is affected. However, by using low-dose TAM applications, genetic recombination can be targeted the hepatocyte compartment [105]. The *RPK* transposon system is our other method of choice to target hepatocytes. Both systems give rise to big solid primary liver tumors after a short period of time. HNF1 β , which is expressed in bile duct cells/cholangiocytes, and SOX9 as a biliary marker are both highly specific for the biliary compartment labelled with a CreER [105]. In our model, hepatocytes and bile duct cells had a normal histology and showed no evidence of aberrant cell behavior or tumor formation in the liver after TAM treatment in aging *RPK;Sox9-CreER* and *RPK;Hnf1b-CreER* mice. Interestingly, *RPK;Hnf1b-CreER* mice had no physical ailments and were healthy until sacrificed. Although the liver of the *RPK;Sox9-CreER* mice was healthy and unremarkable

with no sign of hepatic tumors, lung tumors developed after some time, leading to a lower survival. SOX9 is a transcription factor crucial for the promotion of proliferation, migration and invasion of cells in lung adenocarcinoma [144]. Lung tumors are highly SOX9 positive, 70% show moderate to robust expression of SOX9 [145]. Therefore, it is not surprising that lung tumors arise in the *RPK;Sox9-CreER* mice. While targeting of the bile duct compartment did not give rise to primary liver tumors, the hepatocyte specific CreER transposon in *RPK* mice and the *RPK;Alb^{CreER}* model give rise to solid tumors with mixed, ICC, and HCC differentiation in a time span of 1 to 5 months. This shows that hepatocytes are the primary source of for the cell of origin for primary liver cancer in our model. Although the tumors arising from our *RPK* mouse model are rising from the hepatocytic compartment, the tumors show characteristics of mixed hepatocytic and biliary differentiation. Primary liver cancer which displays biliary compartment marker CK19 and hepatocytic markers are highly aggressive, associated with larger and faster tumor growth and prognoses a poor survival outcome for patients [146].

Ras signaling is crucial for initiation and formation of primary liver tumors in *RPK* mice

Ras signaling, triggered by persistently activated oncogenic KRAS, is a strong driver in a multitude of cancers for controlling cell survival, differentiation, proliferation, metabolism, and motility. Activating KRAS mutations are a sign of rapidly proliferating cells and a poor prognosis in diagnosis for patients. The characterization of the *RPK* tumors showed more ICC than HCC tumors, as well as one third of the tumors were of mixed HCC/ICC differentiation. The variety of ICC and mixed HCC/ICC differentiation in our *RPK* mouse model might be explained by the analysis of human ICC tumor samples. *KRAS* is mutated in 16,7% of ICC tumors and classified as the second most mutated gene in ICC, notably patients with *KRAS* mutations show less survival compared with those without such mutations. p53/RB signaling pathway is in 44% and Ras signaling in 70% of the examined cases mutated [54]. In HCCs mutations in p53/RB signaling pathway are among the most common mutations found, p53 alone is mutated in 21% of examined cases [1]. Oncogenic KRAS was found rarely in patients with HCC, but Ras signaling plays a crucial role in HCC formation and is activated in a majority of human HCCs independent of *RAS* mutations [128]. Our genetic setting in the *RPK* mouse model can give rise to tumors with features of both HCC and ICC, but it seems that the genetic

background leads preferably to ICC formation. Mutations in *Kras* and *p53* are clinically inconvertible, therefore we focused on the downstream effector kinases of Ras signaling, PI3K, AKT, ERK, and MEK. The MEK/ERK and PI3K/AKT pathways show enrichment in *RPK* tumor samples by microarray analysis. We found elevated pERK levels in tumors of *RPK* mice, but not in healthy hepatocytes of the same liver. By inhibition of MEK and thereby ERK activation in *RPK* cell lines *in vitro* we observed a decrease in cell viability. Activated ERK signaling is a major contributor to proliferation and survival and upregulated in human HCC and ICC. Another downstream effector kinase of Ras signaling is AKT, which gets phosphorylated at Threonine³⁰⁸ by PDK1 and phosphorylated at Serin⁴⁷³ by mTORC2. AKT^{Thr308} is highly upregulated in *RPK* tumor tissue. This finding is not surprising, as PDK1-mediated activating phosphorylation of AKT at Thr308 is an effector pathway of *Kras* signaling. AKT is activated by phosphorylation at Thr308 or Ser473, which gets actively phosphorylated by mTORC2. Full activation of AKT can only be achieved if both amino acids are phosphorylated. Interestingly, we observed downregulation of AKT^{Ser473} in *RPK* tumors, possibly by compensatory cell-intrinsic mechanisms or feedback loops.

All our *RPK* cell lines showed a high sensitivity towards the treatment with PI3K/AKT and MEK/ERK inhibitors. The additive effect when combining the inhibitors indicates that both sub-pathways are important for cancer formation in the *RPK* mouse model. After these promising *in vitro* results, we tested the effect a reduced activating phosphorylation of AKT^{Thr308} *in vivo* in the *RPK* mouse model. PDK1 is a Ras downstream effector kinase, which is mainly involved in the phosphorylation of AKT at Thr308 and therefore a good target for investigation of Ras-dependent PI3K/AKT signaling. High pAKT^{Thr308} levels are associated with poor prognosis for patients and the formation of metastases, described as a risk factor for aggressive HCC [147]. As a consequence of genetic *Pdk1* deletion in the liver, significantly less proliferation occurred already after 4 weeks after TAM-induced recombination. Notably, even the knockout of a single *Pdk1* allele already leads to fewer KI67 positive hepatocytes than observed in *Pdk1*-proficient *RPK* mice. Thus, in our mouse model, there seems to be a strong dependence of the proliferation of AKT signaling pathway. This finding indicates that activation of AKT is crucial for early proliferation in *RPK* livers and likely contributes to the increased time to tumor development in *Pdk1*-deficient *RPK* mice. The PI3K/AKT and MEK/ERK signaling pathways are connected via mTOR signaling and inhibition of either one of this sub-pathways may result in recovery by activation of downstream effectors. ERK inhibition by

sorafenib leads to a survival pathway recovery in ICC by the PI3K/AKT signaling pathway. Interestingly, continuous activation of the PI3K/AKT signaling pathway during MEK/ERK inhibition has been described as a mechanism that leads to sorafenib resistance [148]. Therefore, inhibition of both AKT and ERK signaling might be a promising approach to counteract Sorafenib resistance. Whether the inhibition of both sub-pathways of Ras signaling increases the cell cytotoxicity or has other undesired effects, needs further research.

Oncogenic Dmbt1

The search for novel oncogenes is crucial for a better understanding of oncogenic signaling pathways and the identification of new targets for therapies. We screened several highly upregulated genes in our *RPK* mouse model that possibly contribute to cancer initiation and development. Our shRNA screening experiments revealed that Deleted in malignant brain tumors 1 (*Dmbt1*) could present a putative oncogene in primary liver cancer. *DMBT1* is a protein that belongs to the scavenger receptor cysteine-rich superfamily. *DMBT1* deletion was observed in brain tumor cell lines and was therefore first described as a putative tumor suppressor [108]. Additionally studies support the tumor suppressor hypothesis, because of the loss or downregulation of *DMBT1* in melanoma [109], pancreatic adenocarcinoma [110], lung cancer [111, 112], epithelial skin cancer [113], breast cancer [114], oral squamous cell carcinoma [115], prostate cancer [116], and esophageal cancer [117]. Functionally, *DMBT1* is described as a contributor to the innate immune defense system and functions as a pattern recognition molecule for pathogens [118]. In the liver, there are only a few studies that describe a connection between *DMBT1* and cancer, available data from liver models indicate that *DMBT1* has proliferative, oncogenic role, but no reliable mechanism has been presented so far. A splice variant of *DMBT1* called Ebnerin plays a role in liver regeneration from transit-amplifying ductular (oval) cells by deciding their fate and differentiation [119]. *DMBT1* is described as a potential biomarker for bile duct hyperplasia (BDH) [120] and *DMBT1* expression induces a proliferation and differentiation response of cholangiocytes which results in BDH [121]. Downregulation of *DMBT1* by specific shRNA in *RPK* cell lines led to reduced proliferation and viability of transfected cells. This cytostatic effect of sh*DMBT1* might be explained by downregulation of pERK signaling as a result of *DMBT1* knock-down. It seems that *DMBT1* directly or indirectly leads or critically contributes to the activation of the Ras downstream effector kinase ERK leading to proliferation. It was shown that *DMBT1* is

upregulated along the gastric precancerous cascade, in *Dmbt1* knockout mice, pERK levels are reduced, speaking for an indirect or direct activation of ERK by DMBT1 [149]. This could potentially provide a substitute mechanism to mimic or enhance continuously activated Kras signaling, contributing to faster proliferating cells and increased cell viability with a more aggressive tumor and shorter survival. Resistance mechanisms in transfected cells might take place after a certain amount of time and overcome the reduced pERK activation, for example by activation of the mTOR pathway or enhanced activation of PI3K/AKT signaling or activation of downstream targets of ERK. Little is known about the role of DMBT1 in ICC and HCC. In contrast to the described tumor suppressive function of DMBT1, we observed highly upregulated DMBT1 in various tumor samples of *RPK* mice and a prolonged survival of mice treated with *shDMBT1*. Our observations are supported and in line with studies describing high levels of DMBT1 in high-grade biliary intraepithelial neoplasia, dysplastic nodules, hepatitis, and cirrhosis where it presumably contributes to malignant transformation of hepatic cells [122, 131, 150]. In these forms of liver injury or early events that can lead to primary liver cancer, DMBT1 might contribute to tumor initiation or even be crucial for the tumor development [122, 151]. The oncogenic function of DMBT1 is further supported by the finding of high DMBT1 levels in non-invasive ICC with hepatolithiasis and HCC [150, 151], speaking for an important function even during the tumor is already established. However, as a late event in ICC DMBT1 levels seem to go back to normal. DMBT1 is described as expressed by biliary epithelial cells and is maybe lost as a side effect of epithelial to mesenchymal transition, a critical step in the formation of metastasis. An argument against this theory, however, is the presence of high DMBT1 levels in HCC patients with poorer prognosis compared to better prognosis primary liver cancer [150]. Another explanation could be that when the tumor is in an advanced state, the potential tumor suppressive features of DMBT1 outweigh the oncogenic capabilities and DMBT1 gets downregulated or resistance mechanisms take place. It is not clarified which functions DMBT1 has in the liver and one can only speculate about the underlying mechanism by which DMBT1 mediates cancer initiation and development.

Conclusion

We established a new and reliable mouse model which reflects the histology and genetic characteristics of primary liver cancer. The *RPK* mouse model meets the genetic requirements for rapid tumorigenesis, short disease progression, and the emergence of mixed HCC/ICC, pure ICC and HCC, and undifferentiated tumors. Ras signaling was identified as key driver of tumor formation in our model and inhibition of either MEK/ERK or PI3K/AKT signaling has an anti-tumor effect on *RPK* tumors. The *RPK* mouse model could represent a valuable tool to understand the tumor biology and the progression of primary liver cancer with bad prognosis for patients as well as to develop novel therapies for advanced HCC and ICC patients. In addition, the mouse model was used to identify a potential oncogene – *DMBT1* –, that seems to be a poor prognosis marker in human HCC. The role and function of *DMBT1* in cancer initiation and progression needs further investigation.

Publications resulting from my PhD work

- Hubner, E. K., **Lechler, C.**, Kohnke-Ertel, B., Zmoos, A. F., Sage, J., Schmid, R. M., & Ehmer, U. (2017). An in vivo transfection system for inducible gene expression and gene silencing in murine hepatocytes. *J Gene Med*, 19(1-2). doi:10.1002/jgm.2940
- Hubner, E. K., **Lechler, C.**, Rosner, T. N., Kohnke-Ertel, B., Schmid, R. M., & Ehmer, U. (2018). Constitutive and Inducible Systems for Genetic In Vivo Modification of Mouse Hepatocytes Using Hydrodynamic Tail Vein Injection. *J Vis Exp*(132). doi:10.3791/56613

Presentation of my work

- 02/2019 Poster presentation, Deutsche Arbeitsgemeinschaft zum Studium der Leber (GASL), Heidelberg, Germany
- 04/2017 Poster presentation, International Liver Congress (EASL), Amsterdam, Netherlands
- 06/2016 Poster presentation, Federation of American Societies for Experimental Biology Science Research Conference (FASEB), West Palm Beach, Florida, USA
- 01/2015 Poster presentation, Deutsche Arbeitsgemeinschaft zum Studium der Leber (GASL), Munich, Germany

Acknowledgements

I would like to thank all the people who contributed in any way to the success of this doctoral project and supported me in the last 4 years.

First, I would like to thank my group leader PD Dr. Ursula Ehmer for the chance to work in her laboratory and for all the support and patience over the recent years.

Further, I would like to especially thank Prof. Dr. Roland M. Schmid for accepting me as a Ph.D. student at his institute.

Next, I would like to thank PD Dr. Fabian Geisler and Prof. Dr. Gabriele Multhoff for the support and feedback on my project and their active contribution to this work as part of my Thesis Advisory Committee.

I would also like to thank all the members of my working group, especially Eric Hubner, Birgit Kohnke-Ertel and Thomas Rösner.

My special thanks goes to my family and friends, without their continued support, completion of the doctoral thesis would not have been possible.

References

- [1] C. Guichard, G. Amaddeo, S. Imbeaud, Y. Ladeiro, L. Pelletier, I.B. Maad, J. Calderaro, P. Bioulac-Sage, M. Letexier, F. Degos, B. Clement, C. Balabaud, E. Chevet, A. Laurent, G. Couchy, E. Letouze, F. Calvo, J. Zucman-Rossi, Integrated analysis of somatic mutations and focal copy-number changes identifies key genes and pathways in hepatocellular carcinoma, *Nat Genet* 44(6) (2012) 694-8.
- [2] U. Ehmer, A.F. Zmoos, R.K. Auerbach, D. Vaka, A.J. Butte, M.A. Kay, J. Sage, Organ size control is dominant over Rb family inactivation to restrict proliferation in vivo, *Cell Rep* 8(2) (2014) 371-81.
- [3] F. Liu, Y. Song, D. Liu, Hydrodynamics-based transfection in animals by systemic administration of plasmid DNA, *Gene Ther* 6(7) (1999) 1258-66.
- [4] L.A. Torre, F. Bray, R.L. Siegel, J. Ferlay, J. Lortet-Tieulent, A. Jemal, Global cancer statistics, 2012, *CA Cancer J Clin* 65(2) (2015) 87-108.
- [5] R.L. Siegel, K.D. Miller, A. Jemal, Cancer statistics, 2015, *CA Cancer J Clin* 65(1) (2015) 5-29.
- [6] D.L. White, A.P. Thrift, F. Kanwal, J. Davila, H.B. El-Serag, Incidence of Hepatocellular Carcinoma in All 50 United States, From 2000 Through 2012, *Gastroenterology* 152(4) (2017) 812-820 e5.
- [7] H.B. El-Serag, Hepatocellular carcinoma, *The New England journal of medicine* 365(12) (2011) 1118-27.
- [8] A. Jemal, F. Bray, M.M. Center, J. Ferlay, E. Ward, D. Forman, Global cancer statistics, *CA: a cancer journal for clinicians* 61(2) (2011) 69-90.
- [9] M.M. Yeh, Pathology of combined hepatocellular-cholangiocarcinoma, *Journal of gastroenterology and hepatology* 25(9) (2010) 1485-92.
- [10] H.B. El-Serag, Epidemiology of viral hepatitis and hepatocellular carcinoma, *Gastroenterology* 142(6) (2012) 1264-1273 e1.
- [11] H.B. El-Serag, K.L. Rudolph, Hepatocellular carcinoma: epidemiology and molecular carcinogenesis, *Gastroenterology* 132(7) (2007) 2557-76.
- [12] G.L. Tyson, H.B. El-Serag, Risk factors for cholangiocarcinoma, *Hepatology* 54(1) (2011) 173-84.
- [13] F. Kanwal, A. Befeler, R.S. Chari, J. Marrero, J. Kahn, N. Afdhal, T. Morgan, L. Roberts, S.R. Mohanty, J. Schwartz, D. VanThiel, J. Li, A. Zeringue, A. Di'Bisceglie, Potentially curative treatment in patients with hepatocellular cancer--results from the liver cancer research network, *Aliment Pharmacol Ther* 36(3) (2012) 257-65.
- [14] H.C. Spangenberg, R. Thimme, H.E. Blum, Targeted therapy for hepatocellular carcinoma, *Nat Rev Gastroenterol Hepatol* 6(7) (2009) 423-32.
- [15] J.M. Llovet, J. Bruix, Molecular targeted therapies in hepatocellular carcinoma, *Hepatology* 48(4) (2008) 1312-27.
- [16] A. Hollebecque, D. Malka, C. Ferte, M. Ducreux, V. Boige, Systemic treatment of advanced hepatocellular carcinoma: from disillusion to new horizons, *Eur J Cancer* 51(3) (2015) 327-39.
- [17] J. Bruix, S. Qin, P. Merle, A. Granito, Y.H. Huang, G. Bodoky, M. Pracht, O. Yokosuka, O. Rosmorduc, V. Breder, R. Gerolami, G. Masi, P.J. Ross, T. Song, J.P. Bronowicki, I. Ollivier-Hourmand, M. Kudo, A.L. Cheng, J.M. Llovet, R.S. Finn, M.A. LeBerre, A. Baumhauer, G. Meinhardt, G. Han, R. Investigators, Regorafenib for patients with hepatocellular carcinoma who progressed on sorafenib treatment (RESORCE): a randomised, double-blind, placebo-controlled, phase 3 trial, *Lancet* 389(10064) (2017) 56-66.

- [18] A.B. El-Khoueiry, B. Sangro, T. Yau, T.S. Crocenzi, M. Kudo, C. Hsu, T.Y. Kim, S.P. Choo, J. Trojan, T.H.R. Welling, T. Meyer, Y.K. Kang, W. Yeo, A. Chopra, J. Anderson, C. Dela Cruz, L. Lang, J. Neely, H. Tang, H.B. Dastani, I. Melero, Nivolumab in patients with advanced hepatocellular carcinoma (CheckMate 040): an open-label, non-comparative, phase 1/2 dose escalation and expansion trial, *Lancet* 389(10088) (2017) 2492-2502.
- [19] M. Kudo, Immune Checkpoint Inhibition in Hepatocellular Carcinoma: Basics and Ongoing Clinical Trials, *Oncology* 92 Suppl 1 (2017) 50-62.
- [20] R.S. Finn, P. Merle, A. Granito, Y.H. Huang, G. Bodoky, M. Pracht, O. Yokosuka, O. Rosmorduc, R. Gerolami, C. Capareello, R. Cabrera, C. Chang, W. Sun, M.A. LeBerre, A. Baumhauer, G. Meinhardt, J. Bruix, Outcomes of sequential treatment with sorafenib followed by regorafenib for HCC: Additional analyses from the phase III RESORCE trial, *J Hepatol* 69(2) (2018) 353-358.
- [21] A. Forner, J.M. Llovet, J. Bruix, Hepatocellular carcinoma, *Lancet* 379(9822) (2012) 1245-55.
- [22] M. Kumar, X. Zhao, X.W. Wang, Molecular carcinogenesis of hepatocellular carcinoma and intrahepatic cholangiocarcinoma: one step closer to personalized medicine?, *Cell Biosci* 1(1) (2011) 5.
- [23] L. Mishra, T. Banker, J. Murray, S. Byers, A. Thenappan, A.R. He, K. Shetty, L. Johnson, E.P. Reddy, Liver stem cells and hepatocellular carcinoma, *Hepatology* 49(1) (2009) 318-29.
- [24] K. Furuyama, Y. Kawaguchi, H. Akiyama, M. Horiguchi, S. Kodama, T. Kuhara, S. Hosokawa, A. Elbahrawy, T. Soeda, M. Koizumi, T. Masui, M. Kawaguchi, K. Takaori, R. Doi, E. Nishi, R. Kakinoki, J.M. Deng, R.R. Behringer, T. Nakamura, S. Uemoto, Continuous cell supply from a Sox9-expressing progenitor zone in adult liver, exocrine pancreas and intestine, *Nat Genet* 43(1) (2011) 34-41.
- [25] J.S. Lee, J. Heo, L. Libbrecht, I.S. Chu, P. Kaposi-Novak, D.F. Calvisi, A. Mikaelyan, L.R. Roberts, A.J. Demetris, Z. Sun, F. Nevens, T. Roskams, S.S. Thorgeirsson, A novel prognostic subtype of human hepatocellular carcinoma derived from hepatic progenitor cells, *Nature medicine* 12(4) (2006) 410-6.
- [26] F. Zhang, X.P. Chen, W. Zhang, H.H. Dong, S. Xiang, W.G. Zhang, B.X. Zhang, Combined hepatocellular cholangiocarcinoma originating from hepatic progenitor cells: immunohistochemical and double-fluorescence immunostaining evidence, *Histopathology* 52(2) (2008) 224-32.
- [27] C. Coulouarn, C. Cavard, L. Rubbia-Brandt, A. Audebourg, F. Dumont, S. Jacques, P.A. Just, B. Clement, H. Gilgenkrantz, C. Perret, B. Terris, Combined hepatocellular-cholangiocarcinomas exhibit progenitor features and activation of Wnt and TGFbeta signaling pathways, *Carcinogenesis* 33(9) (2012) 1791-6.
- [28] P. Viatour, U. Ehmer, L.A. Saddic, C. Dorrell, J.B. Andersen, C. Lin, A.F. Zmoos, P.K. Mazur, B.E. Schaffer, A. Ostermeier, H. Vogel, K.G. Sylvester, S.S. Thorgeirsson, M. Grompe, J. Sage, Notch signaling inhibits hepatocellular carcinoma following inactivation of the RB pathway, *J Exp Med* 208(10) (2011) 1963-76.
- [29] S. Benhamouche, M. Curto, I. Saotome, A.B. Gladden, C.H. Liu, M. Giovannini, A.I. McClatchey, Nf2/Merlin controls progenitor homeostasis and tumorigenesis in the liver, *Genes & development* 24(16) (2010) 1718-30.
- [30] X. Mu, R. Espanol-Suner, I. Mederacke, S. Affo, R. Manco, C. Sempoux, F.P. Lemaigre, A. Adili, D. Yuan, A. Weber, K. Unger, M. Heikenwalder, I.A. Leclercq, R.F. Schwabe, Hepatocellular carcinoma originates from hepatocytes and not from the progenitor/biliary compartment, *The Journal of clinical investigation* 125(10) (2015) 3891-903.

- [31] K. Nio, T. Yamashita, S. Kaneko, The evolving concept of liver cancer stem cells, *Mol Cancer* 16(1) (2017) 4.
- [32] A. Fujimoto, Y. Totoki, T. Abe, K.A. Boroevich, F. Hosoda, H.H. Nguyen, M. Aoki, N. Hosono, M. Kubo, F. Miya, Y. Arai, H. Takahashi, T. Shirakihara, M. Nagasaki, T. Shibuya, K. Nakano, K. Watanabe-Makino, H. Tanaka, H. Nakamura, J. Kusuda, H. Ojima, K. Shimada, T. Okusaka, M. Ueno, Y. Shigekawa, Y. Kawakami, K. Arihiro, H. Ohdan, K. Gotoh, O. Ishikawa, S. Ariizumi, M. Yamamoto, T. Yamada, K. Chayama, T. Kosuge, H. Yamaue, N. Kamatani, S. Miyano, H. Nakagama, Y. Nakamura, T. Tsunoda, T. Shibata, H. Nakagawa, Whole-genome sequencing of liver cancers identifies etiological influences on mutation patterns and recurrent mutations in chromatin regulators, *Nature genetics* 44(7) (2012) 760-4.
- [33] J. Huang, Q. Deng, Q. Wang, K.Y. Li, J.H. Dai, N. Li, Z.D. Zhu, B. Zhou, X.Y. Liu, R.F. Liu, Q.L. Fei, H. Chen, B. Cai, B. Zhou, H.S. Xiao, L.X. Qin, Z.G. Han, Exome sequencing of hepatitis B virus-associated hepatocellular carcinoma, *Nat Genet* 44(10) (2012) 1117-21.
- [34] w.b.e. Cancer Genome Atlas Research Network. Electronic address, N. Cancer Genome Atlas Research, Comprehensive and Integrative Genomic Characterization of Hepatocellular Carcinoma, *Cell* 169(7) (2017) 1327-1341 e23.
- [35] P. Laurent-Puig, J. Zucman-Rossi, Genetics of hepatocellular tumors, *Oncogene* 25(27) (2006) 3778-86.
- [36] I.P. Pogribny, I. Rusyn, Role of epigenetic aberrations in the development and progression of human hepatocellular carcinoma, *Cancer Lett* 342(2) (2014) 223-30.
- [37] C. Guichard, G. Amaddeo, S. Imbeaud, Y. Ladeiro, L. Pelletier, I.B. Maad, J. Calderaro, P. Bioulac-Sage, M. Letexier, F. Degos, B. Clement, C. Balabaud, E. Chevet, A. Laurent, G. Couchy, E. Letouze, F. Calvo, J. Zucman-Rossi, Integrated analysis of somatic mutations and focal copy-number changes identifies key genes and pathways in hepatocellular carcinoma, *Nature genetics* 44(6) (2012) 694-8.
- [38] J.B. Andersen, S.S. Thorgeirsson, Genetic profiling of intrahepatic cholangiocarcinoma, *Curr Opin Gastroenterol* 28(3) (2012) 266-72.
- [39] J.C. Nault, J. Zucman-Rossi, Genetics of hepatobiliary carcinogenesis, *Seminars in liver disease* 31(2) (2011) 173-87.
- [40] J.B. Andersen, B. Spee, B.R. Blechacz, I. Avital, M. Komuta, A. Barbour, E.A. Conner, M.C. Gillen, T. Roskams, L.R. Roberts, V.M. Factor, S.S. Thorgeirsson, Genomic and genetic characterization of cholangiocarcinoma identifies therapeutic targets for tyrosine kinase inhibitors, *Gastroenterology* 142(4) (2012) 1021-1031 e15.
- [41] D. Sia, Y. Hoshida, A. Villanueva, S. Roayaie, J. Ferrer, B. Tabak, J. Peix, M. Sole, V. Tovar, C. Alsinet, H. Cornella, B. Klotzle, J.B. Fan, C. Cotsoglou, S.N. Thung, J. Fuster, S. Waxman, J.C. Garcia-Valdecasas, J. Bruix, M.E. Schwartz, R. Beroukhim, V. Mazzaferro, J.M. Llovet, Integrative Molecular Analysis of Intrahepatic Cholangiocarcinoma Reveals 2 Classes That Have Different Outcomes, *Gastroenterology* (2013).
- [42] D. Sia, Y. Hoshida, A. Villanueva, S. Roayaie, J. Ferrer, B. Tabak, J. Peix, M. Sole, V. Tovar, C. Alsinet, H. Cornella, B. Klotzle, J.B. Fan, C. Cotsoglou, S.N. Thung, J. Fuster, S. Waxman, J.C. Garcia-Valdecasas, J. Bruix, M.E. Schwartz, R. Beroukhim, V. Mazzaferro, J.M. Llovet, Integrative molecular analysis of intrahepatic cholangiocarcinoma reveals 2 classes that have different outcomes, *Gastroenterology* 144(4) (2013) 829-40.
- [43] D.F. Calvisi, S. Ladu, A. Gorden, M. Farina, E.A. Conner, J.S. Lee, V.M. Factor, S.S. Thorgeirsson, Ubiquitous activation of Ras and Jak/Stat pathways in human HCC, *Gastroenterology* 130(4) (2006) 1117-28.

- [44] L. Chen, Y. Shi, C.Y. Jiang, L.X. Wei, Y.L. Wang, G.H. Dai, Expression and prognostic role of pan-Ras, Raf-1, pMEK1 and pERK1/2 in patients with hepatocellular carcinoma, *Eur J Surg Oncol* 37(6) (2011) 513-20.
- [45] M. Hennig, M.T. Yip-Schneider, S. Wentz, H. Wu, S.K. Hekmatyar, P. Klein, N. Bansal, C.M. Schmidt, Targeting mitogen-activated protein kinase kinase with the inhibitor PD0325901 decreases hepatocellular carcinoma growth in vitro and in mouse model systems, *Hepatology* 51(4) (2010) 1218-25.
- [46] H. Huynh, V.C. Ngo, H.N. Koong, D. Poon, S.P. Choo, H.C. Toh, C.H. Thng, P. Chow, H.S. Ong, A. Chung, B.C. Goh, P.D. Smith, K.C. Soo, AZD6244 enhances the anti-tumor activity of sorafenib in ectopic and orthotopic models of human hepatocellular carcinoma (HCC), *Journal of hepatology* 52(1) (2010) 79-87.
- [47] H. Huynh, AZD6244 (ARRY-142886) enhances the antitumor activity of rapamycin in mouse models of human hepatocellular carcinoma, *Cancer* 116(5) (2010) 1315-25.
- [48] C. Wang, H. Jin, D. Gao, C. Lieftink, B. Evers, G. Jin, Z. Xue, L. Wang, R.L. Beijersbergen, W. Qin, R. Bernards, phospho-ERK is a biomarker of response to a synthetic lethal drug combination of sorafenib and MEK inhibition in liver cancer, *J Hepatol* (2018).
- [49] H. Azechi, N. Nishida, Y. Fukuda, T. Nishimura, M. Minata, H. Katsuma, M. Kuno, T. Ito, T. Komeda, R. Kita, R. Takahashi, K. Nakao, Disruption of the p16/cyclin D1/retinoblastoma protein pathway in the majority of human hepatocellular carcinomas, *Oncology* 60(4) (2001) 346-54.
- [50] A.K. McClendon, J.L. Dean, A. Ertel, Z. Fu, D.B. Rivadeneira, C.A. Reed, R.J. Bourgo, A. Witkiewicz, S. Addya, C.N. Mayhew, H.L. Grimes, P. Fortina, E.S. Knudsen, RB and p53 cooperate to prevent liver tumorigenesis in response to tissue damage, *Gastroenterology* 141(4) (2011) 1439-50.
- [51] H. Symonds, L. Krall, L. Remington, M. Saenz-Robles, S. Lowe, T. Jacks, T. Van Dyke, p53-dependent apoptosis suppresses tumor growth and progression in vivo, *Cell* 78(4) (1994) 703-11.
- [52] T. Shibata, Y. Arai, Y. Totoki, Molecular genomic landscapes of hepatobiliary cancer, *Cancer Sci* 109(5) (2018) 1282-1291.
- [53] B. Bournet, F. Muscari, C. Buscail, E. Assenat, M. Barthelet, P. Hammel, J. Selves, R. Guimbaud, P. Cordelier, L. Buscail, KRAS G12D Mutation Subtype Is A Prognostic Factor for Advanced Pancreatic Adenocarcinoma, *Clin Transl Gastroenterol* 7 (2016) e157.
- [54] S. Zou, J. Li, H. Zhou, C. Frech, X. Jiang, J.S. Chu, X. Zhao, Y. Li, Q. Li, H. Wang, J. Hu, G. Kong, M. Wu, C. Ding, N. Chen, H. Hu, Mutational landscape of intrahepatic cholangiocarcinoma, *Nat Commun* 5 (2014) 5696.
- [55] T. Ikenoue, Y. Terakado, H. Nakagawa, Y. Hikiba, T. Fujii, D. Matsubara, R. Noguchi, C. Zhu, K. Yamamoto, Y. Kudo, Y. Asaoka, K. Yamaguchi, H. Ijichi, K. Tateishi, N. Fukushima, S. Maeda, K. Koike, Y. Furukawa, A novel mouse model of intrahepatic cholangiocarcinoma induced by liver-specific Kras activation and Pten deletion, *Sci Rep* 6 (2016) 23899.
- [56] M.R. O'Dell, J.L. Huang, C.L. Whitney-Miller, V. Deshpande, P. Rothberg, V. Grose, R.M. Rossi, A.X. Zhu, H. Land, N. Bardeesy, A.F. Hezel, Kras(G12D) and p53 mutation cause primary intrahepatic cholangiocarcinoma, *Cancer Res* 72(6) (2012) 1557-67.
- [57] P. Yu, L. Ye, H. Wang, G. Du, J. Zhang, J. Zhang, J. Tian, NSK-01105 inhibits proliferation and induces apoptosis of prostate cancer cells by blocking the Raf/MEK/ERK and PI3K/Akt/mTOR signal pathways, *Tumour Biol* 36(3) (2015) 2143-53.
- [58] J. Avruch, A. Khokhlatchev, J.M. Kyriakis, Z. Luo, G. Tzivion, D. Vavvas, X.F. Zhang, Ras activation of the Raf kinase: tyrosine kinase recruitment of the MAP kinase cascade, *Recent Prog Horm Res* 56 (2001) 127-55.

- [59] Y. Ito, Y. Sasaki, M. Horimoto, S. Wada, Y. Tanaka, A. Kasahara, T. Ueki, T. Hirano, H. Yamamoto, J. Fujimoto, E. Okamoto, N. Hayashi, M. Hori, Activation of mitogen-activated protein kinases/extracellular signal-regulated kinases in human hepatocellular carcinoma, *Hepatology* 27(4) (1998) 951-8.
- [60] C.M. Schmidt, I.H. McKillop, P.A. Cahill, J.V. Sitzmann, Increased MAPK expression and activity in primary human hepatocellular carcinoma, *Biochem Biophys Res Commun* 236(1) (1997) 54-8.
- [61] C.Y. Wang, D.C. Guttridge, M.W. Mayo, A.S. Baldwin, Jr., NF-kappaB induces expression of the Bcl-2 homologue A1/Bfl-1 to preferentially suppress chemotherapy-induced apoptosis, *Mol Cell Biol* 19(9) (1999) 5923-9.
- [62] T. Luedde, R.F. Schwabe, NF-kappaB in the liver--linking injury, fibrosis and hepatocellular carcinoma, *Nat Rev Gastroenterol Hepatol* 8(2) (2011) 108-18.
- [63] F. Feo, M. Frau, M.L. Tomasi, S. Brozzetti, R.M. Pascale, Genetic and epigenetic control of molecular alterations in hepatocellular carcinoma, *Exp Biol Med (Maywood)* 234(7) (2009) 726-36.
- [64] H. Hermeking, C. Rago, M. Schuhmacher, Q. Li, J.F. Barrett, A.J. Obaya, B.C. O'Connell, M.K. Mateyak, W. Tam, F. Kohlhuber, C.V. Dang, J.M. Sedivy, D. Eick, B. Vogelstein, K.W. Kinzler, Identification of CDK4 as a target of c-MYC, *Proc Natl Acad Sci U S A* 97(5) (2000) 2229-34.
- [65] K. Zheng, F.J. Cubero, Y.A. Nevzorova, c-MYC-Making Liver Sick: Role of c-MYC in Hepatic Cell Function, Homeostasis and Disease, *Genes (Basel)* 8(4) (2017).
- [66] J.M. Llovet, S. Ricci, V. Mazzaferro, P. Hilgard, E. Gane, J.F. Blanc, A.C. de Oliveira, A. Santoro, J.L. Raoul, A. Forner, M. Schwartz, C. Porta, S. Zeuzem, L. Bolondi, T.F. Greten, P.R. Galle, J.F. Seitz, I. Borbath, D. Haussinger, T. Giannaris, M. Shan, M. Moscovici, D. Voliotis, J. Bruix, S.I.S. Group, Sorafenib in advanced hepatocellular carcinoma, *N Engl J Med* 359(4) (2008) 378-90.
- [67] G.K. Abou-Alfa, L. Schwartz, S. Ricci, D. Amadori, A. Santoro, A. Figer, J. De Greve, J.Y. Douillard, C. Lathia, B. Schwartz, I. Taylor, M. Moscovici, L.B. Saltz, Phase II study of sorafenib in patients with advanced hepatocellular carcinoma, *J Clin Oncol* 24(26) (2006) 4293-300.
- [68] B.H. O'Neil, L.W. Goff, J.S. Kauh, J.R. Strosberg, T.S. Bekaii-Saab, R.M. Lee, A. Kazi, D.T. Moore, M. Learoyd, R.M. Lush, S.M. Sebti, D.M. Sullivan, Phase II study of the mitogen-activated protein kinase 1/2 inhibitor selumetinib in patients with advanced hepatocellular carcinoma, *J Clin Oncol* 29(17) (2011) 2350-6.
- [69] H.Y. Lim, J. Heo, H.J. Choi, C.Y. Lin, J.H. Yoon, C. Hsu, K.M. Rau, R.T. Poon, W. Yeo, J.W. Park, M.H. Tay, W.S. Hsieh, C. Kappeler, P. Rajagopalan, H. Krissel, M. Jeffers, C.J. Yen, W.Y. Tak, A phase II study of the efficacy and safety of the combination therapy of the MEK inhibitor refametinib (BAY 86-9766) plus sorafenib for Asian patients with unresectable hepatocellular carcinoma, *Clin Cancer Res* 20(23) (2014) 5976-85.
- [70] W.M. Tai, W.P. Yong, C. Lim, L.S. Low, C.K. Tham, T.S. Koh, Q.S. Ng, W.W. Wang, L.Z. Wang, S. Hartano, C.H. Thng, H. Huynh, K.T. Lim, H.C. Toh, B.C. Goh, S.P. Choo, A phase Ib study of selumetinib (AZD6244, ARRY-142886) in combination with sorafenib in advanced hepatocellular carcinoma (HCC), *Ann Oncol* 27(12) (2016) 2210-2215.
- [71] X. Yu, Y. Zheng, X. Zhu, X. Gao, C. Wang, Y. Sheng, W. Cheng, L. Qin, N. Ren, H. Jia, Q. Dong, Osteopontin promotes hepatocellular carcinoma progression via the PI3K/AKT/Twist signaling pathway, *Oncol Lett* 16(4) (2018) 5299-5308.
- [72] I. Nepstad, K.J. Hatfield, T.H.A. Tvedt, H. Reikvam, O. Bruserud, Clonal Heterogeneity Reflected by PI3K-AKT-mTOR Signaling in Human Acute Myeloid Leukemia Cells and Its Association with Adverse Prognosis, *Cancers (Basel)* 10(9) (2018).

- [73] M.J. Ellis, C.M. Perou, The genomic landscape of breast cancer as a therapeutic roadmap, *Cancer Discov* 3(1) (2013) 27-34.
- [74] J. Wang, F. Liu, P. Ao, X. Li, H. Zheng, D. Wu, N. Zhang, J. She, J. Yuan, X. Wu, Correlation of PDK1 expression with clinicopathologic features and prognosis of hepatocellular carcinoma, *Onco Targets Ther* 9 (2016) 5597-602.
- [75] D. Bai, L. Ueno, P.K. Vogt, Akt-mediated regulation of NFkappaB and the essentialness of NFkappaB for the oncogenicity of PI3K and Akt, *Int J Cancer* 125(12) (2009) 2863-70.
- [76] M. Farhan, H. Wang, U. Gaur, P.J. Little, J. Xu, W. Zheng, FOXO Signaling Pathways as Therapeutic Targets in Cancer, *Int J Biol Sci* 13(7) (2017) 815-827.
- [77] Z. Fu, D.J. Tindall, FOXOs, cancer and regulation of apoptosis, *Oncogene* 27(16) (2008) 2312-9.
- [78] V.S. Rodrik-Outmezguine, S. Chandarlapaty, N.C. Pagano, P.I. Poulikakos, M. Scaltriti, E. Moskatel, J. Baselga, S. Guichard, N. Rosen, mTOR kinase inhibition causes feedback-dependent biphasic regulation of AKT signaling, *Cancer Discov* 1(3) (2011) 248-59.
- [79] A. Villanueva, D.Y. Chiang, P. Newell, J. Peix, S. Thung, C. Alsinet, V. Tovar, S. Roayaie, B. Minguez, M. Sole, C. Battiston, S. Van Laarhoven, M.I. Fiel, A. Di Feo, Y. Hoshida, S. Yea, S. Toffanin, A. Ramos, J.A. Martignetti, V. Mazzaferro, J. Bruix, S. Waxman, M. Schwartz, M. Meyerson, S.L. Friedman, J.M. Llovet, Pivotal role of mTOR signaling in hepatocellular carcinoma, *Gastroenterology* 135(6) (2008) 1972-83, 1983 e1-11.
- [80] F. Sahin, R. Kannangai, O. Adegbola, J. Wang, G. Su, M. Torbenson, mTOR and P70 S6 kinase expression in primary liver neoplasms, *Clin Cancer Res* 10(24) (2004) 8421-5.
- [81] M.S. Matter, T. Decaens, J.B. Andersen, S.S. Thorgeirsson, Targeting the mTOR pathway in hepatocellular carcinoma: current state and future trends, *J Hepatol* 60(4) (2014) 855-65.
- [82] W. Yeo, S.L. Chan, F.K. Mo, C.M. Chu, J.W. Hui, J.H. Tong, A.W. Chan, J. Koh, E.P. Hui, H. Loong, K. Lee, L. Li, B. Ma, K.F. To, S.C. Yu, Phase I/II study of temsirolimus for patients with unresectable Hepatocellular Carcinoma (HCC)- a correlative study to explore potential biomarkers for response, *BMC Cancer* 15 (2015) 395.
- [83] A.X. Zhu, M. Kudo, E. Assenat, S. Cattan, Y.K. Kang, H.Y. Lim, R.T. Poon, J.F. Blanc, A. Vogel, C.L. Chen, E. Dorval, M. Peck-Radosavljevic, A. Santoro, B. Daniele, J. Furuse, A. Jappe, K. Perraud, O. Anak, D.B. Sellami, L.T. Chen, Effect of everolimus on survival in advanced hepatocellular carcinoma after failure of sorafenib: the EVOLVE-1 randomized clinical trial, *JAMA* 312(1) (2014) 57-67.
- [84] D. Koeberle, J.F. Dufour, G. Demeter, Q. Li, K. Ribí, P. Samaras, P. Saletti, A.D. Roth, D. Horber, M. Buehlmann, A.D. Wagner, M. Montemurro, G. Lakatos, J. Feilchenfeldt, M. Peck-Radosavljevic, D. Rauch, B. Tschanz, G. Bodoky, R. Swiss Group for Clinical Cancer, Sorafenib with or without everolimus in patients with advanced hepatocellular carcinoma (HCC): a randomized multicenter, multinational phase II trial (SAKK 77/08 and SASL 29), *Ann Oncol* 27(5) (2016) 856-61.
- [85] L. Bakiri, E.F. Wagner, Mouse models for liver cancer, *Mol Oncol* 7(2) (2013) 206-23.
- [86] L. He, D.A. Tian, P.Y. Li, X.X. He, Mouse models of liver cancer: Progress and recommendations, *Oncotarget* 6(27) (2015) 23306-22.
- [87] X. Chen, D.F. Calvisi, Hydrodynamic transfection for generation of novel mouse models for liver cancer research, *Am J Pathol* 184(4) (2014) 912-923.
- [88] Y. Malato, S. Naqvi, N. Schurmann, R. Ng, B. Wang, J. Zape, M.A. Kay, D. Grimm, H. Willenbring, Fate tracing of mature hepatocytes in mouse liver homeostasis and regeneration, *J Clin Invest* 121(12) (2011) 4850-60.

- [89] S.R. Yant, L. Meuse, W. Chiu, Z. Ivics, Z. Izsvak, M.A. Kay, Somatic integration and long-term transgene expression in normal and haemophilic mice using a DNA transposon system, *Nat Genet* 25(1) (2000) 35-41.
- [90] F. Park, K. Ohashi, W. Chiu, L. Naldini, M.A. Kay, Efficient lentiviral transduction of liver requires cell cycling in vivo, *Nat Genet* 24(1) (2000) 49-52.
- [91] A. Baldo, E. van den Akker, H.E. Bergmans, F. Lim, K. Pauwels, General considerations on the biosafety of virus-derived vectors used in gene therapy and vaccination, *Curr Gene Ther* 13(6) (2013) 385-94.
- [92] K. Jooss, N. Chirmule, Immunity to adenovirus and adeno-associated viral vectors: implications for gene therapy, *Gene Ther* 10(11) (2003) 955-63.
- [93] R. Rudalska, D. Dauch, T. Longerich, K. McJunkin, T. Wuestefeld, T.W. Kang, A. Hohmeyer, M. Pesic, J. Leibold, A. von Thun, P. Schirmacher, J. Zuber, K.H. Weiss, S. Powers, N.P. Malek, M. Eilers, B. Sipos, S.W. Lowe, R. Geffers, S. Laufer, L. Zender, In vivo RNAi screening identifies a mechanism of sorafenib resistance in liver cancer, *Nat Med* 20(10) (2014) 1138-46.
- [94] T. Wuestefeld, M. Pesic, R. Rudalska, D. Dauch, T. Longerich, T.W. Kang, T. Yevsa, F. Heinzmann, L. Hoenicke, A. Hohmeyer, A. Potapova, I. Rittelmeier, M. Jarek, R. Geffers, M. Scharfe, F. Klawonn, P. Schirmacher, N.P. Malek, M. Ott, A. Nordheim, A. Vogel, M.P. Manns, L. Zender, A Direct in vivo RNAi screen identifies MKK4 as a key regulator of liver regeneration, *Cell* 153(2) (2013) 389-401.
- [95] W. Xue, S. Chen, H. Yin, T. Tammela, T. Papagiannakopoulos, N.S. Joshi, W. Cai, G. Yang, R. Bronson, D.G. Crowley, F. Zhang, D.G. Anderson, P.A. Sharp, T. Jacks, CRISPR-mediated direct mutation of cancer genes in the mouse liver, *Nature* 514(7522) (2014) 380-4.
- [96] J. Weber, R. Ollinger, M. Friedrich, U. Ehmer, M. Barenboim, K. Steiger, I. Heid, S. Mueller, R. Maresch, T. Engleitner, N. Gross, U. Geumann, B. Fu, A. Segler, D. Yuan, S. Lange, A. Strong, J. de la Rosa, I. Esposito, P. Liu, J. Cadinanos, G.S. Vassiliou, R.M. Schmid, G. Schneider, K. Unger, F. Yang, R. Braren, M. Heikenwalder, I. Varela, D. Saur, A. Bradley, R. Rad, CRISPR/Cas9 somatic multiplex-mutagenesis for high-throughput functional cancer genomics in mice, *Proceedings of the National Academy of Sciences of the United States of America* 112(45) (2015) 13982-7.
- [97] O.C. Hibbitt, R.P. Harbottle, S.N. Waddington, C.A. Bursill, C. Coutelle, K.M. Channon, R. Wade-Martins, Delivery and long-term expression of a 135 kb LDLR genomic DNA locus in vivo by hydrodynamic tail vein injection, *J Gene Med* 9(6) (2007) 488-97.
- [98] E.K. Hubner, C. Lechler, B. Kohnke-Ertel, A.F. Zmoos, J. Sage, R.M. Schmid, U. Ehmer, An in vivo transfection system for inducible gene expression and gene silencing in murine hepatocytes, *J Gene Med* 19(1-2) (2017).
- [99] D. Dauch, R. Rudalska, G. Cossa, J.C. Nault, T.W. Kang, T. Wuestefeld, A. Hohmeyer, S. Imbeaud, T. Yevsa, L. Hoenicke, T. Pantsar, P. Bozko, N.P. Malek, T. Longerich, S. Laufer, A. Poso, J. Zucman-Rossi, M. Eilers, L. Zender, A MYC-aurora kinase A protein complex represents an actionable drug target in p53-altered liver cancer, *Nat Med* 22(7) (2016) 744-53.
- [100] E.K. Hubner, C. Lechler, T.N. Rosner, B. Kohnke-Ertel, R.M. Schmid, U. Ehmer, Constitutive and Inducible Systems for Genetic In Vivo Modification of Mouse Hepatocytes Using Hydrodynamic Tail Vein Injection, *J Vis Exp* (132) (2018).
- [101] C.H. Miao, K. Ohashi, G.A. Patijn, L. Meuse, X. Ye, A.R. Thompson, M.A. Kay, Inclusion of the hepatic locus control region, an intron, and untranslated region increases and stabilizes hepatic factor IX gene expression in vivo but not in vitro, *Mol Ther* 1(6) (2000) 522-32.

- [102] Z. Izsvak, Z. Ivics, R.H. Plasterk, Sleeping Beauty, a wide host-range transposon vector for genetic transformation in vertebrates, *J Mol Biol* 302(1) (2000) 93-102.
- [103] G. Zhang, X. Gao, Y.K. Song, R. Vollmer, D.B. Stolz, J.Z. Gasiorowski, D.A. Dean, D. Liu, Hydroporation as the mechanism of hydrodynamic delivery, *Gene Ther* 11(8) (2004) 675-82.
- [104] C.M. Weisend, J.A. Kundert, E.S. Suvorova, J.R. Prigge, E.E. Schmidt, Cre activity in fetal albCre mouse hepatocytes: Utility for developmental studies, *Genesis* 47(12) (2009) 789-92.
- [105] S. Jors, P. Jeliaskova, M. Ringelhan, J. Thalhammer, S. Durl, J. Ferrer, M. Sander, M. Heikenwalder, R.M. Schmid, J.T. Siveke, F. Geisler, Lineage fate of ductular reactions in liver injury and carcinogenesis, *J Clin Invest* 125(6) (2015) 2445-57.
- [106] J. Ji, X.W. Wang, Clinical implications of cancer stem cell biology in hepatocellular carcinoma, *Seminars in oncology* 39(4) (2012) 461-72.
- [107] L. Wu, Z.Y. Tang, Y. Li, Experimental models of hepatocellular carcinoma: developments and evolution, *Journal of cancer research and clinical oncology* 135(8) (2009) 969-81.
- [108] J. Mollenhauer, S. Wiemann, W. Scheurlen, B. Korn, Y. Hayashi, K.K. Wilgenbus, A. von Deimling, A. Poustka, DMBT1, a new member of the SRCR superfamily, on chromosome 10q25.3-26.1 is deleted in malignant brain tumours, *Nat Genet* 17(1) (1997) 32-9.
- [109] M. Deichmann, J. Mollenhauer, B. Helmke, M. Thome, W. Hartschuh, A. Poustka, H. Naher, Analysis of losses of heterozygosity of the candidate tumour suppressor gene DMBT1 in melanoma resection specimens, *Oncology* 63(2) (2002) 166-72.
- [110] K. Sasaki, K. Sato, Y. Akiyama, K. Yanagihara, M. Oka, K. Yamaguchi, Peptidomics-based approach reveals the secretion of the 29-residue COOH-terminal fragment of the putative tumor suppressor protein DMBT1 from pancreatic adenocarcinoma cell lines, *Cancer Res* 62(17) (2002) 4894-8.
- [111] H. Takeshita, M. Sato, H.O. Shiwaku, S. Semba, A. Sakurada, M. Hoshi, Y. Hayashi, Y. Tagawa, H. Ayabe, A. Horii, Expression of the DMBT1 gene is frequently suppressed in human lung cancer, *Jpn J Cancer Res* 90(9) (1999) 903-8.
- [112] W. Wu, B.L. Kemp, M.L. Proctor, A.F. Gazdar, J.D. Minna, W.K. Hong, L. Mao, Expression of DMBT1, a candidate tumor suppressor gene, is frequently lost in lung cancer, *Cancer Res* 59(8) (1999) 1846-51.
- [113] J. Mollenhauer, M. Deichmann, B. Helmke, H. Muller, G. Kollender, U. Holmskov, T. Ligtenberg, I. Krebs, S. Wiemann, U. Bantel-Schaal, J. Madsen, F. Bikker, S.M. Klauck, H.F. Otto, G. Moldenhauer, A. Poustka, Frequent downregulation of DMBT1 and galectin-3 in epithelial skin cancer, *Int J Cancer* 105(2) (2003) 149-57.
- [114] J. Mollenhauer, B. Helmke, D. Medina, G. Bergmann, N. Gassler, H. Muller, S. Lyer, L. Diedrichs, M. Renner, R. Wittig, S. Blaich, U. Hamann, J. Madsen, U. Holmskov, F. Bikker, A. Ligtenberg, A. Carlen, J. Olsson, H.F. Otto, B. O'Malley, A. Poustka, Carcinogen inducibility in vivo and down-regulation of DMBT1 during breast carcinogenesis, *Genes Chromosomes Cancer* 39(3) (2004) 185-94.
- [115] M.A. Imai, T. Moriya, F.L. Imai, M. Shiiba, H. Bukawa, H. Yokoe, K. Uzawa, H. Tanzawa, Down-regulation of DMBT1 gene expression in human oral squamous cell carcinoma, *Int J Mol Med* 15(4) (2005) 585-9.
- [116] J. Du, M. Guan, J. Fan, H. Jiang, Loss of DMBT1 expression in human prostate cancer and its correlation with clinical progressive features, *Urology* 77(2) (2011) 509 e9-13.
- [117] M. Mori, T. Shiraishi, S. Tanaka, M. Yamagata, K. Mafune, Y. Tanaka, H. Ueo, G.F. Barnard, K. Sugimachi, Lack of DMBT1 expression in oesophageal, gastric and colon cancers, *Br J Cancer* 79(2) (1999) 211-3.

- [118] A.J. Ligtenberg, E.C. Veerman, A.V. Nieuw Amerongen, J. Mollenhauer, Salivary agglutinin/glycoprotein-340/DMBT1: a single molecule with variable composition and with different functions in infection, inflammation and cancer, *Biol Chem* 388(12) (2007) 1275-89.
- [119] H.C. Bisgaard, U. Holmskov, E. Santoni-Rugiu, P. Nagy, O. Nielsen, P. Ott, E. Hage, K. Dalhoff, L.J. Rasmussen, N. Tygstrup, Heterogeneity of ductular reactions in adult rat and human liver revealed by novel expression of deleted in malignant brain tumor 1, *Am J Pathol* 161(4) (2002) 1187-98.
- [120] R. T. Borchardt, E. H. Kerns, M. Hageman, D. R. Thakker, J. L. Stevens, *Optimizing the "Drug-Like" Properties of Leads in Drug Discovery*, 2006.
- [121] M.A. Otieno, V. Bhaskaran, E. Janovitz, Y. Callejas, W.B. Foster, W. Washburn, J.R. Megill, L. Lehman-McKeeman, B. Gemzik, Mechanisms for Hepatobiliary Toxicity in Rats Treated with an Antagonist of Melanin Concentrating Hormone Receptor 1 (MCHR1), *Toxicol Sci* 155(2) (2017) 379-388.
- [122] B. Goepfert, S. Roessler, N. Becker, M. Zucknick, M.N. Vogel, A. Warth, A. Pathil-Warth, A. Mehrabi, P. Schirmacher, J. Mollenhauer, M. Renner, DMBT1 expression in biliary carcinogenesis with correlation of clinicopathological data, *Histopathology* 70(7) (2017) 1064-1071.
- [123] S.R. Yant, Y. Huang, B. Akache, M.A. Kay, Site-directed transposon integration in human cells, *Nucleic Acids Res* 35(7) (2007) e50.
- [124] J.C. Nault, J. Zucman-Rossi, Genetics of hepatocellular carcinoma: the next generation, *J Hepatol* 60(1) (2014) 224-6.
- [125] B. Fan, Y. Malato, D.F. Calvisi, S. Naqvi, N. Razumilava, S. Ribback, G.J. Gores, F. Dombrowski, M. Evert, X. Chen, H. Willenbring, Cholangiocarcinomas can originate from hepatocytes in mice, *The Journal of clinical investigation* 122(8) (2012) 2911-5.
- [126] R. Feil, J. Brocard, B. Mascrez, M. LeMeur, D. Metzger, P. Chambon, Ligand-activated site-specific recombination in mice, *Proc Natl Acad Sci U S A* 93(20) (1996) 10887-90.
- [127] N. Oishi, M.R. Kumar, S. Roessler, J. Ji, M. Forgues, A. Budhu, X. Zhao, J.B. Andersen, Q.H. Ye, H.L. Jia, L.X. Qin, T. Yamashita, H.G. Woo, Y.J. Kim, S. Kaneko, Z.Y. Tang, S.S. Thorgeirsson, X.W. Wang, Transcriptomic profiling reveals hepatic stem-like gene signatures and interplay of miR-200c and epithelial-mesenchymal transition in intrahepatic cholangiocarcinoma, *Hepatology* 56(5) (2012) 1792-803.
- [128] L. Li, G.D. Zhao, Z. Shi, L.L. Qi, L.Y. Zhou, Z.X. Fu, The Ras/Raf/MEK/ERK signaling pathway and its role in the occurrence and development of HCC, *Oncol Lett* 12(5) (2016) 3045-3050.
- [129] B. Delire, P. Starkel, The Ras/MAPK pathway and hepatocarcinoma: pathogenesis and therapeutic implications, *Eur J Clin Invest* 45(6) (2015) 609-23.
- [130] B.A. Hemmings, D.F. Restuccia, PI3K-PKB/Akt pathway, *Cold Spring Harb Perspect Biol* 4(9) (2012) a011189.
- [131] H. Deng, Y.B. Gao, H.F. Wang, X.L. Jin, J.C. Xiao, Expression of deleted in malignant brain tumours 1 (DMBT1) relates to the proliferation and malignant transformation of hepatic progenitor cells in hepatitis B virus-related liver diseases, *Histopathology* 60(2) (2012) 249-60.
- [132] J. Mollenhauer, S. Herberth, U. Holmskov, M. Tolnay, I. Krebs, A. Merlo, H.D. Schroder, D. Maier, F. Breitling, S. Wiemann, H.J. Grone, A. Poustka, DMBT1 encodes a protein involved in the immune defense and in epithelial differentiation and is highly unstable in cancer, *Cancer Res* 60(6) (2000) 1704-10.

- [133] X. Jiang, K. Feng, Y. Zhang, Z. Li, F. Zhou, H. Dou, T. Wang, Sorafenib and DE605, a novel c-Met inhibitor, synergistically suppress hepatocellular carcinoma, *Oncotarget* 6(14) (2015) 12340-56.
- [134] J.S. Kim, G.H. Choi, Y. Jung, K.M. Kim, S.J. Jang, E.S. Yu, H.C. Lee, Downregulation of Raf-1 kinase inhibitory protein as a sorafenib resistance mechanism in hepatocellular carcinoma cell lines, *J Cancer Res Clin Oncol* 144(8) (2018) 1487-1501.
- [135] Z. Zhang, L. Xu, C. Sun, Comprehensive characterization of cancer genes in hepatocellular carcinoma genomes, *Oncol Lett* 15(2) (2018) 1503-1510.
- [136] T. Ozaki, A. Nakagawara, Role of p53 in Cell Death and Human Cancers, *Cancers (Basel)* 3(1) (2011) 994-1013.
- [137] H. Shiraha, K. Yamamoto, M. Namba, Human hepatocyte carcinogenesis (review), *Int J Oncol* 42(4) (2013) 1133-8.
- [138] R.B. Matondo, M.J. Toussaint, K.M. Govaert, L.D. van Vuuren, S. Nantasanti, M.W. Nijkamp, S.K. Pandit, P.C. Tooten, M.H. Koster, K. Holleman, A. Schot, G. Gu, B. Spee, T. Roskams, I.B. Rinkes, B. Schotanus, O. Kranenburg, A. de Bruin, Surgical resection and radiofrequency ablation initiate cancer in cytokeratin-19+ liver cells deficient for p53 and Rb, *Oncotarget* 7(34) (2016) 54662-54675.
- [139] A. Fernandez-Medarde, E. Santos, Ras in cancer and developmental diseases, *Genes Cancer* 2(3) (2011) 344-58.
- [140] F. McCormick, K-Ras protein as a drug target, *J Mol Med (Berl)* 94(3) (2016) 253-8.
- [141] J. Bruix, A.L. Cheng, G. Meinhardt, K. Nakajima, Y. De Sanctis, J. Llovet, Prognostic factors and predictors of sorafenib benefit in patients with hepatocellular carcinoma: Analysis of two phase III studies, *J Hepatol* 67(5) (2017) 999-1008.
- [142] J.E. Visvader, Cells of origin in cancer, *Nature* 469(7330) (2011) 314-22.
- [143] A. Wang, L. Wu, J. Lin, L. Han, J. Bian, Y. Wu, S.C. Robson, L. Xue, Y. Ge, X. Sang, W. Wang, H. Zhao, Whole-exome sequencing reveals the origin and evolution of hepatocarcinoma, *Nat Commun* 9(1) (2018) 894.
- [144] J. Shi, J. Guo, X. Li, Role of LASP-1, a novel SOX9 transcriptional target, in the progression of lung cancer, *Int J Oncol* 52(1) (2018) 179-188.
- [145] A. Matheu, M. Collado, C. Wise, L. Manterola, L. Cekaite, A.J. Tye, M. Canamero, L. Bujanda, A. Schedl, K.S. Cheah, R.I. Skotheim, R.A. Lothe, A. Lopez de Munain, J. Briscoe, M. Serrano, R. Lovell-Badge, Oncogenicity of the developmental transcription factor Sox9, *Cancer Res* 72(5) (2012) 1301-15.
- [146] J.I. Lee, J.W. Lee, J.M. Kim, J.K. Kim, H.J. Chung, Y.S. Kim, Prognosis of hepatocellular carcinoma expressing cytokeratin 19: comparison with other liver cancers, *World J Gastroenterol* 18(34) (2012) 4751-7.
- [147] K. Nakanishi, M. Sakamoto, S. Yamasaki, S. Todo, S. Hirohashi, Akt phosphorylation is a risk factor for early disease recurrence and poor prognosis in hepatocellular carcinoma, *Cancer* 103(2) (2005) 307-12.
- [148] K. Yokoi, A. Kobayashi, H. Motoyama, M. Kitazawa, A. Shimizu, T. Notake, T. Yokoyama, T. Matsumura, M. Takeoka, S.I. Miyagawa, Survival pathway of cholangiocarcinoma via AKT/mTOR signaling to escape RAF/MEK/ERK pathway inhibition by sorafenib, *Oncol Rep* 39(2) (2018) 843-850.
- [149] J. Garay, M.B. Piazuelo, L. Lopez-Carrillo, Y.A. Leal, S. Majumdar, L. Li, N. Cruz-Rodriguez, S.J. Serrano-Gomez, C.S. Busso, B.G. Schneider, A.G. Delgado, L.E. Bravo, A.M. Crist, S.M. Meadows, M.C. Camargo, K.T. Wilson, P. Correa, J. Zabaleta, Increased expression of deleted in malignant brain tumors (DMBT1) gene in precancerous gastric lesions: Findings from human and animal studies, *Oncotarget* 8(29) (2017) 47076-47089.

- [150] M. Frau, M.M. Simile, M.L. Tomasi, M.I. Demartis, L. Daino, M.A. Seddaiu, S. Brozzetti, C.F. Feo, G. Massarelli, G. Solinas, F. Feo, J.S. Lee, R.M. Pascale, An expression signature of phenotypic resistance to hepatocellular carcinoma identified by cross-species gene expression analysis, *Cell Oncol (Dordr)* 35(3) (2012) 163-73.
- [151] M. Sasaki, S.F. Huang, M.F. Chen, Y.Y. Jan, T.S. Yeh, A. Ishikawa, J. Mollenhauer, A. Poustka, K. Tsuneyama, Y. Nimura, K. Oda, Y. Nakanuma, Decrease of deleted in malignant brain tumour-1 (DMBT-1) expression is a crucial late event in intrahepatic cholangiocarcinoma, *Histopathology* 43(4) (2003) 340-6.
- [152] Cheng AL, Kang YK, Chen Z, Tsao CJ, Qin S, Kim JS, Luo R, Feng J, Ye S, Yang TS, Xu J, Sun Y, Liang H, Liu J, Wang J, Tak WY, Pan H, Burock K, Zou J, Voliotis D, Guan Z, Efficacy and safety of sorafenib in patients in the Asia-Pacific region with advanced hepatocellular carcinoma: a phase III randomised, double-blind, placebo-controlled trial, *Lancet Oncol* 10(1) (2009) 25-34.
- [153] Al-Lazikani B, Banerji U, Workman P, Combinatorial drug therapy for cancer in the post-genomic era, *Nat Biotechnol.* 30(7) (2012) 679-92.
- [154] Gotwals P, Cameron S, Cipolletta D, Cremasco V, Crystal A, Hewes B, Mueller B, Quarantino S, Sabatos-Peyton C, Petruzzelli L, Engelman JA, Dranoff G, Prospects for combining targeted and conventional cancer therapy with immunotherapy, *Nat Rev Cancer* 2017 17(5) (2017) 286-301.